UNIVERSITÀ DEGLI STUDI DI MILANO-BICOCCA
Facoltà di Scienze Matematiche, Fisiche e Naturali
Dottorato di Ricerca in Biologia XXIII ciclo

ROLE OF PHOSPHORYLATION OF ATAXIN-3 AND OXIDATIVE STRESS IN THE PATHOGENESIS OF SPINOCEREBELLAR ATAXIA TYPE 3 (SCA3)

Tutor: Dott.ssa Paola Fusi

Valentina Pastori

Matr: 040403

INDEX

ABSTRACT

Spinocerebellar ataxia type 3 (SCA3) is a dominantly inherited, neurodegenerative disease caused by the presence of an expanded polyglutamine repeat inside ataxin-3, the protein encoded by MJD1 gene (located on chromosome 14).

Bioinformatic analysis, using *NetPhos 2.0*, *PHOSIDIA* and *ScanProsite*, showed the presence of eight casein kinase 2 (CK2) phosphorylation sites and three glycogen synthase kinase 3 (GSK3) phosphorylation sites in ataxin-3 sequence. CK2 is a pleiotropic kinase involved in many cellular processes and GSK3 has turned out to have a key role in the regulation of many cell functions, both kinases are involved in neurodegenerative diseases. In order to investigate the possible role of ataxin-3 phosphorylation by CK2 and GSK3 on its sub-cellular localization, *in vitro* phosphorylated AT-3Q6 was analyzed by mass spectrometry phosphomapping. The analysis identified 7 phosphorylation sites for CK2: the serines 29, 272, 277, 329, 341, 344 and the threonine 271 and 3 phosphorylation sites for GSK3: the serines 29, 268 and 273. We obtained mutants lacking phosphorylation sites for CK2 and GSK3 by PCR, substituting serines and threonine with alanines: S29A, S272A, S277A, DM (S272A and S277A), TM (T271A, S272A and S277A) and QM (S268A, T271A, S272A, S273A and S277A).

Sub-cellular localization of these mutants was investigated in COS7 transfected cells, through sub-cellular fractionation, mitochondria extraction and confocal microscopy.

Only S29A mutant showed a phenotype, in fact it had a lower localization in the nucleus than the wild-type, suggesting that this phosphorylation site might be involved in nuclear ataxin-3 import.

In order to confirm the role of S29 phosphorylation on ataxin-3 nuclear uptake, this residue was substituted by PCR with an aspartic acid, yielding S29D mutant, mimicking the presence of the phosphate negative charge.

Confocal microscopy and sub-cellular fractionation showed that this mutant has the same sub-cellular localization of wild-type, demonstrating that the identified phenotype is due to lack of phosphorylation and not to amino acidic substitution.

Sub-cellular localization was also investigated in SHSY-5Y cells, a human neuronal cancer cell line, and also in these cells the S29A mutant showed a lower nuclear localization than the wild-type.

COS-7 cells expressing either AT-3Q6 or AT-3Q6S29D were grown in the presence of CK2 inhibitor TBB (tetrabromobenzotriazole) and GSK3 inhibitor SB216763. Inhibitors were added to growth media either separately or in combination. When the culture medium was supplemented with TBB alone, both wild-type AT-3Q6 and S29D mutant were found evenly distributed between the cytosol and the nucleus, suggesting that TBB could not prevent S29 phosphorylation. The same happened when only GSK3 inhibitor SB216763 was administered. However, when both inhibitors were added to culture medium, nuclear translocation of wild-type AT-3Q6 appeared to be reduced, a behaviour closely mirroring that of S29A mutant. These data clearly show that CK2 and GSK3 can substitute each other in the phosphorylation of S29, promoting AT-3 nuclear uptake.
Mueller and coworkers (Mueller t. *et al*., 2009) demonstrated that serine 340 and 352 within the third ubiquitin-interacting motif of AT-3 were particularly important for nuclear localization of normal and expanded AT-3. To demonstrate if the combination of S29A with Mueller's mutants could suppress AT-3 nuclear uptake, we obtained AT-3Q6M substituting S29, S329 and S341 with alanines, in fact S329 and S341 correspond to S340 and S352 respectively in human AT-3. Our data demonstrated that removal of S329 and S341 does not further reduce S29A nuclear uptake.
To demonstrate if S29 was also involved in nuclear uptake of AT-3 pathological form we mutated S29 of AT-3Q72 to alanine. Our results demonstrated that the mutation does not change AT-3Q72 nuclear localization.

VCP/p97 is a key protein essential for the extraction of substrates from the endoplasmic reticulum (ER) to the cytosol in ER-associated degradation (ERAD). Since VCP/p97 interacts with ataxin-3 in a region between aminoacids 257 and 291 (Boeddrich A. *et al*.,2006), we studied the interaction between the mutants lacking phosphorylation sites in this region, and VCP to understand if phosphorylation was involved in this interaction. In this region of interaction with VCP there are 3 phosphorylation sites for CK2 (T271, S272 and S277) and 2 phosphorylation sites for GSK3 (S268 and S273).
We studied the interaction between VCP/p97 and AT-3Q6 or the mutants TM (T271A, S272A and S277A) and QM (S268A, T271A, S272A, S273A and S277A) by immunoprecipitation of AT-3 from COS7 cells co-transfected with VCP and AT-3.

The mutants showed the same interaction with VCP as the wild-type, suggesting that these phosphorylation sites are not involved in interaction with VCP/p97.
To assess whether the phosphorylation sites had an effect on the interaction between VCP/p97 and its substrates, we treated transfected cells with DTT to obtain an ER stress. No difference between AT-3Q6 and its mutants was detected in these conditions. Nevertheless, in the presence of ERAD stress, AT-3 showed a weaker interaction with VCP than in normal conditions. This suggests that when ER is under stress, VCP/p97 must increase its interaction with its normal partner Ufd1 and with polyubiquitin chains to degrade ERAD substrates, so VCP/p97 must decrease its interaction with AT-3.
We also studied the interaction between VCP/p97 and AT-3Q72 with or without inducing ER stress conditions and we showed that there was no change in the interaction between AT-3Q72 and VCP/p97 under stress condition. Nevertheless AT-3Q72 has a stronger interaction with VCP than AT-3Q6, as demonstrated by Zhong and coworkers (Zhong X. *et al.,* 2006). Therefore the pathological form of AT-3 interacts aberrantly with VCP/p97 also in ER stress condition, leading to a deregulation of ERAD.

Overproduction of reactive nitrogen species (RNS) and reactive oxygen species (ROS), which lead to neuronal cell injury and death, is a potential mediator of neurodegenerative disorders. To understand the role of nitrosative stress in Spinocerebellar Ataxia Type 3 we studied the expression of NO synthase in Neuro2a cells transfected with AT-3Q6 or AT-3Q72. The results demonstrated that in presence of AT-3 pathological form there was an increase in NOS expression. Thus we studied nitration pattern through mono and bidimensional analysis and we observed that in presence of pathological form of AT-3 there was a remarkable increase in protein nitration, both as nitration level and as number of nitrated proteins. Therefore the presence of AT-3 pathological form causes activation of nitrosative stress.

1. Introduction

1.1 TRINUCLEOTIDE REPEAT EXPANSION DISEASES (TREDs)

Many regions rich in trinucleotide repeats have been found in different positions in the genome of eukaryotes, both in coding and in non coding sequences. Some of these expansions are related to the genesis of pathology, typically a neuropathology, when exceeding a typical threshold. These pathologies are now known as trinucleotide repeat expansion diseases (TREDs) (Richards R. I. *et al*., 1997)

If the repetition is located in a non coding region it can influence the regulation of the nearest genes, but if it stands in a coding one it leads to the formation of an aberrant protein. These regions containing expanded repetitions are subject to a dynamic instability, which can cause an elongation of the repetition in the offspring, a phenomenon called anticipation (Richards R. I. *et al*., 1997). This depends on the propensity of a highly repeated DNA sequence to undergo a wrong crossing over, the so called mitotic, meiotic or post mitotic instability (Ross C. A., 1995; Perutz M. F., 1996).

TREDs can be divided in two classes. The first one includes all the diseases caused by expansions in non coding regions which influence nearby genes regulation. It includes diseases as X fragile syndrome, myotonic dystrophy, Friedreich ataxia and EPM1, a monogenic progressive form of epilepsy (Mandel J. L., 1997). Pathologies classified as class II are caused by expansions within the coding regions of different genes. They consist mainly of CAG triplet repeats, which are translated in polyglutamine (poly-Q) stretches. Diseases caused by this kind of mutations depends on the production of a protein which can loose its physiological function and gain a new toxic one; these mutated proteins show a cytotoxic behaviour, which leads to the death of peculiar neuronal cell populations.
Nine poly-Q diseases are known so far: Huntington disease (HD), dentatorubral pallidoluysian atrophy (DRPLA), spinobulbar muscular atrophy (SBMA) and 6 different types of spinocerebellar ataxias (SCA): 1, 2, 3, 6, 7, and 17.

1.2 POLY-Q DISEASES

SBMA is the only pathology linked to the X chromosome (Kakizuka A., 1998); the gene involved codes for the androgen receptor. The

poly-Q stretch is located near the N-terminus of the protein and is not necessary for the receptor function, but it causes the pathology when its length exceeds a threshold of 38 consecutive glutamines (Zoghbi H. Y. *et al.*, 2000).
In DRPLA the aberrant protein contains a minimum of 49 repetitions, is mainly cytoplasmic and does not present any homology with any known protein.

The most studied amongst class II pathologies is certainly Huntington disease (HD), which is caused by a 348 kDa protein, called huntingtin, which is found in the cytosol, where it associates to microtubules and to presinaptic vescicles in neurons. This protein seems to be essential during neurogenesis (Bates G. P. *et al.*, 1998), as well as for the transcription of Brain-derived neurotrophic factor (BDNF) which is fundamental for the survival of striatal neurons (Zuccato C. *et al.*, 2001). Pathology occurs if the repetition is longer than 36 consecutive residues.

Spinocerebellar ataxias show many similarities in pathological symptoms, such as a diffused degeneration of cerebellum, and superiors tracts of the spinal cord, although the proteins involved are completely different.
Ataxin 1 is a protein of 792-830 aminoacids which does not present any similarities with other known proteins; its pathological threshold is over 44 consecutive glutamines (Servadio A. *et al.*, 1995). Ataxin 2 is a cytosolic protein that becomes pathological if the glutamine stretch exceeds 36 repetitions. Ataxin-3 is the protein responsible for Spinocerebellar ataxia type 3 or Machado Joseph disease and is the subject of our studies. Ataxin 7 is a nuclear protein of 130-180 kDa with the poly-Q stretch at its N-terminus. Unlike ataxin 1 and 2 it presents no interruptions in the repetitions which are considered non pathologic when shorter than 35 residues (Zoghbi H. Y. *et al.*, 2000). Spinocerebellar ataxia type 17 has been recently characterized (Maltecca F. *et al.*, 2003). The protein causing this pathology is TBP (TATA box-binding protein), a very important factor for transcription; the pathological threshold corresponds to 47 consecutive residues.
A really interesting observation about all these pathologies is that the proteins involved are structurally different from one another, except for the presence of the poly-Q stretch; moreover their functions (when known) are not necessary linked, nevertheless it seems likely that the mechanisms causing the diseases are similar in all cases, since they all

share many peculiar features. The length of the poly-Q stretch and the age of onset of the pathology are inversely related: the longer the repetition, the earlier the onset of the pathology. Nevertheless each disease shows a different threshold in the repeat length, as well as a different correlation between the length of the poly-Q and the severity of the syndrome, maybe due to the different physiological contest (Gusella J. F. *et al.*, 2000). In all cases the allele carrying the expanded triplets is dominant on the wild-type one even if the genesis of the pathology and its severity are more closely linked to the length of the poly-Q stretch than to the homozygosis for the mutation. Poly-Q diseases affect particular cell lines, despite their sharing a common pathological mechanism; this is probably due to the different physiological contest and to differences in the protein functions and cellular partners.

1.3 MODELS FOR POLY-Q DISEASES

The mechanism leading to the onset of poly-Q diseases has not yet been fully elucidated, in particular it has not been clearly established if the major role is played by the poly-Q itself or by the whole expanded protein.
Many experimental models have been set up in order to better understand the genetic causes of these pathologies: transgenic mice, cultured cells or other non complex organisms that over-produce the expanded protein and show a cellular degeneration similar to that found in affected patients (Gusella J. F. *et al.*, 2000).

For instance, in cultured cells an expanded poly-Q stretch always leads to the formation of aggregates even though this does not always cause cell death. Transgenic mice expressing HD exon 1 carrying 150 consecutive glutamines, showed neuropathology and diabetes; moreover, many nuclear inclusions (NI) have been found in their encephalic neurons, even though they did not show the massive striatal neuronal loss typical of HD (Gusella J. F. *et al.*, 2000); many observations suggested that the phenotypic manifestations of HD were linked to insoluble amyloid material aggregated in the nucleus. Mice models of SBMA, DRPLA, SCA1, SCA3 and HD, in which the whole protein was expressed, also presented NI in their neurons.

These results led to the “gain of function” hypothesis; according to this hypothesis the expanded protein gains a new toxic function that

leads to cell death. In 1994 Perutz proposed that expanded poly-Q stretches would organize into β-strand that can interact by hydrogen bonds forming the so called “polar zippers”, responsible for the formation of protein aggregates (Perutz M. F. *et al.*, 1994); however, it is still debated whether the expanded stretch is sufficient for the onset of the pathology. Recently it has been proposed that aggregation does not depend directly on poly-Q, but that the latter only destabilizes the structure of the protein, which goes through aggregation with itself and other cellular partners (Chai Y. *et al.*, 2001).

The localization of the proteins involved in poly-Q diseases seems to be an important factor for the pathogenesis; it has been demonstrated that the non pathological proteins are mainly cytosolic, while the expanded forms are usually found aggregated inside the nucleus (Zoghbi H. Y. *et al.*, 2000). Interestingly a study from Yang and colleagues, on isolated poly-Q fragments, suggests that the expanded protein exerts its new toxic function only when translocated inside the nucleus (Yang W. *et al.*, 2002). Another debated point is the importance of NI in the pathogenesis: it has been shown that mouse models of SCA1 presented neuronal loss even in the absence of inclusions (Klement I. A. *et al.*, 1998); moreover, Fujigasaki and colleagues have demonstrated that many other proteins, besides the expanded form, are sequestered in NI and this can be a very important step, leading to neuronal dysfunction and death (Fujigasaki H. *et al.*, 2001). Cellular partners sequestering suggests the idea that the proteins involved in these pathologies play a more important role in the pathogenesis than poly-Q alone. Expanded poly-Q stretches aggregate and have a cytotoxic effect, but cannot reproduce the pathological manifestation of the disease. Moreover many transcriptional factors are found to be sequestered in NI and a loss in transcriptional regulation can be important in the way to cell death. It has been demonstrated beyond any doubt that the formation of insoluble intranuclear amyloid aggregates is linked to the pathology.

Recently Chiti and colleagues have found that many proteins not linked to these pathologies, such as acilphosphatase, can form amyloid fibrils after destabilization of their secondary structure (Chiti F. *et al.*, 2000). These data support the increasingly more accepted idea that the poly-Q stretch is important for the onset of the pathology, but that its progression depends on the protein involved.

The poly-Q stretch is nowadays a topic of discussion: its possible function and structure are still unknown. Long repetitions of glutamines (Gln) are present in many transcriptional factors, like Drosophila homeoboxes. Here the loss of the poly-Q tract does not affect the protein binding to DNA, but alters its transcriptional activity (Perutz M. F. *et al.*, 1994). Studies on human transcriptional factor Sp1 showed that its zinc-fingers become active only when the repetition undergoes splicing (Perutz M. F. *et al*., 1994). Nevertheless, the poly-Q stretch is not always associated to a function. Murine ataxin-3 (AT-3) presents only 5-6 consecutive Gln while the human range varies between 12 and 84; this suggests that here the poly-Q stretch does not have a specific function.

Another question regards how the expanded poly-Q stretch can lead to the formation of insoluble, well structured aggregates.
Many *in vitro* experiments showed that expanded poly-Q stretch always aggregate, both in a protein context and as synthetic peptides: the longer the expansion, the faster the process. One of the most widely accepted model on the intrinsic aggregation properties of expanded poly-Q stretches, suggests that it can form a β-helix structure composed of at least two turns of 20 residues each (Perutz M. F. *et al*., 2002; Merlino A. *et al.*, 2006), a novel conformational motif rich in parallel β-sheets that has been found in many protein structures in the PDB (Zanuy D. *et al*., 2006). These helices seem to be stabilized by hydrogen bonds and can work as nucleation centres for the formation of bigger aggregates. This hypothesis is supported by Circular Dicroism (CD) data obtained on ataxin-3, the protein involved in the Machado Joseph Disease, showing that the pathological form undergoes an increase in β-sheet structure together with a decrease in α-helices. This suggests the importance of the expanded poly-Q stretch in destabilizing the native structure of the protein (Bevivino A. E. *et al*., 2001; Shehi E. *et al*., 2003).

1.4 NUCLEAR INCLUSIONS (NI) AND PATHOLOGICAL MECHANISMS

The typical midlife onset of the pathology suggests that the molecular mechanism of pathogenesis goes through the accumulation of a toxic intermediate that leads to the selective degeneration of a peculiar cell line (Paulson H. L., 1999). Moreover an expanded poly-Q stretch could facilitate the misfolding of the protein involved and of any other

protein whose structure can be perturbed by interactions with poly-Q expansion, leading to the accumulation of aggregates. In particular caspase cleavage could very likely promote misfolding and aggregation, through the release of the poly-Q stretch or an alteration of the intracellular trafficking of the polyglutaminated protein (Paulson H. L., 1999).

Many studies suggest the importance of nuclear translocation of the pathological proteins, to form aggregates: nuclear environment seems to promote aggregation more readily than cytoplasmic. This might be due to the fact that nucleus is less efficient in degrading, refolding or disaggregating misfolded proteins. Alternatively, the intricate structure of the nucleus might concentrate expanded proteins in subdomains that foster aggregation (Paulson H. L., 1999).

The formation of nuclear inclusions is a common feature of all poly-Q diseases and seems to be important in the development of the pathology, as supported by the discovery, in the NI, of many different cellular proteins apart, from the polyglutaminated proteins and their wild-type forms. The existence of glutamine-rich transcription factors suggests that expanded proteins might improperly bind such factors, thus altering the transcription of genes that are critical for neuronal functions; other nuclear functions could be disrupted in a similar manner (Paulson H. L., 1999). The hypothesis that the polyglutamine domain is an important component of the recruitment process was demonstrated by Evert and colleagues, by coexpressing a polyglutamine-containing green fluorescent protein (GFP) with a fragment of ataxin-3 containing an expanded poly-Q: recruitment of GFP into NIs was observed (Evert B. O. *et al.*, 2000), but it was also demonstrated that expression of expanded poly-Q stretches alone leads to aggregation and citotoxicity, although it does not fully reproduce pathologic manifestations.

Although NIs are a common feature of poly-Q neurodegenerative disease, every pathology displays a unique pattern of neuronal degeneration, even though the protein involved is ubiquitously expressed. This implies that the protein context plays an important role in establishing selective neurotoxicity. This idea is supported by a study on ataxin-3, conducted by Chai and colleagues who demonstrated that the protein sequence surrounding the poly-Q

specifies the constituents of nuclear inclusions (NIs) formed by the disease protein (Chai Y. *et al.*, 2001).

The fact that NIs are present in vulnerable neurons supports the notion that their presence is relevant to pathogenesis. However, many studies strongly suggest that aggregation is neither necessary nor sufficient for neuronal dysfunction. It may be that expanded proteins are most toxic when roaming freely, and that aggregates represent the cell's effort to minimize the toxicity of the strands (Zoghbi H. Y. *et al.*, 2000). Moreover, the fact that NIs also contain proteins normally associated with protein folding, such as ubiquitin, parts of the proteasome complex and many molecular chaperones, suggests that the proteins involved are not completely folded and that the formation of fibrils overwhelms the defensive mechanisms of the cell (Paulson H. L., 1999).

Nowadays it is widely accepted that the formation of large NIs is driven by the formation of the so called "protofibrils" or "nucleation centres" which are mainly composed of fragments of the pathological protein containing an expanded poly-Q stretch. NIs growing starts from these small aggregates, through the addition of the whole pathological protein and other proteins.
This mechanism supports both the loss of function and the gain of function hypothesis: the presence of an expanded poly-Q would confer the protein the ability to aggregate and form NIs, but the pathology could also be caused by the loss of the protein function or of peculiar proteins sequestered in the aggregates.

A cell cultured model of cells transiently transfected with truncated ataxin-3 constructs containing expanded repeats correlated with an increased susceptibility to apoptotic cell death (Ikeda H. *et al.*, 1996).
Evidence has accumulated that specific caspases are activated and recruited during poly-Q induced cell death. Sanchez and coworkers (Sanchez I. *et al.*, 1999) showed that transient expression of a truncated ataxin-3 with 79 glutamine residues fused to green fluorescent protein (GFP) in cultured striatal, cerebellar, and cortical neurons resulted in apoptotic cell death characterized by cell body shrinkage and chromosomal DNA condensation.
A commonly held view is that caspase cleavage may generate fragments of expanded proteins that might serve to initiate the formation of aggregates that could recruit other cellular proteins and

could be translocated into the nucleus. Moreover, the availability of different caspases in different neurons may further play an important role in the cell specificity of neuronal degeneration (Evert B. O. *et al.*, 2000).

1.5 ROLE OF PROTEOLYSIS

All the proteins involved in poly-Q diseases share ubiquitous expression, although each one affects a peculiar neuronal population. One hypothesis suggests that this characteristic distribution of the injury depends on different, newly gained or lost intracellular interactions. Another one states that the pathogenesis needs a proteolytic event leading to the formation of a toxic fragment containing the poly-Q stretch, intending that the distribution of the damage depends on the different proteases specific for the different proteins. (Tarlac V. *et al*., 2003).

Proteolysis takes place in neurodegeneration in different ways: it can be enhanced or reduced by the presence of the poly-Q stretch; the protein containing the expansion can became more or less susceptible to proteolytic cleavage. Evidence for proteolytic cleavages *in vivo* and *in vitro* have been found for HD, SBMA, DRPLA, SCA2, 3 and 7. In particular, in DPRLA an N-terminal fragment containing the poly-Q stretch is translocated to the nucleus increasing death in cultured cells (Nucifora F. C., *et al*., 2003). In HD it has been seen that the expansion of the poly-Q fragment seems to inhibit proteolysis (Trottier Y. *et al*., 1995).

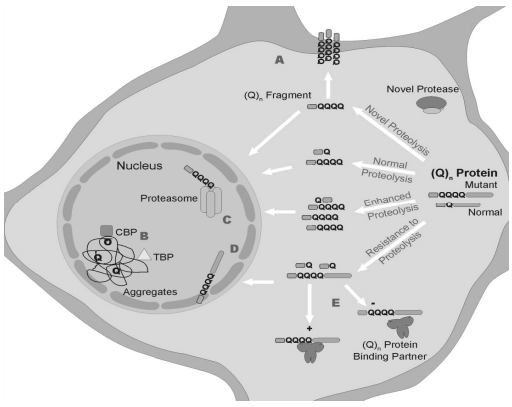

Figure 1.1 Possible outcomes of proteolysis of expanded (Q)n proteins (Tarlac V. *et al*., 2003). Whether proteolysis of expanded (Q)n proteins is unaffected,

enhanced, reduced, or the result of novel proteolysis, there are several possible toxic outcomes for the cell. Proteolysis of the expanded (Q)n protein resulting in production of an expanded (Q)n toxic fragment may cause several deleterious effects to the cell. First, the expanded (Q)n toxic fragment may form cationic channels in membranes (A). The expanded (Q)n fragment may enter the nucleus where it can form macroaggregates that can recruit other (Q)n containing proteins such as TBP, chaperones, and components of the proteasome (B). Another possibility is that the initial expanded (Q)n cleavage fragment could be resistant to further proteolysis by the proteasome (C). If the expanded (Q)n protein is resistant to proteolysis, toxicity could be caused by disruption of the nuclear matrix by the full-length protein (D), or by an alteration of normal protein partner interaction (E).

1.6 ROLE OF MITOCHONDRIA IN NEURODEGENERATIVE DISEASES

Recently, mitochondrial dysfunction has emerged as an increasingly convincing 'lowest common denominator' linking many neurodegenerative disorders like Huntington's disease, Parkinson's disease, Alzheimer's disease and Friedreich ataxia (Kwong, J.Q. *et al.*, 2006).

Mitochondria are the driving force behind life, as mitochondrial oxidative phosphorylation provides the main source of energy in the cell. In addition to energy production, mitochondria play a crucial role in mediating amino acid biosynthesis, fatty acid oxidation, steroid metabolism, intermediate metabolic pathways, calcium homeostasis, and free radical scavenging. The mitochondrion is especially complex as it is the only cellular organelle under the dual control of both the nuclear and its own (mitochondrial) genomes. The majority of mitochondrial proteins are encoded for by the nuclear DNA, synthesized in the cytosol, imported into the organelle and targeted to one of the four sub mitochondrial compartments: the outer mitochondrial membrane, the intermembrane space, the inner mitochondrial membrane and the matrix. The intermembrane space sequesters many pro-apoptotic factors such as cytochrome c, Smac/DIABLO, and endonuclease G. A multiplicity of mitochondrial insults can cause the release of cytochrome c into the cytosol, which can then bind to Apaf1 and pro-caspase 9 to form the apoptosome and initiate a downstream caspase cascade, leading to cell death.
Because mitochondria are positioned at the gateway to apoptosis and combined with the fact that neurons are highly energy dependent, mitochondrial dysfunction is a prime suspect for both the initiation and the execution of neuronal death.

Parkinson's disease

Parkinson's disease is a common neurodegenerative movement disorder clinically characterized by resting tremor, rigidity, bradykinesia, and postural instability.

Mutations in α-synuclein have been found to be linked to an autosomal dominant form of Parkinson's disease. α-synuclein is localized at synaptic terminals and in the cytosol, where it may be involved in modulating the release of dopamine from synaptic vesicles. Despite the lack of a direct connection to mitochondria, there is evidence that mutant α-synuclein may cause mitochondrial dysfunction, in fact it has been found that overexpression of mutant α-synuclein in cultured cells impairs mitochondrial function and leads to oxidative damage.

Mutations in parkin have been found to cause autosomal recessive juvenile Parkinson's disease. Parkin encodes for an ubiquitin E3 ligase, which is a component of the ubiquitin-proteasome system involved in cellular protein degradation. Parkin has been found to be associated with the outer mitochondrial membrane, where it protects against mitochondrial swelling and the release of cytochrome c induced by treatment with ceramide, suggesting that it might be involved in degrading mitochondrial proteins. It has also recently been found that parkin is localized within mitochondria in proliferating cells but exhibits cytosolic localization in differentiated cells. Furthermore, parkin interacts with the mitochondrial transcription factor A and enhances mtDNA transcription and replication. These results suggest that parkin may directly modulate mitochondrial function by mechanisms independent of the ubiquitin-proteasome pathway.

Friedreich ataxia

Friedreich ataxia, the most common form of inherited ataxia, is an autosomal recessive degenerative disorder characterized by progressive gait and limb ataxia, axonal sensory neuropathy, loss of deep tendon reflexes, spasticity, and extensor plantar responses. The genetic basis for Friedreich ataxia is an abnormal GAA trinucleotide repeat expansion in the first intron of the Friedreich ataxia gene.

This trinucleotide repeat can adopt a triple helical structure to inhibit Friedreich ataxia transcription, leading to a reduced expression of the protein frataxin. Frataxin is a highly conserved, mitochondrial protein involved in heme biosynthesis, the formation of ironsulfur clusters, and the detoxification of iron. Studies in yeast and mice show that

frataxin defects lead to accumulation of iron in mitochondria and decrease in iron-sulfur cluster-containing enzymes such as aconitase, and complexes I–III of the electron transport chain. While the mechanisms of Friedreich ataxia pathogenesis are still unclear, one possibility is oxidative stress, in fact accumulation of mitochondrial iron may lead to oxidative damage through the production of free radicals. Studies have shown that loss of frataxin leads to increased sensitivity to oxidative stress.

Huntington's disease

Huntington's disease is an autosomal dominant neurodegenerative disorder characterized by cognitive impairment, emotional disturbances and choreoathetotic movements.

Mitochondrial dysfunction in the pathogenesis of Huntington's disease has been demonstrated in patients, mutant htt transgenic mice, and cell culture models. Mitochondria from Huntington's disease brain or lymphoblasts exhibit a polyglutamine length dependent decrease in mitochondrial membrane potential and depolarize at lower calcium concentrations, indicating impaired calcium homeostasis. In fact htt has also been shown to bind to neuronal mitochondrial membranes as shown by electron microscopy, and it is found predominantly in the outer mitochondrial membrane in cells overexpressing the mutant protein. Furthermore, by interacting with mitochondria, mutant htt induces calcium dependent membrane permeability transition pore opening and reduces the calcium load needed to induce the opening.

These studies suggest an involvement of mitochondrial damage also in other neurodegenerative disease, as spinocerebellar ataxia type 3.

1.7 NITROSATIVE STRESS AND NEURODEGENERATIVE DISEASES

Overproduction of reactive nitrogen species (RNS) and reactive oxygen species (ROS), which lead to neuronal cell injury and death, is a potential mediator of neurodegenerative disorders including: Parkinson's disease (PD), Alzheimer's disease (AD), amyotrophic lateral sclerosis (ALS) and polyglutamine (poly-Q) diseases such as Huntington's disease (Nakamura T. and Lipton S.A., 2007).

Accumulation of nitrosative stress due to excessive generation of nitric oxide (NO) appears to be a potential factor contributing to neuronal cell damage and death. A well-established model for NO production entails a central role of the N-methy-D-aspartate (NMDA)-type glutamate receptors in nervous system. Excessive activation of NMDA receptors drives Ca^{2+} influx, which in turn activates neuronal NO synthase (nNOS) as well as the generation of ROS. Importantly, normal mitochondrial respiration also generates free radicals, principally ROS, and one such molecule, superoxide anion ($O2^{-}$) reacts rapidly with free radical $NO^{\bullet}$ to form the very toxic product peroxynitrite ($ONOO^{-}$) (Nakamura T. and Lipton S.A., 2007).
An additional feature of most neurodegenerative diseases is accumulation of misfolded and/or aggregated proteins. These protein aggregates can be cytosolic, nuclear, or extracellular. Importantly, protein aggregation can result from either a mutation in the disease-related gene encoding the protein, or post-translational changes to the protein engendered by nitrosative/oxidative stress (Nakamura T. and Lipton S.A., 2007).

Glutamate is the major excitatory neurotransmitter in the brain and is important for normal functioning of the nervous system; however, excessive activation of glutamate receptors is implicated in neuronal damage in many neurological disorders. This form of toxicity is mediated at least in part by excessive activation of NMDA-type receptors, resulting in excessive Ca^{2+} influx through a receptor's associated ion channel. Excessive Ca^{2+} leads to the production of damaging free radicals (NO and ROS) and other enzymatic processes, contributing to cell death. Intracellular Ca^{2+} triggers the generation of NO by activating nNOS in a Ca^{2+}/calmodulin (CaM)-dependent manner. NO is a gaseous free radical (thus highly diffusible) and a key molecule that plays a vital role in normal signal transduction but in excess can lead to neuronal cell damage and death. Three subtypes of NOS have been identified; two constitutive forms of NOS – nNOS and endothelial NOS (eNOS) – take their names from the cell type in which they were first found. The name of the third subtype – inducible NOS (iNOS) – indicates that expression of the enzyme is induced by acute inflammatory stimuli. All three isoforms are widely distributed in the brain (Nakamura T. and Lipton S.A., 2007).

Recently, a novel cellular mechanism for Ca^{2+}-dependent release of NO was discovered in dorsal root ganglion neurons and pancreatic

acinar cells. This Ca^{2+}-dependent NO release occurs not as a result of *de novo* synthesis by NO but instead via liberation of NO from an S-nitrosothiol (SNO) pool, whereby NO is reversibly bound to specific cysteine residues (Nakamura T. and Lipton S.A., 2007).

Recent studies further pointed out the potential connection between ROS/RNS and mitochondrial dysfunction in neurodegenerative diseases, especially in PD. Administration to animal models of complex I inhibitors, which result in overproduction of ROS/RNS, reproduces many of the features of sporadic PD. In addition, it has recently been proposed that mitochondrial cytochrome oxidase can produce NO in a nitrite (NO_2^-)- and pH-dependent but non-Ca^{2+}-dependent manner (Nakamura T. and Lipton S.A., 2007).

In general, NO exerts physiological and some pathophysiological effects via stimulation of guanylate cyclase to form cyclic guanosine-3',5'-monophosphate (cGMP) or through S-nitros(yl)ation of regulatory protein thiol groups. S-nitrosylation is the covalent addition of an NO group to a critical cysteine thiol/sulfhydryl (RSH or, more properly, thiolate anion, RS^-) to forman S-nitrosothiol derivative (R-SNO). Such modification modulates the function of a broad spectrum of mammalian, plant, and microbial proteins. In general, a consensus motif of amino acids comprised of nucleophilic residues (generally an acid and a base) surrounds a critical cysteine, which increases the cysteine sulfhydryl's susceptibility to S-nitrosylation (Nakamura T. and Lipton S.A., 2007).

NO is neuroprotective via S-nitrosylation of NMDA receptors (as well as other subsequently discovered targets, including caspases), and yet can also be neurodestructive by formation of peroxynitrite. Over the past decade, accumulating evidence has suggested that S-nitrosylation can regulate the biological activity of a great variety of proteins, in some ways akin to phosphorylation (Nakamura T. and Lipton S.A., 2007).

Analyses of mice deficient in either nNOS or iNOS confirmed that NO is an important mediator of cell injury and death after excitotoxic stimulation; NO generated from nNOS or iNOS is detrimental to neuronal survival. In addition, inhibition of NOS activity ameliorates the progression of disease pathology in animal models of PD, AD, and ALS, suggesting that excess generation of NO plays a pivotal role in

the pathogenesis of several neurodegenerative diseases. In fact S-nitrosylation modulates the ubiquitin E3 ligase activity of parkin, and chaperone and isomerase activities of PDI, contributing to protein misfolding and neurotoxicity in models of neurodegenerative disorders (Nakamura T. and Lipton S.A., 2007). Additionally, Cohen et al. (Cohen E. *et al*., 2006) recently demonstrated that insulin/insulin-like growth factor-I (IGFI) signaling, which influences longevity and lifespan in many species in part via down-regulation of ROS/RNS generation, can affect aggregation of toxic proteins such as Aβ.

Parkinson's disease

Nitrosative and oxidative stress are potential causal factors for protein accumulation in the much more common sporadic form of PD. Nitrosative/oxidative stress, commonly found during normal aging, can mimic rare genetic causes of disorders, such as PD, by promoting protein misfolding in the absence of a genetic mutation. For example, S-nitrosylation and further oxidation of parkin or Uch-L1 result in dysfunction of these enzymes and thus of the UPS (ubiquitin-proteasome system). SNO-parkin initially stimulates ubiquitin E3 ligase activity, resulting in enhanced ubiquitination as observed in Lewy bodies, followed by a decrease in enzyme activity, producing a futile cycle of dysfunctional UPS. Moreover, S-nitrosylation appears to compromise the neuroprotective effect of parkin. These mechanisms involve S-nitrosylation of critical cysteine residues in the first RING domain of parkin (Nakamura T. and Lipton S.A., 2007).

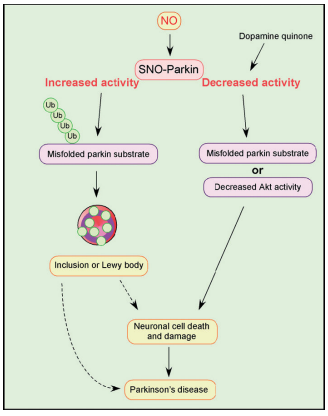

Figure 1.2 Possible mechanism of S-nitrosylated parkin (SNO-Parkin) contributing to the accumulation of aberrant proteins and damage or death of

dopaminergic neurons (Nakamura T. and Lipton S.A., 2007). Nitrosative stress leads to S-nitrosylation of parkin, and, initially, to a dramatic increase followed by a decrease in its E3 ubiquitin ligase activity. The initial increase in this E3 ubiquitin ligase activity leads to enhanced ubiquitination of parkin substrates (e.g., synphilin-1, Pael-R, and parkin itself). Increased parkin E3 ubiquitin ligase activity may contribute to Lewy body formation and impair parkin function, as also suggested by Sriram et al. (Sriram S.R. *et al*., 2005). The subsequent decrease in parkin activity may allow misfolded proteins to accumulate. Down-regulation of parkin may also result in decreased Akt neuroprotective activity because of enhanced epidermal growth factor receptor (EGFR) internalization. Dopamine quinone can also modify cysteine thiols of parkin and reduce its activity.

Alzheimer's disease

Several mechanisms have been proposed to underlie AD pathogenesis; however, there is accumulating evidence that oxidative stress plays an important role in this disease pathophysiology. Either the oxidants or the products of oxidative stress could modify the proteins or activate other pathways that may lead to additional impairment of cellular functions and neuronal loss (Sultana R. *et al*., 2005).

Oxidative stress could stimulate the additional damage via the overexpression of inducible and neuronal specific nitric oxide synthase (NOS: iNOS and nNOS, respectively). Previous studies suggested that an increase production of peroxynitrite, a product of reaction of nitric oxide (NO) with superoxide, could cause nitration of proteins that may lead to irreversible damage to the proteins.

Recently, several studies suggested that protein nitration could be a cellular signaling mechanism, as is often a reversible and selective process, similar to protein phosphorylation. In addition, proteins that are nitrated are more prone to proteosomal degradation than their counterparts. Ubiquitin carboxyl-terminal hydrolase L-1 (UCH L-1), one of the components of the proteosomal pathway, was found to be oxidized in the IPL and hippocampus of AD, a finding that could be one of the reasons for the observed increase in nitrated proteins in this disorder (Sultana R. *et al*., 2005).

1.8 SPINOCEREBELLAR ATAXIA TYPE 3

Spinocerebellar ataxia type 3 (SCA3) or Machado-Joseph disease is the most common dominantly inherited ataxia. The protein involved, called ataxin-3 (AT-3), is coded by the MJD1 gene which presents a CAG repetition next to its 3' which is highly polymorphic. This repetition becomes pathologic when it exceeds 50 consecutive triplets. The neurological phenotype includes cerebellar ataxia, spasticity,

ophthalmoplegia and dysarthria. Pathologically, SCA3 is characterized by selective neuronal degeneration within the basal ganglia, brainstem, cerebellum and spinal cord (Takiyama Y. *et al*., 1994).

The gene coding for SCA3 is located on the long arm of chromosome 14 (14q32.1) and encodes for a cDNA of about 1800 basepairs (Kawaguchi Y. et al., 1994). AT-3, whose aminoacidic sequence is reported in figure 1.3, is a protein with a predicted molecular weight of 42 kDa in its unexpanded form. It has been found that it presents many homologous in many different organisms. The gene encoding murine AT-3 shows about 88% sequence identity with the human one, the main differences being found in the C-terminus, downstream from the poly-Q; another difference concerns the poly-Q stretch, which consists of only 6 consecutive glutamines in the murine form (Schmitt I. *et al.*, 1997).

Ataxin-3 is a cytoplasmic protein ubiquitously expressed throughout the body. In affected individuals expanded ataxin-3 is predominantly found in NIs in neurons of the ventral pons, whereas it is normally cytoplasmic (Paulson H. L. *et al*., 1997a; Paulson H. L. *et al*., 1997b; Trottier Y. *et al.*, 1998; Schmidt T. *et al.*, 1998).

MESIFHEKQEGSLCAQHCLNNLLQGEYFSPVELSSIAHQLDEEERMR
MAEGGVTSEDYRTFLQQPSGNMDDSGFFSIQVISNALKVWGLELILF
NSPEYQRLRIDPINERSFICNYKEHWFTVRKLGKQWFNLNSLLTGPE
LISDTYLALFLAQLQQEGYSIFVVKGDLPDCEADQLLQMIRVQQMHR
PKLIGEELAQLKEQRVHKTDLERVLEANDGSGMLDEDEEDLQRALAL
SRQEIDMEDEEADLRRAIQLSMQGSSRNISQDMTQTSGTNLTSEELR
KRREAYFEKQQQKQQQQQQQQQQQQQQQQQQQQQQQRDLSGQSS
HPCERPATSSGALGSDLGKACSPFIMFATFTLYLT

Figure 1.3 Aminoacidic sequence of human ataxin-3.

It has been demonstrated that the pathological form of AT-3 aggregates in physiological conditions while the normal one remains soluble (Bevivino A. E. *et al*., 2001). The length of the poly-Q also affects secondary structure thermostability: a moderately expanded variant containing 36 consecutive Gln undergoes the formation of insoluble amyloid aggregates at 85°C, while human AT-3 with 26 Gln

and the murine form with 6 Gln remain soluble even at higher temperature (Shehi E. *et al*., 2003). Similarly a non pathological form containing 28 consecutive glutamines undergoes amyloid aggregation in chemical denaturing conditions (Chow M. K. *et al.*, 2004). These and other experiments suggest that the expansion of the poly-Q stretch leads to the instability of the structure of the protein with the formation of an instable intermediate prone to aggregation.

Analysis of the aminoacidic sequence of the protein showed the presence of different domains and functional motifs. The N-terminus domain of the protein, (stretching from aminoacid 1 to 180) is a globular domain known as Josephin domain, while the C-terminus is mainly unstructured and contains the poly-Q stretch, together with two or three ubiquitin interacting motives (UIMs), depending on the splicing. UIMs are peculiar sequences that can recognize and interact with ubiquitin; they are found in proteins involved in ubiquitination and successive degradation of misfolded proteins or involved in the metabolism of ubiquitin.

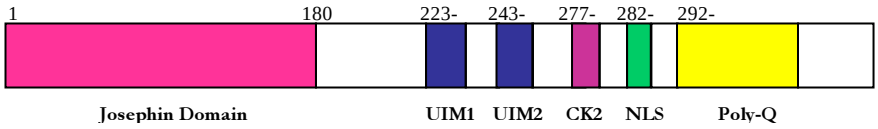

Figure 1.4 The domains of ataxin-3.

Recently the structure of the Josephin domain has been resolved by NMR (Nicastro G. *et al.*, 2005). Results show that it consists of a globular domain divided in two subdomains, one rich in α-helices, the other rich in β-strand forming an antiparallel β-sheet (Fig. 1.5). The C-terminal domain seems to be less structured with the poly-Q tract exposed to the solvent (Masino L. *et al*., 2003).

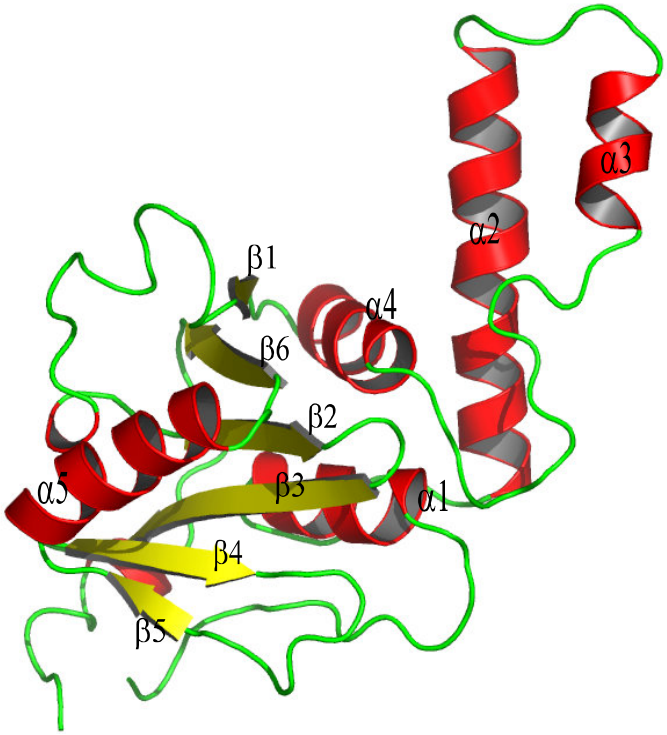

Figure 1.5 Josephin domain tridimensional structure. Representation of the Josephin domain (PDB ID code: 1yzb) with the software pyMOL. Loops are evidenced in green, β-sheets in yellow and α-helices in red.

1.9 ATAXIN-3 INTRACELLULAR LOCALIZATION

It is now known that ataxin-3 has a heterogeneous distribution both in the whole organism and in the cellular environment. In transfected HeLa cells, for example, Trottier and colleagues showed that the protein is mainly cytosolic, but is found also in the nucleus and in mitochondria (Trottier Y. *et al.*, 1998).

The pathological form of AT-3 was found to be localized mainly in the nucleus of different neuronal cell types; moreover it was found that these cells present ubiquitinilated nuclear inclusions (Paulson H. L. *et al.*, 1997a). These inclusions, called Marinesco bodies, also contains AT-3 in its normal form indicating that even in the absence of a poly-Q stretch the protein is able to enter the nucleus and form aggregates (Fujigasaki H. *et al.*, 2001). These inclusions, that contain ubiquitin, can represent the cellular response to a stress condition or to protein misfolding, aberrant aggregation or degradation. It is

interesting that AT-3 is the only protein causing a neuropathology that is recruited in Marinesco Bodies.

Nuclear localization seems to be crucial for pathogenesis. This has been clearly demonstrated on a mouse model of ataxin 1 in which the pathological protein was modified so that it could not enter the nucleus: these mice did not develop the pathology. Ataxin-3 has been demonstrated to be constitutively translocated to the nucleus and the normal form was shown to interact with the nuclear matrix (Tait D. *et al.*, 1998) and become reactive to antibody 1C2 that usually recognizes expanded poly-Q stretches; this suggests a conformational change of the protein (Perez M. K. *et al.*, 1999). PSORT database searches found a putative NLS and two phosphorylation sites for Caseine Kinase 2 (CK2) just upstream of the poly-Q stretch. A hypothesis suggests that NLS facilitates nuclear translocation of the protein, while the two phosphorylation sites would modulate the transport rate. Although it can be considered a fundamental step in the pathogenesis, since inclusions are found only in the nucleus, nuclear localization of AT-3 has still not been demonstrated to require NLS. It has been demonstrated that the concentration of the pathological protein or of its toxic fragment is important for the formation of the aggregates involved in cytotoxicity; in this way nuclear localization can be important because of the compartmentalization of the protein, which can favour aberrant interactions with other proteins found in aggregates (Cemal C. K. *et al.*, 2002).

Pozzi and coworkers investigated subcellular localization and proteolytic cleavage of different forms of ataxin-3 (AT-3). Normal (AT-3Q6 and AT-3Q26) and pathological (AT-3Q72) ataxins-3, as well as two truncated forms lacking poly-Q, were studied. Full-length proteins were also expressed as C14A mutants, in order to assess whether AT-3 autoproteolytic activity was involved in its fragmentation. Both normal and pathological proteins were found to localize in the cytoplasm and in the nucleus, as expected, but also in the mitochondria. Microsequencing showed that all ataxins-3 underwent the same proteolytic cleavage, removing the first 27 aminoacids. Interestingly, while normal ataxins were further cleaved at a number of caspase sites, pathological AT-3 was proteolyzed to a much lesser extent. This may play a role in the pathogenesis, hampering degradation of aggregation-prone expanded AT-3. In

addition, autolytic cleavage was apparently not involved in AT-3 proteolysis (Pozzi C. *et al.*, 2008).

Heat shock, a general proteotoxic stress, also induces wild-type and pathogenic AT-3 to accumulate in the nucleus where AT-3 has a protective function in the cellular response to heat shock, in particular serine-111 of AT-3 is required for nuclear localization in these conditions. Reina and colleagues found that oxidative stress also induced nuclear localization of AT-3 (Reina C. P. *et al.*, 2010). In fact Macedo-Ribeiro and coworkers demonstrated that AT-3 is actively imported to and exported from the cell nucleus, and that its nuclear export activity is dependent on a motif located at its N-terminal region (Macedo-Ribeiro S. *et al.*, 2009).

1.10 ATAXIN-3 FUNCTIONS

A bioinformatic analysis (Scheel H. *et al.*, 2003) revealed that ataxin-3 possess the typical catalytic triad of cystein proteases, identified in aminoacids Cys 14 (which is supposed to be the key catalytic residue), His 119 and Asn 134. Moreover it has been shown that the folding of both the Josephin domain and the catalytic site are similar to that of different cystein proteases (Nicastro G. *et al.*, 2005) even though, unlike all other cystein protease families, the Josephin domain is always in its active form with the catalytic site exposed. In particular the Josephin domain structure is highly similar to that of *ubiquitin C-terminal hydrolase* (Mao Y. *et al.*, 2005), supporting the accepted hypothesis that AT-3 is a deubiquitylating enzyme, possibly involved in the proteasome pathway. *In vitro* analysis confirmed that AT-3 can cut polyubiquitin chains (Burnett B. *et al.*, 2003); moreover, in cultured cells the expression of a C14A mutated form of the protein with the catalytic cysteine substituted with an alanine, leads to the accumulation of polyubiquitylated proteins; the same result is obtained through pharmacological inhibition of the proteasome (Berke S. J. *et al.*, 2005).

AT-3 can bind ubiquitylated substrates thanks to its two or three ubiquitin interacting motives (UIMs), depending on the splicing to which the mRNA has been subjected. Expanded AT-3 can bind ubiquitylated proteins (Berke S. J. *et al.*, 2005), although it is supposed to assume an altered conformation (Albrecht M. *et al.*,

2003); however, the authors do not rule out the possibility that the two forms can bind different proteins.
All these studies suggest that AT-3 is a deubiquitylating enzyme that binds polyubiquitylated proteins through its UIMs and deubiquitylates the substrates through its N-terminal active domain.

A very recent study reports that AT-3 binds VCP/p97, a key protein essential for the extraction of substrates from the endoplasmic reticulum (ER) to the cytosol in ER-associated degradation (ERAD), a quality control system in the secretory pathway responsible for degrading misfolded proteins (Zhong X. *et al.*, 2006). Recent studies revealed that VCP may be involved in the pathogenesis of protein misfolding diseases (Boeddrich A. *et al*, 2006). It colocalizes with abnormal inclusion bodies containing insoluble protein aggregates, which are characteristic features of many neurodegenerative diseases, including Alzheimer's, Parkinson's, and Huntington's disease.
Zhong and coworkers describe the interaction between AT-3 and VCP which seems to decrease binding of the latter with its normal partner Ufd1 and with polyubiquitin chains resulting in a decreased degradation of ERAD substrates. The authors suggest that AT-3 would regulate flow through the ERAD pathway by adjusting the rate of extraction of ERAD substrates and that this regulation is dependent on the poly-Q tract, so that a pathologic AT-3 would aberrantly interact with VCP leading to a deregulation of ERAD (Zhong X. *et al.*, 2006).

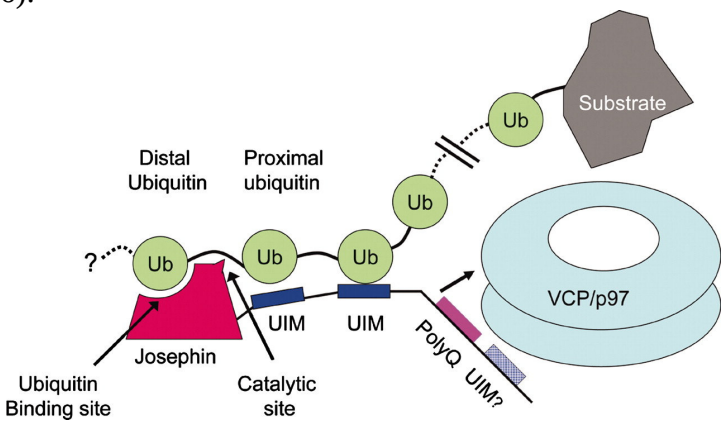

Figure 1.6 Putative model of ataxin-3 function (Mao Y. *et al.*, 2005). Several functional groups are arranged in a linear fashion in ataxin-3. The Ub-binding site in the JD is followed in order by the catalytic site, the tandem UIMs, the poly-Q stretch, and the variable C terminus that may contain a putative UIM. The tandem UIMs may recruit a polyubiquitinated substrate and present it to the JD. The JD

holds a distal Ub in a tetrahedral intermediate state before releasing it after catalytic cleavage. The model implies that optimal substrates of ataxin-3 should have a minimum polyubiquitin chain length to allow engagement of both the second UIMs and the JD in Ub binding.

VCP/p97 is characterized by an N-terminal domain followed by two highly conserved AAA domains (D1 and D2) that are important for ATP binding and hydrolysis. The N-terminal domain (aa 1-199) is essential for the interaction with ataxin-3 (Wang Q. *et al*., 2003). Ataxin-3 interacts with VCP/p97 in a region (aa 257-291) localized between the second ubiquitin interacting motif (UIM) and the poly-Q. VCP/p97 does not bind the poly-Q of proteins but to an arginin/lysine rich motif (^{282}RKRR) called VBM (VPC binding motif), in the ataxin-3 aminoacid sequence this motif overlaps the nuclear localization sequence (Boeddrich A. *et al,* 2006).
Previous studies have demonstrated that VCP hexamers have different conformations in the ATP-free and ATP-bound states (DeLaBarre and Brunger, 2005). Full-length ataxin-3 interacts with VCP in the absence as well as in the presence of ATP or its nonhydrolyzable analog, ATP-γS. In striking contrast, no interaction was detected in the presence of ADP, suggesting that VCP might adopt an alternative conformation that is unable to bind ataxin-3. Interestingly, the inhibitory effect of ADP was lost when N-terminally truncated ataxin-3 fragments lacking the conserved Josephine domain were used for binding experiments. As ataxin-3 is composed of a folded N-domain and most likely has an unstructured poly-Q tail (Masino et al, 2003), probably the N-terminally truncated ataxin-3 fragments are more flexible than the full-length protein and are therefore able to associate with the VCP-binding site in the ADP state. However *in vivo* full-length ataxin-3 binds to VCP in the ATP state, and is released after ATP hydrolysis in the ADP state. N-terminally truncated ataxin-3 fragments with expanded poly-Q sequences, which are generated under disease conditions (Goti et al, 2004), might lose their ability to dissociate from VCP in the ADP state. Thus, altered binding of truncated ataxin-3 proteins to VCP in neurons could contribute critically to neuronal dysfunction in SCA3 (Boeddrich A. *et al,* 2006).
VCP modulates ataxin-3 aggregation in a concentration-dependent manner. Low or intermediate concentrations of VCP significantly stimulated ataxin-3 aggregation, while a fourfold molar excess of the chaperone completely prevented fibrillogenesis. Currently, the molecular mechanism of this effect is unclear. Probably at low or

equimolar VCP concentrations the hexamers provide an optimal catalytic surface for the efficient conversion of bound ataxin-3 molecules into fibrillar structures. At higher VCP concentrations (four hexamers with one ataxin-3 molecule), however, the access to the aggregation-prone ataxin-3 molecules exposed by the hexamers might be masked, because the chaperone molecules themselves start to form oligomeric structures (Boeddrich A. *et al*, 2006).
Studies suggest that increasing the levels of VCP in SCA3 patients might have beneficial effects on disease pathogenesis. In fact VCP overexpression, similar to Hsp40/70, can protect neurons because it may reduce the amount of toxic protein aggregates (most likely oligomers or protofibrils) or mask the surface of toxic soluble ataxin-3 molecules. However, *in vivo*, higher concentrations of VCP might also stimulate the selective degradation of misfolded ataxin-3 molecules by the ubiquitin–proteasome system (Boeddrich A. *et al*, 2006).

AT-3 UIMs mediate binding of the protein to ubiquitylated substrates, but also AT-3 self-ubiquitylation. In particular it seems that AT-3 would undergo polyubiquitylation and can become a target of its own deubiquitylation activity (Berke S. J. *et al.*, 2005). The authors suggest that this control of the trans ubiquitynilation could regulate AT-3 intracellular localization and its activity as ubiquitylation can be a regulatory modification.
Different data suggest that AT-3 can also regulate the activity of different transcriptional factors, through the control of their oligo-ubiquitylation; transcriptional deregulation is one of the most plausible pathological mechanisms of poly-Q diseases. Li and colleagues showed that AT-3 interacts with two histone acetyl transferase: the cAMP response element binding protein (CBP) and p300, and with other factors associated to these two proteins (Li F. *et al.*, 2002). Cultured cells analysis showed that the Josephin domain is able to bind chromatine and can inhibit histone acetylation; moreover both normal and pathological AT-3 can repress transcription mediated by CBP and p300 when overexpressed.
Chou and colleagues demonstrated that polyglutammine-expanded ataxin-3-Q79 causes cerebellar transcriptional downregulation of SCA3 transgenic mice by inducing histone hypoacetylation and that HDAC inhibitor sodium butyrate alleviates cerebellar malfunction and ataxic symptoms (Chou A. H. *et al.*, 2010)
Through a yeast two hybrid system study Wang and colleagues demonstrated that both normal and mutant form of AT-3 interact with

RAD23, a yeast ortholog of the human proteins HHR23B and HHR23A, which are involved in DNA reparation (Wang G. *et al.*, 2000). The elucidation of the structure of the Josephin domain allowed demonstrating the binding between the N-terminal domain of AT-3 and the ubiquitin-like (Ubl) domain of HHR23B.

Mazzucchelli and coworkers found that different ataxin-3 constructs bind alpha- and beta-tubulin from soluble rat brain extracts; this suggests an involvement of ataxin-3 in directing aggregated protein to aggresomes, and shed light on the mode of interaction among the different molecular partners participating in the process (Mazzucchelli S. *et al.*, 2009). In addition, siAT-3-silenced cells exhibit marked morphological changes such as rounder shape and loss of adhesion protrusions. At a structural level, the microtubule, microfilament and intermediate filament networks are severely compromised and disorganized. This cytoskeletal phenotype is reversible and dependent on AT-3 levels (Rodrigues A. J. *et al.*, 2010)

1.11 SCA3 PATHOGENIC MECHANISMS

It is known that the formation of nuclear inclusions (NI) is a common feature of all poly-Q pathologies; NI seem to be important in the pathogenesis even though their effective role is still debated: they could represent the core cause for the genesis of the pathology or a defensive cellular mechanism against the pathologic protein. NI in SCA3 are mainly constituted of the expanded and normal forms of AT-3, AT-3 C-terminal fragments and others components such as ubiquitin, molecular chaperons and proteasome components.
Many works suggest the involvement of a 28kDa C-terminal fragment in SCA3 pathogenesis. This hypothesis is supported by the presence of nine caspases cleavage sites on AT-3 sequence and by the fact that AT-3 undergoes proteolysis during apoptotic process (Berke S. J. *et al.*, 2004). Moreover Paulson and colleagues suggested that a C-terminal fragment of the protein containing the poly-Q stretch promotes intracellular and perinuclear aggregation recruiting the full-length protein (Paulson H. L. *et al.*, 1997b). In cultured neuroblastoid cells it has been seen that a construct coding for the C-terminus of the protein containing an expanded poly-Q tract leads to the formation of aggregates and to cells death (Yoshizawa T. *et al.*, 2000). Transgenic mice expressing pathologic AT-3 in the brain and in the spinal

marrow develop symptoms similar to SCA3 patients and poly-Q containing fragments are found in crude brain extracts (Goti D. *et al.*, 2004).

On the other hand, Chai Y. et colleagues (Chai Y. *et al.*, 2001) discovered that many proteins found in nuclear aggregates had been recruited thanks to protein-protein interactions, thus implying that the whole protein and not only a fragment, is required for aggregation. This hypothesis was confirmed by the lack of AT-3 fragments in cell lines transiently transfected with the full-length pathologic protein that led to cytotoxicity and aggregates formations (Yoshizawa T. *et al.*, 2001). The same result was obtained in transgenic mice where AT-3 was expressed under control of its own regulatory elements: mice developed SCA3-like symptoms with the formation of intranuclear aggregates in cerebellum cells but without the formation of any proteolytic fragment (Cemal C. K. *et al.*, 2002). Moreover a clear difference has been demonstrated in the composition of NI caused by the full-length pathological protein and that deprived of the N-terminal domain (Chai Y. *et al.*, 2001).
Another debated topic is the apoptotic or non-apoptotic nature of cell death after the onset of the disease. Wullner et al. (Wullner U. *et al.*, 1999) observed a necrotic death following the formation of intranuclear inclusions in stable transfected cells, whereas another study found a big misregulation in the expression of pro and anti-apoptotic proteins after overexpression of a pathological variant of AT-3 (Tsai H. F. *et al.*, 2004). Tsai and colleagues found that full-length expanded ataxin-3 significantly impaired the expression of Bcl-2 protein. This may be responsible for the weak tolerance to polyglutamine toxicity at an early stage of disease and ultimately resulted in an increase of stress-induced cell death upon apoptotic stress, apoptosis being considered the main cause of neuronal cell death in SCA3 patients.

Furthermore the proteasome can participate in the pathologic mechanism as it recognizes and proteolyses misfolded proteins and since it has been seen that its inhibition increase aggregate formation in cultured cells transfected with mutated AT-3 (Chai Y. *et al.*, 2004). Actually aggregation seems to be depended on protein concentration (Scherzinger E. *et al.*, 1997) and it may be supposed that an expanded poly-Q tract can assume a β strand stable conformation (Perutz M. F. *et al.*, 2002) which can interfere with proteasome mediated

degradation (Chai Y. *et al.*, 1999), thus leading to an increase in the aberrant protein concentration.
Other data show that AT-3 associate with the nuclear matrix after nuclear translocation (Tait D. *et al.*, 1998) undergoing a conformational change that cause the poly-Q tract to be exposed, even when not expanded (Perez M. K. *et al.*, 1999), a modification that could lead to aberrant new interactions both with the nuclear matrix and with other nuclear proteins in the case of an expanded poly-Q.

Moreover it was shown that a cycle arrest in G0/G1 enhances the C−terminal fragment toxicity (Yoshizawa T. *et al.*, 2001).

Several lines of evidence demonstrate that poly-Q also accumulates in mitochondria and causes mitochondrial dysfunction. Sugiura and coworkers demonstrated that MITOL, a novel mitochondrial ubiquitin ligase localized in the mitochondrial outer membrane, promoted AT-3Q71 degradation via the ubiquitin-proteasome pathway and attenuated mitochondrial accumulation of AT-3Q71. Thus, MITOL plays a protective role against poly-Q toxicity, and may thereby be a potential target for therapy in poly-Q diseases (Sugiura A. *et al.*, 2010).

Chou and coworkers demonstrated that polyglutamine-expanded ataxin-3-Q79 activates mitochondrial apoptotic pathway and induces neuronal death by upregulating Bax expression and downregulating Bcl-xL expression (Chou A. H. *et al.*, 2006). In a recent work Chou and colleagues also demonstrated that mutant polyglutamine ataxin-3 upregulates Bax expression of cerebellar and pontine nuclei neurons by increasing transcriptional activity of p53, in fact it increased the protein level of active phospho-p53^{Ser15} without affecting mRNA or protein level of p53 (Chou A. H. *et al.*, 2010)

Yu and coworkers demonstrated a significant reduction in the ratio of GSH/GSSG and total glutathione content (GSH + 2X GSSG) in mutant MJD cells compared with the wild-type cells under normal or stressful conditions. They also showed that both SK-NSH-MJD78 and COS7-MJD78-GFP cell lines have lower activities of catalase, glutathione reductase, and superoxide dismutase compared with the wild-type cell lines. In addition, it is known that, when cells are under oxidative stress, the mitochondrial DNA is prone to damage. Their results demonstrated that mitochondrial DNA copy numbers are

decreased in mutant cells and SCA3 patients' samples compared with the normal controls. Furthermore, the amount of common mitochondrial DNA 4,977-bp deletion is higher in SCA3 patients compared with that in normal individuals. Overall, mutant ataxin-3 may influence the activity of enzymatic components to remove O_2^- and H_2O_2 efficiently and promote mitochondrial DNA damage or depletion, which leads to dysfunction of mitochondria. Therefore, they suggest that the cell damage caused by greater oxidative stress in SCA3 mutant cells plays an important role, at least in part, in the disease progression (Yu Y. C. *et al.*, 2009)

Chou and colleagues also tested the involvement of transcriptional deregulation in ataxin-3-Q79-induced cerebellar malfunction and they demonstrated that ataxin-3-Q79 mice exhibited downregulated mRNA expression of proteins involved in glutamatergic neurotransmission, intracellular calcium signaling/mobilization or MAP kinase pathways, GABA(A/B) receptor subunits, heat shock proteins and transcription factor regulating neuronal survival and differentiation (Chou A. H. *et al.*, 2008).

1.12 CASEIN KINASE 2 (CK2)

The reversible phosphorylation of proteins is a major mechanism for the regulation of a broad spectrum of fundamental cellular processes. Given the importance of this covalent modification, it may not be surprising that the human genome encodes several hundred distinct protein kinases, that a third of all cellular proteins appear to be phosphorylated, and that many proteins are phosphorylated at several distinct sites (Litchfield D. W., 2003).

Protein kinase CK2 is distributed ubiquitously in eukaryotic organisms, where it most often appears to exist in tetrameric complexes consisting of two catalytic subunits and two regulatory subunits. In many organisms, distinct isoenzymic forms of the catalytic subunit of CK2 have been identified. For example, in humans, two catalytic isoforms, designated CK2α and CK2α', have been well characterized, while a third isoform, designated CK2α'', has been identified recently. In humans, only a single regulatory subunit, designated CK2β, has been identified (Litchfield D. W., 2003).

At a very early stage after its discovery, CK2, together with a distinct casein kinase designated CK1, was distinguished among known protein kinases for its ability to phosphorylate serine or threonine residues that are proximal to acidic amino acids. Systematic studies, particularly those performed by Pinna and colleagues, subsequently led to the definition of a minimal consensus sequence for phosphorylation by CK2 (Ser-Xaa-Xaa-Acidic, where the acidic residue may be Glu, Asp, pSer or pTyr) that remains distinct from the minimal consensus sequence for any other protein kinase that has been characterized to date. While delineation of this minimal consensus sequence has greatly facilitated the identification of many new potential CK2 targets, there are limitations to the use of such a consensus sequence for the identification of such targets. For example, there are sites, such as Ser392 in the p53 tumour suppressor, that are efficiently phosphorylated by CK2 despite the fact that they do not conform to this consensus sequence (Litchfield D. W., 2003).

It is both exciting and confounding that CK2 appears to reside in a variety of cellular compartments and to participate in the phosphorylation and regulation of a broad array of cellular targets. In fact, CK2 has been detected within the nucleus and cytoplasm, and is also associated with specific structures or organelles, including the plasma membrane, Golgi, endoplasmic reticulum and ribosomes, and has even been detected as an ectoprotein kinase activity on the outer surface of the plasma membrane. Therefore it may not be surprising that CK2 has been implicated in such a broad array of cellular functions. Based on evidence from genetically tractable organisms such as yeast and slime mould, it has been demonstrated that CK2 is essential for viability. Furthermore, there is mounting evidence indicating that CK2 is a component of regulatory protein kinase networks that are involved in various aspects of transformation and cancer. In this respect, abnormally high levels of CK2 have been observed in a number of cancers, including those of the mammary gland, prostate, lung, head and neck and kidney. CK2 also participates in the regulation of various stages of the cell cycle, presumably through the phosphorylation and regulation of proteins that have important functions associated with cell cycle progression (Litchfield D. W., 2003).

A role has been proposed for CK2 in apoptosis. It has been demonstrated that for at least five proteins, phosphorylation by CK2

can inhibit caspase cleavage suggesting a possible anti-apoptotic function. A complementary mechanism for the regulation of caspases by CK2 has recently emerged with the demonstration that phosphorylation by CK2 is required for the apoptotic protein ARC (apoptosis repressor with caspase recruitment domain) to exert its inhibitory activity towards caspase 8. Together with the ability of CK2 to protect individual proteins from caspase-mediated cleavage, this latter observation suggests that CK2 may have general anti-apoptotic functions (Litchfield D. W., 2003).

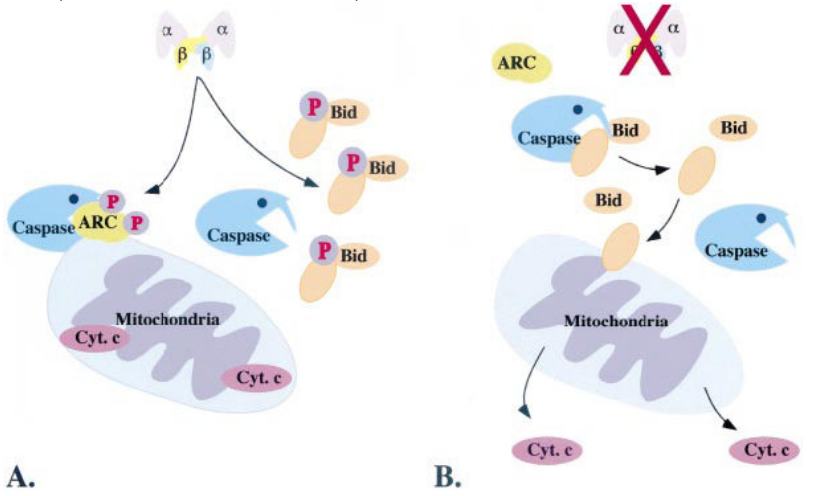

Figure 1.7 Dual role of CK2 in the regulation of apoptosis. (*A*) Under survival conditions, CK2 phosphorylates proteins such as ARC and Bid. When phosphorylated by CK2, ARC is targeted to mitochondria, where it inhibits caspase 8. Bid is resistant to cleavage by caspase 8 when it is phosphorylated by CK2. (*B*) Under apoptotic conditions and/or when CK2 is compromised, CK2 phosphorylation sites on proteins such as Bid and ARC are not phosphorylated. Under these conditions, ARC is not targeted to mitochondria and does not inhibit caspase 8. In the absence of phosphorylation, Bid is susceptible to cleavage by caspase 8. The subsequent translocation of Bid to the mitochondria is followed by release of cytochrome *c* (Cyt. c) that results in the amplification of caspase activation.

CK2 is much more abundant in the brain than in any other tissue. Zetina (Zetina C. R., 2001) observed that CK2 consensus sequences show a high similarity with those found in helix-unfolding motifs in naturally unfolded proteins. This suggests that CK2 phosphorylation could modulate the folding to unfolding check point that leads to the final formation of toxic aggregates; this hypothesis is supported by the fact that CK2 can phosphorylate other proteins involved in

neuropathies, such as α-synuclein, β-amyloid precursor and the prion protein (Meggio F. *et al*., 2003).

Tait and colleagues (Tait D. *et al.*, 1998) have shown the presence, in AT-3 primary structure, of two putative casein kinase (CK2) phosphorylation sites. In fact Tao and coworkers demonstrated that ataxin-3 is CK2 substrate with *in vitro* experiments (Tao R.S. *et al*., 2008).
Mueller and coworkers (Mueller t. *et al*., 2009) demonstrated that CK2-dependent phosphorylation controls the nuclear localization, aggregation, and stability of ataxin-3. Serine 340 and 352 within the third ubiquitin-interacting motif of AT-3 were particularly important for nuclear localization of normal and expanded AT-3 and mutation of these sites robustly reduced the formation of nuclear inclusions; a putative nuclear leader sequence was not required. AT-3 associated with CK2α and pharmacological inhibition of CK2 decreased nuclear AT-3 levels and the formation of nuclear inclusions. Moreover, they found that AT-3 shifted to the nucleus upon thermal stress in a CK2-dependent manner, indicating a key role of CK2-mediated phosphorylation of AT-3 in SCA3 pathophysiology (Mueller t. *et al*., 2009).

1.13 GLYCOGEN SYNTHASE KINASE 3 (GSK3)

Glycogen synthase kinase 3 (GSK3) is a serine/threonine kinase whose function was confined to glycogen metabolism, but in the recent years, GSK3 has turned out to have a key role in the regulation of many cell functions, including signalling by insulin, growth factors and nutrients, and the specification of cell fates during embryonic development. It is also implicated in the control of cell division, apoptosis and microtubule function (Cohen P. *et al.*, 2001).

GSK3 was identified as one of several protein kinases that could phosphorylate glycogen synthase, the enzyme that catalyses the last step in glycogen synthesis. In contrast to many other kinases, which induce the activation of a substrate, the action of GSK3 inhibits glycogen synthase. This kinase also inhibits synthesis of proteins phosphoryling eIF2B factor that in this way is inactivated.

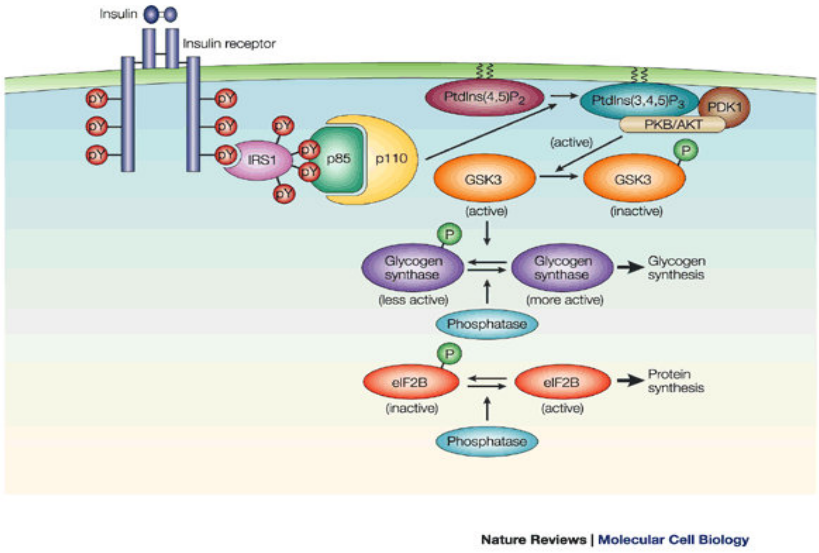

Figure 1.8 The signalling pathway by which insulin inhibits GSK3 and contributes to the stimulation of glycogen and protein synthesis.

The specificity of GSK3 is unique among protein kinases, requiring that many of its substrates are first phosphorylated by another protein kinase at a serine or threonine residue (termed the 'priming phosphate') located four residues carboxy-terminal to the site of GSK3 phosphorylation (Fiol C. J. e*t al.*, 1987).

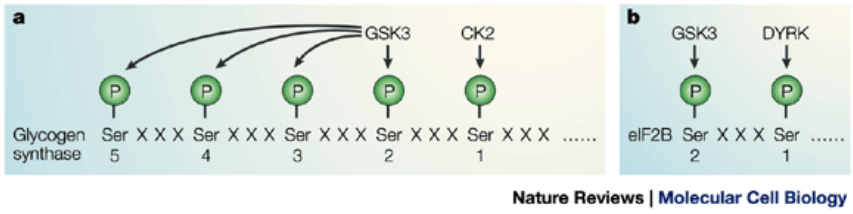

Figure 1.9 The unique substrate specificity of GSK3. Most substrates of GSK3 must first be phosphorylated by another protein kinase at a serine or threonine residue located four residues carboxyterminal to the site of GSK3 phosphorylation. **a** | In the case of glycogen synthase, phosphorylation of a serine residue by casein kinase 2 (CK2; site 1) allows GSK3 to phosphorylate site 2. Phosphorylation of site 2 in turn allows the phosphorylation of site 3 and so on, until five serine residues have become phosphorylated. **b** | Similarly, phosphorylation of eIF2B at site 1 by a protein kinase that might be DYRK (dual-specificity tyrosine-phosphorylated and

regulated kinase) 54 allows GSK3 to phosphorylate site 2 and inhibit eIF2B. (eIF2B, eukaryotic initiation factor 2; Ser, serine.)

The binding site for the priming phosphate on GSK3 has only recently been identified, and was found to contain three crucial basic residues: arginine 96 (Arg96), Arg180 and lysine 205 (Lys205) (Frame S. *et al.*, 2001). Interestingly, the three-dimensional structure of GSK3 most closely resembles that of mitogen-activated protein kinase (MAPK) family members, the activation of which requires the phosphorylation of a threonine and a tyrosine residue that lie in a TXY consensus sequence (T, threonine; X, any amino-acid residue; Y, tyrosine). Intriguingly, the phosphothreonine residue in MAPKs interacts with the same three basic residues that bind the priming phosphate in substrates of GSK3. Moreover, GSK3 is itself phosphorylated constitutively in mammalian cells at a tyrosine residue that is located in a position equivalent to the phosphotyrosine residue in MAPKs. So, the activation of GSK3 seems to be analogous to that of MAPKs, except that the active conformation is induced when the priming phosphate of the substrate binds to GSK3 (Hughes K., *et al.*, 1993).
So, when the serine residue near the amino terminus of GSK3 becomes phosphorylated, it can interact with the same residues that are involved in binding the priming phosphate. Phosphorylation, therefore, suppresses activity by turning the amino terminus of GSK3 into a 'pseudosubstrate'. This not only prevents substrates from binding, but also blocks access to the catalytic centre.

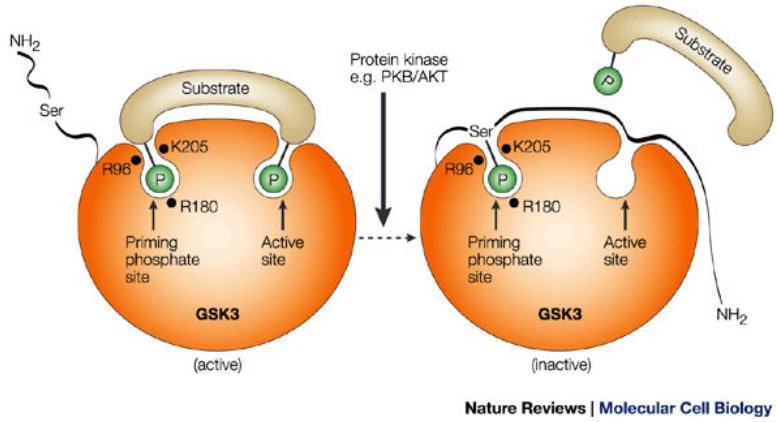

Figure 1.10 The molecular mechanism by which phosphorylation inhibits GSK3. The microtubule-associated protein Tau, which is thought to stabilize microtubules *in vivo* and to promote their polymerization, is phosphorylated at relatively high levels in fetal brain and in the brains of newborn animals, but at much lower levels in adult brain. However, in Alzheimer's disease and several other

neurodegenerative diseases, Tau is found in an abnormally hyperphosphorylated, filamentous and insoluble form. Such hyperphosphorylation is believed to be an early event that precedes its assembly into filaments. Whether hyperphosphorylation is necessary or sufficient for filament assembly is unclear; however, hyperphosphorylation of Tau does prevent it from binding to microtubules, leaving it free and available to undergo the aberrant filament assembly that might underlie the degeneration of nerve cells in these diseases. Many of the sites that are hyperphosphorylated in filamentous Tau are phosphorylated efficiently by GSK3 *in vitro* (Hanger D.P. *et al.,* 1992). Moreover, inhibitors of GSK3, such as lithium ions and insulin, induce a partial dephosphorylation of Tau in newborn animals and human neuronal cells. These observations raise the possibility that GSK3 inhibitors might reduce the abnormal hyperphosphorylation of Tau, thereby enhancing its interaction with microtubules and reducing the pool of Tau available for aberrant assembly (Bienz M., *et al,* 2000).

GSK3 is also involved in another neurodegenerative disease: spinocerebellar ataxia type 3. In fact Villén and coworkers demonstrated that GSK3 phosphorylates *in vivo* Ser268 and Ser273 residues in the sequence of ataxin-3 (Villén J. *et al,* 2007).
Phosphorylation is a common post-translational modification that controls protein function. In many neurodegenerative diseases the phosphorylation of involved proteins has an important role in pathogenesis. Fei and coworkers demonstrated that ataxin-3 is a GSK3 substrate and they identified Ser256 as a phosphorylated residue. In fact upon mutating Ser256 to alanine, ataxin-3 aggregation increases in the pathologic form but not in the normal form, suggesting that phosphorylation of ataxin-3 by GSK3 controls aggregation of ataxin-3 (Fei E., *et al.,* 2007).

AIM OF THE WORK

The aim of this work was the study of role of ataxin-3 phosphorylation and oxidative stress in the pathogenesis of spinocerebellar ataxia type 3.

A bioinformatic analysis showed the presence of 8 putative phosphorylation sites for CK2 and 3 putative phosphorylation sites for GSK3 in the sequence of the wild-type murine form of ataxin-3 (AT-3Q6). An *in vitro* phosphorylation assay was performed to confirm, through mass spectrometry analysis, the phosphorylation sites for CK2 and GSK3.

The identified phosphorylation sites were mutated to alanines to study the involvement of these residues in the subcellular localization of ataxin-3. The experiments were performed in mammalian cells, COS-7 or SHSY-5Y cells, and using subcellular fractionation, mitochondria isolation and confocal microscopy.

In this work the involvement of phosphorylation sites in the interaction between ataxin-3 and VCP/p97 was also studied. In fact ataxin-3 and VCP/p97 interact at ataxin-3 C-terminal in a region with 5 phosphorylation sites for CK2 and GSK3. The co-immunoprecipitation between VCP/p97 and ataxin-3 was analyzed in COS-7 cells under reticular stress or not. The constructs used were AT-3Q6, its mutants lacking phosphorylation sites in the region of interaction with VCP/p97 and the human pathological form of ataxin-3 (AT-3Q72).

Overproduction of reactive nitrogen species (RNS) and reactive oxygen species (ROS), which lead to neuronal cell injury and death, is a potential mediator of neurodegenerative disorders including poly-Q diseases. Thus in this work the role of oxidative stress in the pathogenesis of Spinocerebellar Ataxia Type 3 was studied. In particular the expression of NO synthase in Neuro-2a cells, transfected with AT-3Q6 or AT-3Q72, was analyzed by western blotting. Moreover the nitration pattern in cells was studied in presence of wild-type or pathological form of ataxin-3, with bidimensional analysis.

2. Materials and Methods

2.1 *IN VITRO* PHOSPHORYLATION OF ATAXIN-3

2.1.1 PURIFICATION FROM *E.coli*

AT-3Q6-encoding cDNA, cloned into plasmid *pGEX-6P-1*, was used to transform *E. coli* strain BL21 codon plus RIL, to express AT-3 as a GST-fusion protein.

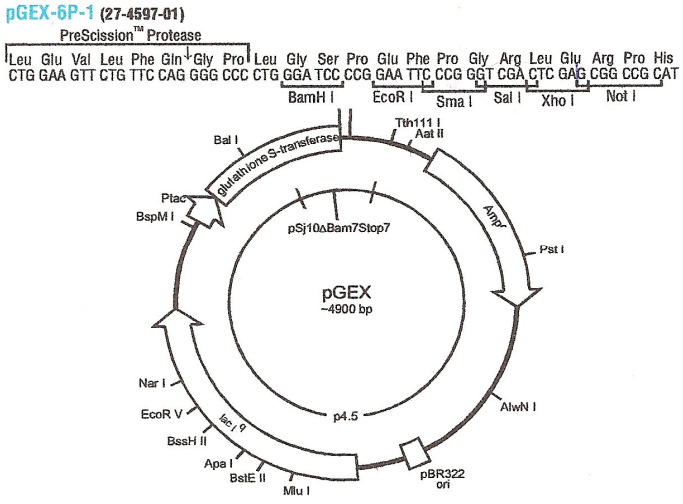

Figure 2.1 Schematic representation of the plasmid *pGEX-6P-1*

Cells were grown at 37°C in LB-ampicillin medium and induced for 3 h with 50 μM IPTG at A_{600} 0.8. In order to obtain crude extracts, cells were resuspended in lysis buffer (10 mM potassium phosphate, pH 7.2, 150 mM NaCl, 1 mM phenylmethanesulfonyl fluoride, 5 mM DTT, 100 mM $MgCl_2$) plus 1 mg/ml lysozyme and incubated for 1 h at 4°C. Cell suspension was then frozen at -80°C for 20 min and thawed; DNase I (0.15 mg/g of cells, wet weight) and 1% Triton X-100 were added, and the sample further incubated for 30 min at room temperature. After centrifugation for 30 min at 18000 x g, the supernatant was incubated with Glutathione Sepharose 4B resin (1 ml/g of cells, wet weight) (GE Healthcare, Uppsala, Sweden) for 40 min at 4°C; the sample was subsequently loaded onto the column. After washing with 10 volumes of PBS (10 mM potassium phosphate, pH 7.2, 150 mM NaCl) and equilibration with 10 volumes of cold Cleavage Buffer (50 mM Tris-HCl, pH 7.0, 150 mM NaCl, 1 mM

EDTA, 1 mM DTT), AT-3 was cleaved from fusion partner by overnight incubation at 4°C with Prescission Protease (80 U/ml resin) (GE Healthcare, Uppsala, Sweden). Purified AT-3 was eluted with 10 ml of Cleavage buffer. Protein concentration was assayed through Coomassie brilliant blue G-250 from Pierce (Pierce Biotechnology, Rockford, IL), using bovine plasma immunoglobulin as a standard protein.

2.1.2 *IN VITRO* PHOSPHORYLATION BY CK2

AT-Q6 purified from *E. coli* was dialyzed for 3 h at 4°C against 50 mM Tris pH 8, 150 mM NaCl, 10 mM $MgCl_2$, with a 14 kD cut-off membrane. AT-3Q6 (40 μg) was then incubated for 30 min at 30°C, under shaking, with 1 μg (200U) CK2 (BIOMOL international, Plymouth Meeting, PA USA) in the presence of 1 mM ATP. The sample was then subjected to MALDI-TOF analysis.

2.1.3 *IN VITRO* PHOSPHORYLATION BY GSK3

AT-3Q6 purified from *E. coli* was dialyzed for 3 h at 4°C in GSK3 buffer (25 mM MOPS pH 7.2, 12.5 mM β-glycerophosphate, 5 mM EGTA, 2 mM EDTA, 25 mM $MgCl_2$, 0.25 mM DTT, 50 ng/μl BSA) with a 14 kD cut-off membrane. AT-3Q6 (40 μg) was then incubated with 1 μg (100U) GSK3 (BIOMOL international, Plymouth Meeting, PA USA) and ATP 100 μM at 30°C for 30 min. The sample was then subjected to analysis.

2.1.4 MASS SPECTROMETRY ANALYSIS

AT-3Q6, phosphorylated *in vitro* by either CK2 or GSK3 as described above, was subjected to reduction and alkylation in solution by iodoacetamide and incubated with GluC endoproteinases (1:25 enzyme/protein, w/w) overnight at 37°C. Following acidification, the peptide mixture was loaded onto a MALDI plate using ZipTip C18 (Millipore, Bedfor, MA-USA) with a matrix of α-ciano-4-hydroxy-cinnamic acid. Mass spectrometry analysis was carried out on a Bruker Daltonics Reflex IV instrument (Bruker Daltonics, Milano, Italy) equipped with a nitrogen laser, operating in positive and negative linear mode. Each spectrum was accumulated for at least 200 laser shots and Bruker peptide calibration standards were used for calibration.

MS/MS analysis was carried out on a MALDI TOF/TOF Autoflex III (Bruker Daltonics, Milano, Italy). Data were acquired and processed using Biotools software (Bruker Daltonics, Milano, Italy).

2.2 SUB-CELLULAR LOCALIZATION OF ATAXIN-3 PHOSPHORYLATION MUTANTS

2.2.1 CONSTRUCTS

cDNAs encoding for murine AT-3Q6 and human AT-3Q72, previously subcloned in our laboratory into plasmid *pGEX-6P-1*, were cut with *BamHI* and *XhoI* restriction enzymes and subcloned into plasmid *pcDNA3X(+)HA* (Invitrogen UK Ltd. Paisley, England).

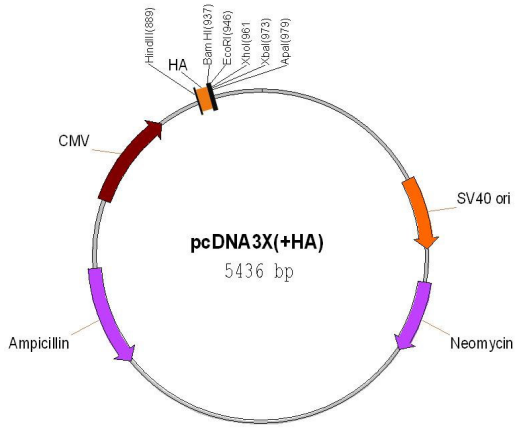

Figure 2.2 Schematic representation of the plasmid *pcDNA3X(+)HA*

Subsequently, AT-3 coding cDNAs, tagged with an HA epitope at the N-terminal, were retrieved by PCR from *pcDNA3X(+)HA* and subcloned into plasmid *pcDNA3.1/myc-His*, digested with the same enzymes, in frame with a *c-myc* epitope, mutating the STOP codon by PCR using Quik-Change Site directed Mutagenesis Kit (Stratagene La Jolla, CA USA), according to the manufacturer's instructions.

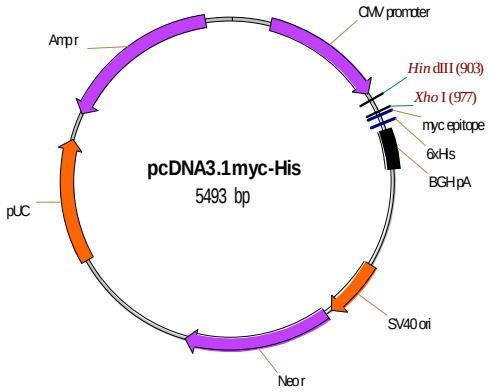

Figure 2.3 Schematic representation of the plasmid *pcDNA3.1/myc-His*

S272A, S277A, DM (S272A and S277A), TM (T271A, S272A and S277A), QM (S268A, T271A, S272A, S273A and S277A), S29A, S29D and M (S29A, S329A and S341A) mutants were obtained by PCR using Quik-Change Site directed Mutagenesis Kit (Stratagene La Jolla, CA USA), according to the manufacturer's instructions. The correct insertion of cDNAs in expression vectors and the presence of the mutations were verified by automated sequencing using vector oligonucleotide primers (T7 and BGH).

2.2.2 CELL CULTURES

All constructs in *pcDNA3.1/myc-His*, carrying N-terminal HA and C-terminal *c-myc* epitopes, were hosted and amplified in *E. coli* strain DH5α, while protein expression was achieved after transient transfection of COS-7 cells or SHSY-5Y cells. Cultures were carried out in 94 mm plates or onto coverslips in DMEM containing 10% fetal bovine serum (FBS), 100 U/ml penicillin, 100 µg/ml streptomycin and 4 mM glutamine (COS-7 cells) or in F12 and DMEM containing 10% fetal bovine serum (FBS), 100 U/ml penicillin, 100 µg/ml streptomycin and 4 mM glutamine (SHSY-5Y cells). Cells were subsequently transiently transfected with FuGENE6 (Roche Diagnostics Mannheim, Germany), according to the manufacturer's instructions (with a proportion of 3 µl of FuGENE6 / 1 µg of DNA for COS-7 cells and with a proportion of 3 µl of FuGENE6 / 2 µg of DNA for SHSY-5Y cells).
To inhibit CK2 and GSK3, COS-7 cells were incubated for 24 hours at 37°C with either 5 or 10 µM CK2 inhibitor (TBB, Sigma St. Louis,

Mo, USA) and/or with 10 µM GSK3 inhibitor (SB216763, Sigma St. Louis, Mo, USA). 24 h after transfection, cells were harvested and tested for sub-cellular localization of exogenous AT-3 by blotting and detection with anti-*c-myc* or Z46 antibodies. Cell viability was assessed through MTT test (Sigma St. Louis, Mo, USA), performed according to the manufacturer's instructions. Statistical analysis was performed using t-Student test, results significance was indicated with $p<0.05$.

2.2.3 IMMUNOFLUORESCENCE AND CONFOCAL ANALYSIS

COS-7 cells were plated onto coverslips (2.5×10^4 cells/coverslip) and grown for 24 h before transfection. Cells were transfected overnight with FuGENE6 (Roche Diagnostics Mannheim, Germany); 24 h after transfection, cells were fixed for 20 min in 3% (w/v) paraformaldehyde in PBS and quenched for 30 min with 50 mM NH_4Cl in PBS. Permeabilization was carried out by incubating the cells in the presence of 0.3% (w/v) saponin in PBS (7 min for 3 times). Cells were then doubly stained with anti-*c-myc* mouse monoclonal antibody (Santa Cruz Cruz Biotechnology Inc. Santa Cruz, CA USA, 1:50) and anti-HA rabbit polyclonal antibody (Sigma St. Louis, Mo USA, 1:50). Cells were also incubated with anti-*c-myc* rabbit monoclonal antibody (Sigma St. Louis, Mo USA, 1:50) and mouse anti-*cyt-c* monoclonal antibody (Promega Corporation Madison, WI USA, 1:200) for mitochondria visualization. After extensive washes, cells were incubated with donkey anti-mouse Cy3 conjugated antibody (1:350) and donkey anti-rabbit Cy2 conjugated antibody (1:150) or with donkey anti-rabbit Cy3 (1:350) and donkey anti-mouse Cy2 (1:150) antibodies. All antibodies were from Jackson ImmunoResearch Laboratories (West Grove, PA USA). Incubations and washes were carried out at room temperature in PBS, 0.3% (w/v) saponin. At the end cells were incubated for 15 min with the nuclear marker TO-PRO-3 iodide (Molecular Probes, Invitrogen UK Ltd Paisley, England). Confocal microscopy was performed using a Leica Mod. TCS-SP2 (Leica Microsystem). Image processing was performed with Leica Confocal Software (LCS) and Adobe Photoshop Software. Confocal microscopy images were collected under the same conditions in order to compare fluorescence intensities among different images. About 120 cells were examined in 6 images; the mean fluorescence intensity of the nuclear region was evaluated.

Statistical analysis was performed using t-Student test, results significance was indicated with $p<0.01$.

2.2.4 CELL FRACTIONATION

24 h after transfection, COS-7 cells (6×10^5 cells/plate, cultured in 94 mm plates) or SHSY-5Y cells (1×10^6 cells/plate, cultured in 94 mm plates) were harvested and resuspended in 10 mM (Na)PO_4, 100 mM NaCl, pH 7.4, 0.5% NP-40, supplemented with protease inhibitors (Roche Diagnostics Mannheim, Germany). After incubating 40 min on ice, nuclei were pelleted by centrifugation at 4000 ×g for 15 min at 4 °C. The supernatant was centrifuged at 15000 ×g for 30 min at 4 °C, yielding the cytosolic fraction. Nuclei were resuspended in 50 mM HEPES pH 7.9, 0.75 mM $MgCl_2$, 0.5 mM EDTA, 0.5 M NaCl, 12.5% glycerol, 5 mM DTT and protease inhibitors. After incubating 1 h on ice nuclei were centrifuged at 15000 ×g for 30 min at 4 °C: the supernatant represented the nuclear fraction.

2.2.5 MITOCHONDRIA ISOLATION

To separate soluble mitochondrial proteins from mitochondrial membranes, Mitochondria Isolation Kit for Cultured Cells (Pierce Biotechnology Rockford, IL USA) was used according to the manufacturer's protocol. Briefly Reagent A was added to 2×10^7 COS-7 cells harvested 24 h after transfection. After incubating 2 min on ice, Reagent B was added. After incubating 5 min on ice vortexing every minute, cells were resuspended in Reagent C and centrifuged at 700 x g for 10 min at 4°C. The supernatant was centrifuged at 3000 x g for 5 min at 4°C: the supernatant represented the cytosolic fraction, while the pellet contained isolated mitochondria. Mitochondria were washed with Reagent C and centrifuged at 12000 x g for 5 min at 4°C. To separate mitochondrial membranes from the matrix, mitochondria were lysed with 2% (w/v) CHAPS in PBS. After vortexing for 1 min, mitochondria were centrifuged at high speed for 2 min. The supernatant represented the mitochondrial soluble fraction (containing soluble mitochondrial proteins), while the pellet represented the mitochondrial membranes. To confirm the homogeneity of the mitochondrial soluble fraction, acid phosphatase (a lysosomal enzyme) and malic dehydrogenase (a mitochondrial enzyme) were assayed. The first was assayed, following the production of nitrophenol from p-nitrophenyl phosphate and the assay confirmed

that mitochondrial fraction was not contaminated by lysosomes. The latter was assayed following NADH absorbance decrease at 340nm; results showed that the soluble fraction contained mitochondrial proteins.

2.2.6 IMMUNOPRECIPITATION

1000 μg of total protein extract obtained from AT-3Q6 overexpressing COS-7 cells (treated or not with CK2 and GSK3 inhibitors) was incubated with 2 μg of Z46 antibody (an anti-ataxin-3 polyclonal antibody) (Primm Cambridge, MA USA), overnight at 4°C. The total extract was subsequently incubated with Protein A-Sepharose ™-CL-4B (Amersham GE Healthcare, Uppsala, Sweden) for 2 h at 4°C. After incubation the resin was washed 3 times with NP40 buffer (50 mM Tris pH 7.5, 150 mM NaCl, 15 mM $MgCl_2$ and 1% NP40) and ataxin-3 was eluted by boiling in SDS buffer.

2.2.7 SDS-PAGE AND WESTERN-BLOT ANALYSIS

SDS-PAGE and Western-blot were carried out by standard procedures. PVDF Immobilon™ P (Millipore Billerica, MA USA) membranes were blocked for 1 h in PBS, containing either 5% (w/v) dried milk (for anti-*c-myc*, Z46, anti-vinculin, anti-VDAC and anti-SOD2 antibodies) or in 5% (w/v) bovine serum albumin (BSA) (Sigma St. Louis, Mo, USA) (for anti-fibrillarin and anti-Phosphoglycerate kinase (PGK) antibodies). Membranes were subsequently probed overnight in 1% dried milk in PBS with anti-*c-myc* mouse monoclonal antibody (1:1000) (Santa Cruz Biotechnology Inc. Santa Cruz, CA. USA) and in 5% dried milk in PBS, 0.3% Tween20 with Z46 rabbit polyclonal antibody (1:5000) (Primm Cambridge, MA USA). Control incubations for cell fractionation with anti-fibrillarin (1:5000) (Encor Biotechnology Gainesville, FL, USA), with 22C5 anti-PGK (1:1000) (Molecular Probes, Invitrogen UK Ltd. Paisley, England) and with anti-vinculin (1:10000) (Sigma St. Louis, Mo, USA) mouse monoclonal antibodies were also carried out overnight in PBS, containing 1% (w/v) BSA, 0.1% (v/v) Tween20, 1% (w/v) BSA and 5% (w/v) dried milk, 0,05% Tween20 respectively. Control incubations for mitochondria isolation with anti-VDAC (1:1000) and anti-SOD2 (1:5000) rabbit polyclonal antibodies (Abcam Inc. Cambridge, MA USA) were also carried out overnight in PBS containing 5% (w/v) BSA. Membranes, probed with mouse

antibodies, were incubated for 1 h with an anti-mouse horseradish peroxidase-conjugated IgG (1:3000) (Calbiochem Darmstadt, Germany) in PBS, 0.1% (v/v) Tween20 containing 1% (w/v) dried milk, while membranes probed with rabbit antibodies were incubated for 1 h with an anti-rabbit horseradish peroxidase-conjugated IgG (1:15000) (Sigma St. Louis, Mo, USA) in PBS containing 5% (w/v) dried milk. Detection of antibody binding was carried out with ECL (Amersham GE Healthcare, Uppsala, Sweden), according to the manufacturer's instructions.
Protein levels were quantified by densitometry of scanned not saturated X-ray films using the NIH Image-based software Scion Image (Scion Corporation). Quantification data are a mean of three independent experiments; bands intensities were normalized on fibrillarin and PGK controls. Statistical analysis was performed using t-Student test, results significance was indicated with $p<0.05$.

2.2.8 ACID SILVER STAIN

To analyze AT-3 immunoprecipitated from COS-7 cells by mass spectrometry, SDS-PAGE was fixed for 1h in 40% Ethanol, 10% acid acetic and for 2 days in 5% ethanol, 5% acid acetic; the gel was subsequently washed in 30% ethanol 3 times for 20 min and incubated for 1 min in 0.8 mM sodium tiosulfate. The gel was then incubated in 11.8 mM silver nitrate, 0.02% formaldehyde for 20 min and subsequently washed twice with water for 20 sec and developed with 556 mM sodium carbonate, 0.02% formaldehyde, 0.02 mM sodium tiosulfate. Developing was stopped with 50% ethanol, 12% acid acetic; the gel was washed with water for 10 min and conserved at 4°C in 1% acid acetic.

2.2.9 MASS SPECTROMETRY ANALYSIS

AT-3, immunoprecipitated from COS-7 transfected cells as described above and separated by SDS-PAGE, was subjected to *in situ* digestion with GluC endoproteinase (1:10 enzyme/protein, w/w) and peptide extraction with 40% CH_3CN in 0.1% TFA before loading onto the MALDI plate using ZipTip C18 (Millipore, Bedfor, MA-USA) with a matrix of α-ciano-4-hydroxy-cinnamic acid. Mass spectrometry analysis was carried out on a Bruker Daltonics Reflex IV instrument (Bruker Daltonics, Milano, Italy) equipped with a nitrogen laser, operating in positive and negative linear mode. Each spectrum was

accumulated for at least 200 laser shots and Bruker peptide calibration standards were used for calibration.
MS/MS analysis was carried out on a MALDI TOF/TOF Autoflex III (Bruker Daltonics, Milano, Italy). Data were acquired and processed using Biotools software (Bruker Daltonics, Milano, Italy).

2.3 INTERACTION BETWEEN AT-3 AND VCP/p97

2.3.1 CONSTRUCTS

cDNA encoding for murine AT-3Q6, previously subcloned in our laboratory into plasmid *pGEX-6P-1*, was cut with *BamHI* and *XhoI* restriction enzymes and subcloned into plasmid *pcDNA3X(+)HA* (Invitrogen UK Ltd. Paisley, England).
cDNA encoding for human AT-3Q72 was cloned into plasmid *pcDNA3.1/myc-His* in frame with HA epitope at N-terminal and *c-myc* epitope at C-terminal.

TM (T271A, S272A and S277A) mutant, cloned into plasmid *pcDNA3.1/myc-His*, was cut with *HindIII* and *XhoI* restriction enzymes and subcloned into plasmid *pcDNA3X(+)HA*, introducing the STOP codon by PCR using Quik-Change Site directed Mutagenesis Kit (Stratagene La Jolla, CA USA), according to the manufacturer's instructions.
QM (S268A, T271A, S272A, S273A and S277A) mutant was obtained by PCR using Quik-Change Site directed Mutagenesis Kit (Stratagene La Jolla, CA USA), according to the manufacturer's instructions.

cDNA encoding for VCP/p97, cloned into plasmid *pCMV-Sport6ccdB*, was retrieved by PCR and subcloned into plasmid *pcDNA3.1/myc-His*, digested with the same enzymes, in frame with a *c-myc* epitope, mutating the STOP codon by PCR using Quik-Change Site directed Mutagenesis Kit (Stratagene La Jolla, CA USA), according to the manufacturer's instructions.

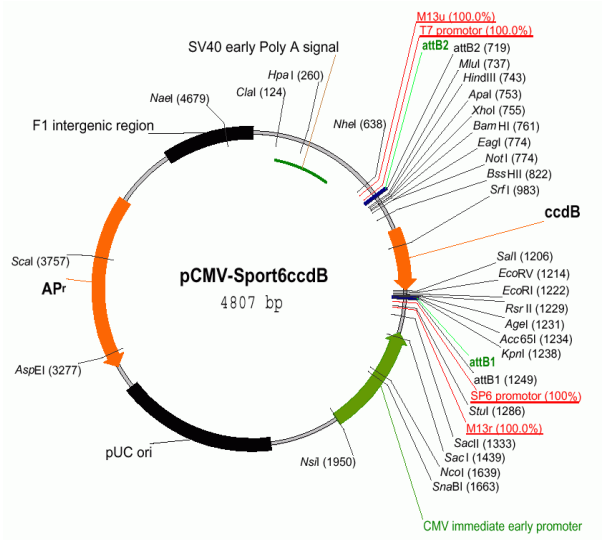

Figure 2.4 Schematic representation of the plasmid *pCMV-Sport6ccdB*

The PCR program was:

1	98°C	2 min.
1	98°C	30 sec.
	53°C	30 sec.
	72°C	3 min.
30	98°C	30 sec.
	63°C	30 sec.
	72°C	3 min.
1	72°C	10 min.

The correct insertion of cDNAs in expression vectors and the presence of the mutations were verified by automated sequencing using vector oligonucleotide primers (T7 and BGH for *pcDNA3.1/myc-His*, T7 and SP6 for *pcDNA3X(+)HA*).

2.3.2 CELL CULTURES

All constructs in *pcDNA3X(+)HA*, carrying N-terminal HA epitope, and VCP/p97 and AT-3Q72 encoding cDNAs in *pcDNA3.1/myc-His*, carrying C-terminal *c-myc* epitope, were hosted and amplified in *E. coli* strain DH5α, while protein expression was achieved after transient transfection of COS-7 cells. Cultures were carried out in 94 mm plates in DMEM containing 10% fetal bovine serum (FBS), 100 U/ml penicillin, 100 μg/ml streptomycin and 4 mM glutamine. Cells were subsequently transiently co-transfected with FuGENE6 (Roche Diagnostics Mannheim, Germany), according to the manufacturer's instructions (with a proportion of 3 μl of FuGENE6 / 1 μg of DNA and with a 1:1 proportion of DNAs molecular weights).
To induce an ERAD stress condition, 24 h after transfection, cells were treated with 10 mM DTT (Sigma St. Louis, Mo, USA) for 1 h at 37°C (Lai C. W. *et al.*, 2010).
24 h after transfection, cells were harvested and tested for immunoprecipitation of exogenous AT-3 and exogenous VCP/p97 by blotting and detection with anti-*c-myc* and anti-HA antibodies.

2.3.3 CELL FRACTIONATION

24 h after transfection, COS-7 cells (6×10^5 cells/plate, cultured in 94 mm plates) were harvested and resuspended in 10 mM (Na)PO_4, 100 mM NaCl, pH 7.4, 0.5% NP-40, supplemented with protease inhibitors (Roche Diagnostics Mannheim, Germany). After incubating 40 min on ice, nuclei were pelleted by centrifugation at 4000 ×g for 15 min at 4 °C. The supernatant was centrifuged at 15000 ×g for 30 min at 4 °C, yielding the cytosolic fraction. Nuclei were resuspended in 50 mM HEPES pH 7.9, 0.75 mM $MgCl_2$, 0.5 mM EDTA, 0.5 M NaCl, 12.5% glycerol, 5 mM DTT and protease inhibitors. After incubating 1 h on ice nuclei were centrifuged at 15000 ×g for 30 min at 4 °C: the supernatant represented the nuclear fraction.

2.3.4 IMMUNOPRECIPITATION

1000 μg of total protein extract was incubated with 2 μg of Z46 antibody (an anti-ataxin-3 polyclonal antibody) (Primm Cambridge, MA USA), overnight at 4°C. The total extract was subsequently incubated with Protein A-Sepharose ^{TM}-CL-4B (Amersham GE Healthcare, Uppsala, Sweden) for 2 h at 4°C. After incubation the

resin was washed 3 times with NP40 buffer (50 mM Tris pH 7.5, 150 mM NaCl, 15 mM $MgCl_2$ and 1% NP40) and ataxin-3 was eluted by boiling in SDS buffer.

2.3.5 SDS-PAGE AND WESTERN-BLOT ANALYSIS

SDS-PAGE and Western-blot were carried out by standard procedures. PVDF Immobilon™ P (Millipore Billerica, MA USA) membranes were blocked for 1 h in PBS, containing 5% (w/v) dried milk. Membranes were subsequently probed overnight in 1% dried milk in PBS with anti-*c-myc* mouse monoclonal antibody (1:1000) (Santa Cruz Biotechnology Inc. Santa Cruz, CA. USA) to visualize VCP/p97 or AT-3Q72 and with anti-HA mouse monoclonal antibody (1:1000) (Santa Cruz Biotechnology Inc. Santa Cruz, CA. USA) to visualize AT-3Q6. Membranes, probed with mouse antibodies, were incubated for 1 h with an anti-mouse horseradish peroxidase-conjugated IgG (1:3000) (Calbiochem Darmstadt, Germany) in PBS, 0.1% (v/v) Tween20 containing 1% (w/v) dried milk. Detection of antibody binding was carried out with ECL (Amersham GE Healthcare, Uppsala, Sweden), according to the manufacturer's instructions.
Protein levels were quantified by densitometry of scanned not saturated X-ray films using the NIH Image-based software Scion Image (Scion Corporation). Quantification data are a mean of three independent experiments. Statistical analysis was performed using t-Student test, results significance was indicated with $p<0.05$.

2.4 NITRATION AND AT-3

2.4.1 CONSTRUCTS

cDNAs encoding for murine AT-3Q6 and human AT-3Q72, previously subcloned in our laboratory into plasmid *pGEX-6P-1*, were cut with *BamHI* and *XhoI* restriction enzymes and subcloned into plasmid *pcDNA3X(+)HA* (Invitrogen UK Ltd. Paisley, England).
Subsequently, AT-3 coding cDNAs, tagged with an HA epitope at the N-terminal, were retrieved by PCR from *pcDNA3X(+)HA* and subcloned into plasmid *pcDNA3.1/myc-His*, digested with the same enzymes, in frame with a *c-myc* epitope, mutating the STOP codon by PCR using Quik-Change Site directed Mutagenesis Kit (Stratagene La Jolla, CA USA), according to the manifacturer's instructions.

2.4.2 CELL CULTURES

All constructs in *pcDNA3.1/myc-His*, carrying C-terminal *c-myc* and N-terminal HA epitopes, were hosted and amplified in *E. coli* strain DH5α, while protein expression was achieved after transient transfection of Neuro2a cells. Cultures were carried out in 94 mm plates in DMEM containing 10% fetal bovine serum (FBS), 100 U/ml penicillin, 100 μg/ml streptomycin and 4 mM glutamine. Cells were subsequently transiently transfected with FuGENE6 (Roche Diagnostics Mannheim, Germany), according to the manufacturer's instructions (with a proportion of 3 μl of FuGENE6 / 2 μg of DNA). 24 h after transfection, cells were harvested and tested for expression of endogenous NOS by blotting and detection with anti-NOS antibody.

2.4.3 CELL FRACTIONATION

24 h after transfection, Neuro2a cells (1×10^6 cells/plate, cultured in 94 mm plates) were harvested and resuspended in 10 mM (Na)PO_4, 100 mM NaCl, pH 7.4, 0.5% NP-40, supplemented with protease inhibitors (Roche Diagnostics Mannheim, Germany). After incubating 40 min on ice, nuclei were pelleted by centrifugation at 4000 ×g for 15 min at 4 °C. The supernatant was centrifuged at 15000 ×g for 30 min at 4 °C, yielding the cytosolic fraction. Nuclei were resuspended in 50 mM HEPES pH 7.9, 0.75 mM $MgCl_2$, 0.5 mM EDTA, 0.5 M NaCl, 12.5% glycerol, 5 mM DTT and protease inhibitors. After incubating 1 h on ice nuclei were centrifuged at 15000 ×g for 30 min at 4 °C: the supernatant represented the nuclear fraction.

2.4.4 2-D PAGE

2-D PAGE was carried out on the total extracts obtained by cell fractionation, after reduction and alkylation. The samples were solubilized in 50 mM Tris-HCl pH 6.8, 4% SDS and 5% b-mercaptoethanol, heated at 70°C, sonicated for 1 min and centrifuged at 10000 x g for 5 min. The supernatants were treated with 5 mM tributylphosphine in NH_4HCO_3 0.1 M as a reductant and stored at room temperature for 1.5 h. After this step, the samples were incubated with 20 mM iodoacetamide at room temperature for 1.5 h. The samples were then precipitated in an anhydrous solution of acetone and methanol (8:1 v/v). Precipitates were resuspended in the

2-D PAGE sample buffer (7 M urea, 2 M thiourea, 2% NP-40, 0.5% Resolyte 3.5–10 NL, bromophenol blue) and sonicated for 1 min. For the first dimension, 80 μg of proteins were applied to a rehydrated IPG strip (110 mm, pH 3–10 NL; Amersham Biosciences, Cologno Monzese, Italy) and IEF was carried out at 20000 V total voltage, for 6 h. Before the second dimension, the strips were rinsed with buffer (6 M urea in 0.375 M Tris-HCl pH 8.8, 2% SDS, 20% glycerol, bromophenol blue). The second dimension was performed on a homemade 10% SDS minigel at 180 mA for 1 h. Finally, the gels were blotted onto a PVDF membrane.

2.4.5 SDS-PAGE AND WESTERN-BLOT ANALYSIS

SDS-PAGE and Western-blot were carried out by standard procedures. PVDF Immobilon™ P (Millipore Billerica, MA USA) membranes were blocked for 1 h in PBS, containing 5% (w/v) dried milk, or o.n. in PBS containing 6% (w/v) dried milk and 0.05% Tween20 for anti-nitrotyrosine antibody. Membranes were subsequently probed overnight in 1% dried milk in PBS with anti-*c-myc* mouse monoclonal antibody (1:1000) (Santa Cruz Biotechnology Inc. Santa Cruz, CA. USA) to visualize AT-3 and in 5% dried milk in PBS with anti-NOS rabbit polyclonal antibody (1:1000) (Abcam Inc. Cambridge, MA USA) to visualize NOS. To visualize nitrated proteins membranes were probed for 2 h in PBS containing 6% dried milk, 0.05% Tween20 with anti-nitrotyrosine rabbit polyclonal antibody (1:750) kindly supplied by Professor Arce (Universitad Nacional de Cordoba, Argentina). Control incubation with anti-vinculin (1:10000) (Sigma St. Louis, Mo, USA) mouse monoclonal antibody was carried out overnight in PBS, containing 5% (w/v) dried milk, 0.05% Tween20. Membranes, probed with mouse antibodies, were incubated for 1 h with an anti-mouse horseradish peroxidase-conjugated IgG (1:3000) (Calbiochem Darmstadt, Germany) in PBS, 0.1% (v/v) Tween20 containing 1% (w/v) dried milk, while membranes probed with rabbit antibodies were incubated for 1 h with an anti-rabbit horseradish peroxidase-conjugated IgG (1:15000) (Sigma St. Louis, Mo, USA) in PBS containing 5% (w/v) dried milk. Detection of antibody binding was carried out with ECL (Amersham GE Healthcare, Uppsala, Sweden), according to the manufacturer's instructions.

Protein levels were quantified by densitometry of scanned not saturated X-ray films using the NIH Image-based software Scion

Image (Scion Corporation). Quantification data are a mean of three independent experiments; bands intensities were normalized on vinculin control. Statistical analysis was performed using t-Student test, results significance was indicated with $p<0.05$.

In nitration pattern analysis protein levels were quantified by densitometry of scanned not saturated X-ray films using Quantity-one Analysis software and profiles were obtained through the parameter Trace quantity (the quantity of a band as measured by the area under its intensity profile curve).

3. Results

3.1 *IN VITRO* PHOSPHORYLATON OF AT-3

3.1.1 ATAXIN-3 AND CK2

In our laboratory, using *NetPhos 2.0*, *ScanProsite* and *PHOSIDIA* servers, eight putative phosphorylation sites for casein kinase 2 (CK2) were identified in the murine ataxin-3 (AT-3Q6) sequence (Table 3.1 and Figure 3.1).

Table 3.1 Putative phosphorylation sites for CK2 in AT-3Q6 sequence.

aa 29-32	SPVE
aa 236-239	SRQE
aa 263-266	SMCE
aa 271-274	TSSP
aa 272-275	SSPD
aa 277-280	SSEE
aa 329-332	SEED
aa 344-347	TAKD

```
  1          11         21         31         41         51
  |          |          |          |          |          |

  1 MESIFHEKQE GSLCAQHCLN NLLQGEYFSP VELSSIAHQL DEEERLRMAE GGVTSEDYRT 60
 61 FLQQPSGNMD DSGFFSIQVI SNALKVWGLE LILFNSPEYQ RLRIDPINER SFICNYKEHW 120
121 FTVRKLGKQW FNLNSLLTGP ELISDTYLAL FLAQLQQEGY SIFVVKGDLP DCEADQLLQM 180
181 IKVQQMHRPK LIGEELAHLK EQSALKADLE RVLEAADGSG IFDEDEDDLQ RALAISRQEI 240
241 DMEDEEADLR RAIQLSMQGS SRSMCENSPQ TSSPDLSSEE LRRRREAYFE KQQQQQQEVD 300
301 RPGPLSYPRE RPTTSSGGRR SDQGGDAVSE EDMLRAAVTM SLETAKDNLK
```

Figure 3.1 AT-3Q6 sequence. CK2 putative phosphorylated residues are evidenced in red.

AT-3Q6 purified from *E.coli* was phosphorylated *in vitro* by CK2 and analized by mass spectrometry. Seven phosphorylated residues were identified (Table 3.2).

Table 3.2 Phosphorylation sites for CK2 in AT-3Q6 sequence.

aa 29-32	SPVE
aa 271-274	TSSP
aa 272-275	SSPD
aa 277-280	SSEE
aa 329-332	SEED
aa 341-344	SLET
aa 344-347	TAKD

3.1.2 ATAXIN-3 AND GSK3

In our laboratory, using *PHOSIDIA* server, three putative phosphorylation sites for glycogen synthase kinase 3 (GSK3) were identified in the murine ataxin-3 (AT-3Q6) sequence (Table 3.3 and Figure 3.2).

Table 3.3 Putative phosphorylation sites for GSK3 in AT-3Q6 sequence.

aa 29-32	SPVE
aa 268-271	SPQT
aa 273-276	SPDL

```
   1          11         21         31         41         51
   |          |          |          |          |          |

  1 MESIFHEKQE GSLCAQHCLN NLLQGEYFSP VELSSIAHQL DEEERLRMAE GGVTSEDYRT 60
 61 FLQQPSGNMD DSGFFSIQVI SNALKVWGLE LILFNSPEYQ RLRIDPINER SFICNYKEHW 120
121 FTVRKLGKQW FNLNSLLTGP ELISDTYLAL FLAQLQQEGY SIFVVKGDLP DCEADQLLQM 180
181 IKVQQMHRPK LIGEELAHLK EQSALKADLE RVLEAADGSG IFDEDEDDLQ RALAISRQEI 240
241 DMEDEEADLR RAIQLSMQGS SRSMCENSPQ TSSPDLSSEE LRRRREAYFE KQQQQQQEVD 300
301 RPGPLSYPRE RPTTSSGGRR SDQGGDAVSE EDMLRAAVTM SLETAKDNLK
```

Figure 3.2 AT-3Q6 sequence. GSK3 putative phosphorylation residues are evidenced in red.

AT-3Q6 purified from *E.coli* was phosphorylated *in vitro* by GSK3 and analized by mass spectrometry. Three phosphorylated residues were identified (Table 3.4).

Table 3.4 Phosphorylation sites for GSK3 in AT-3Q6 sequence.

aa 29-32	SPVE
aa 268-271	SPQT
aa 273-276	SPDL

3.1.3 S29 IS PHOSPHORYLATED BY CK2 AND GSK3

Mass spectrometry analysis demonstrated that serine 29 is phosphorylated by CK2 and GSK3.

a)

AT-3	Kinase	Peptide	Species	Predicted mass	Identified mass
	CK2				
Wild type		^{27}YFSPVE^{32}	P-Ser -18	723.34	723.30
		^{27}YFSPVELSSIAHQLDEEE^{44}	P-Ser +80	2172.97	2172.32
		^{8}KQEGSLCAQHCLNNLLQGEYFSPVE^{32}	P-Ser +80	3001.35	3002.13
		^{3}SIFHEKQEGSLCAQHCLNNLLQGEYFSPVE^{32}	P-Ser -18	3516.64	3516.00
	GSK3				
Wild type		^{27}YFSPVE^{32}	P-Ser -18	723.34	723.53
		^{27}YFSPVELSSIAHQLDEEE^{44}	P-Ser +80	2172.97	2173.00
		^{8}KQEGSLCAQHCLNNLLQGEYFSPVE^{32}	P-Ser +80	3001.35	3001.00

b)

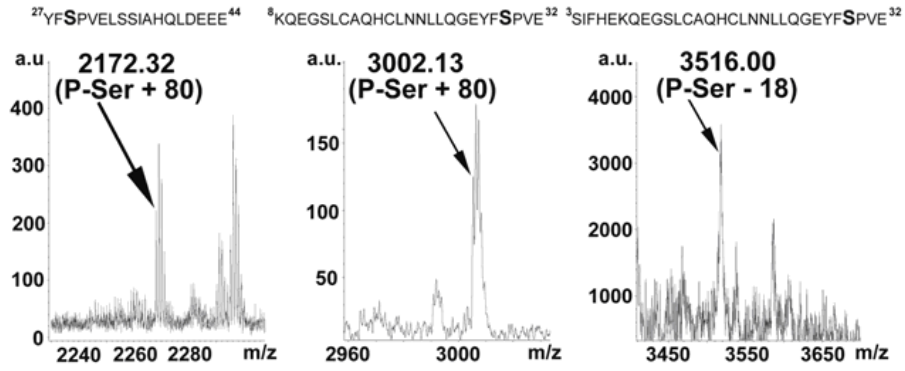

Figure 3.3 AT-3 is phosphorylated on Ser 29 by CK2 and GSK3 (a) 8 µg of AT-3 was phosphorylated *in vitro* either by CK2 or GSK3. Samples were denatured in 8 M urea and subjected to reduction and alkylation in solution by iodoacetamide. After dilution and incubation with GluC endoproteinases (1:25 enzyme/protein, w/w) overnight at 37°C, samples were analysed by Mass analysis. The presence of the phosphate group results in an increase in mass of 80 units or in a decrease of 18

units due to the loss of the phosphate and a water molecule. **(b)** Peak at 2172.32 *m/z* corresponding to the CK2 phosphorylated peptide 27-44 (^{27}YF**S**PVELSSIAHQLDEEE^{44}, calculated average mass 2172.97), peak at 3002.13 *m/z* corresponding to the CK2 phosphorylated peptide 8-32 (^{8}KQEGSLCAQHCLNNLLQGEYF**S**PVE^{32}, calculated monoisotopic mass 3001.35) and peak at 3516.00 *m/z* corresponding to the CK2 phosphorylated peptide 3-32 (^{3}SIFHEKQEGSLCAQHCLNNLLQGEYF**S**PVE^{32}, calculated monoisotopic mass 3516.64) are indicated. Data are representative of one of three experiments.

Operating in the linear mode, upon incubation of wild-type AT-3 with either CK2 or GSK3, it was possible to detect peaks corresponding to monophosphorylated peptides containing S29 (Figure 3.3). A list of the phosphorylated peptides identified through mass spectrometry is reported in Figure 3.3a. The peak at 3002.13 *m/z* was also analyzed by MS/MS TOF-TOF analysis unequivocally confirming the phosphorylation of AT-3 on S29 residue (data not shown). Upon phosphatase treatment the corresponding non-phosphorylated peaks were detected (data not shown). Figure 3.3b reports three of the spectra relative to the peptides, obtained after phosphorylation with CK2: peak at 2172.32 *m/z* corresponds to the phosphorylated peptide 27-44 (^{27}YF**S**PVELSSIAHQLDEEE^{44}, calculated average mass 2172.97), peak at 3002.13 *m/z* corresponds to the phosphorylated peptide 8-32 (^{8}KQEGSLCAQHCLNNLLQGEYF**S**PVE^{32}, calculated monoisotopic mass 3001.35) and peak at 3516.00 *m/z* corresponds to the phosphorylated peptide 3-32 (^{3}SIFHEKQEGSLCAQHCLNNLLQGEYF**S**PVE^{32}, calculated monoisotopic mass 3516.64).
Taken together, these results provide evidence that AT-3 is phosphorylated *in vitro* on residue S29 by CK2 and GSK3 and suggest a direct role of these kinases in *in vivo* phosphorylation of AT-3 within the Josephin domain.

3.2 SUB-CELLULAR LOCALIZATION OF ATAXIN-3 PHOSPHORYLATION MUTANTS

3.2.1 CONSTRUCTS

cDNAs encoding for murine ataxin-3 (AT-3Q6) and human pathological ataxin-3 (AT-3Q72) were subcloned from plasmid *pcDNA3X(+HA)* into plasmid *pcDNA3.1/myc-His*; the recombinant proteins carry N-terminal HA and C-terminal *c-myc* epitopes.

Phosphorylation mutants were obtained by PCR substituting serines and threonine with alanines or aspartate (to mimic phosphorylation as a control); the following mutants were obtained:

- AT-3Q6S272A
- AT-3Q6S277A
- AT-3Q6DM (S272A and S277A)
- AT-3Q6TM (T271A, S272A and S277A)
- AT-3Q6QM (S268A, T271A, S272A, S273A and S277A)
- AT-3Q6S29A
- AT-3Q6S29D
- AT-3Q72S29A
- AT-3Q6M (S29A, S329A and S341A)

All constructs were hosted and amplified in *E. coli* strain DH5α, while protein expression was achieved after transient transfection of COS-7 or SHSY-5Y cells. Cultures were carried out in 94 mm plates or onto coverslips in DMEM containing 10% fetal bovine serum (FBS), 100 U/ml penicillin, 100 μg/ml streptomycin and 4 mM glutamine (COS-7 cells) or in F12 and DMEM containing 10% fetal bovine serum (FBS), 100 U/ml penicillin, 100 μg/ml streptomycin and 4 mM glutamine (SHSY-5Y cells). Cells were subsequently transiently transfected with FuGENE6.

3.2.2 AT-3Q6S272A AND AT-3Q6S277A

3.2.2.1 CONFOCAL MICROSCOPY ANALYSIS

COS-7 cells were plated onto coverslips (2.5×10^4 cells/coverslip) and grown for 24 h before transfection. Cells were transfected overnight with FuGENE6 and AT-3Q6, AT-3Q6S272A or AT-3Q6S277A. 24 h after transfection cells were doubly stained with anti-*c-myc* mouse monoclonal antibody to visualize C-terminal fragments of AT-3 and anti-HA rabbit polyclonal antibody to visualize N-terminal fragments of AT-3. After extensive washes, cells were incubated with donkey anti-mouse Cy3 conjugated antibody (red) and donkey anti-rabbit Cy2 conjugated antibody (green).

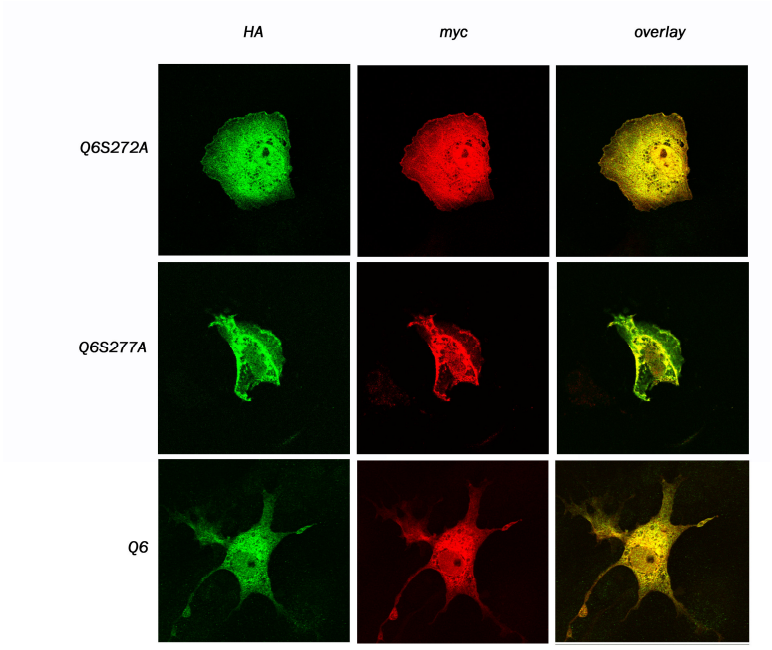

Figure 3.4 Confocal microscopy analysis of AT-3Q6S272A and AT-3Q6S277A sub-cellular localization. COS-7 cells were transfected with cDNAs coding for AT-3Q6, AT-3Q6S272A or AT-3Q6S277A mutants. To investigate sub-cellular localization of AT-3, cells were fixed in PFA and probed with mouse monoclonal anti-*c-myc* (red) and rabbit monoclonal anti-HA antibodies (green).

Confocal microscopy analysis (Figure 3.4) shows that AT-3Q6S272A and AT-3Q6S277A localize in the cytoplasm as well as in the nucleus, showing the same localization of the wild-type. The overlays show that N-terminal and C-terminal fragments co-localize.

Cells were also incubated with anti-*c-myc* rabbit monoclonal antibody to visualize AT-3 and mouse anti-*cyt-c* monoclonal antibody for mitochondria visualization. After extensive washes, cells were incubated with donkey anti-rabbit Cy3 (red) and donkey anti-mouse Cy2 (green) antibodies.

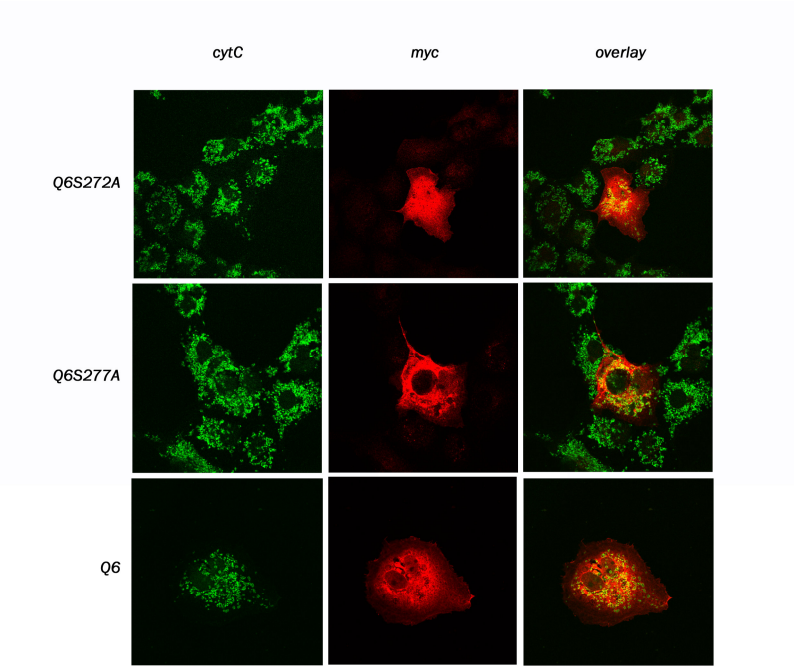

Figure 3.5 Confocal microscopy analysis of AT-3Q6S272A and AT-3Q6S277A mitochondrial localization. COS-7 cells were transfected with cDNAs coding for AT-3Q6, AT-3Q6S272A or AT-3Q6S277A mutants. To investigate mitochondrial localization of AT-3, cells were fixed in PFA and probed with rabbit monoclonal anti-*c-myc* (red) and mouse monoclonal anti-*cytocrome-c* antibodies (green).

Confocal microscopy analysis (Figure 3.5) shows that AT-3Q6S272A and AT-3Q6S277A localize also in mitochondria as wild-type. The overlays show that AT-3 co-localizes with *cytocrome-c* in mitochondria.

3.2.2.2 CELL FRACTIONATION

COS-7 cells were cultured in 94 mm plates (6×10^5 cells/plate) and grown for 24 h before transfection. Cells were transfected overnight with FuGENE6 and *pcDNA3.1/mic-His*, AT-3Q6, AT-3Q6S272A or AT-3Q6S277A. 24 h after transfection cells were harvested and cytosolic and nuclear fractions were obtained. After SDS-PAGE and Western blot, membranes were incubated with anti-*c-myc* mouse monoclonal antibody to visualize AT-3 and with anti-vinculin, anti-

fibrillarin and anti-PGK mouse monoclonal antibodies as fractionation and loading controls.

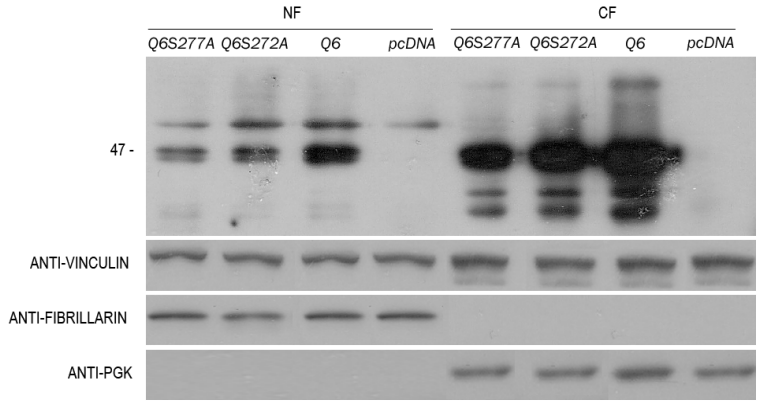

Figure 3.6 Western-blot analysis of AT-3Q6S272A and AT-3Q6S277A sub-cellular localization. *c-myc* tagged AT-3Q6 and its mutants AT-3Q6S272A and AT-3Q6S277A were expressed in COS-7 cells. Western-blots of cytosolic and nuclear fractions were probed with a monoclonal anti-*c-myc* antibody. Cytosolic and nuclear fractions controls were performed with anti-fibrillarin and anti-PGK antibodies, while loading control was performed with anti-vinculin antibody. COS-7 cells were transfected also with empty *pcDNA3.1/myc-His* as control.

Western-blot analysis of AT-3Q6S272A and AT-3Q6S277A sub-cellular localization (Figure 3.6) shows that they localize in cytosol and also in the nucleus as the wild-type. Moreover both mutants are subjected to the same proteolytic cleavage as the wild-type.

3.2.2.3 MITOCHONDRIA ISOLATION

COS-7 cells were cultured in 94 mm plates (6×10^5 cells/plate) and grown for 24 h before transfection. Cells were transfected overnight with FuGENE6 and *pcDNA3.1/myc-His*, AT-3Q6, AT-3Q6S272A or AT-3Q6S277A. 24 h after transfection cells were harvested and mitochondria membranes, lysosomal, mitochondria and cytosolic soluble fractions were obtained. After SDS-PAGE and Western blot, membranes were incubated with Z46 rabbit polyclonal antibody to visualize AT-3 and with anti-VDAC and anti-SOD2 rabbit polyclonal antibodies as mitochondria isolation controls.

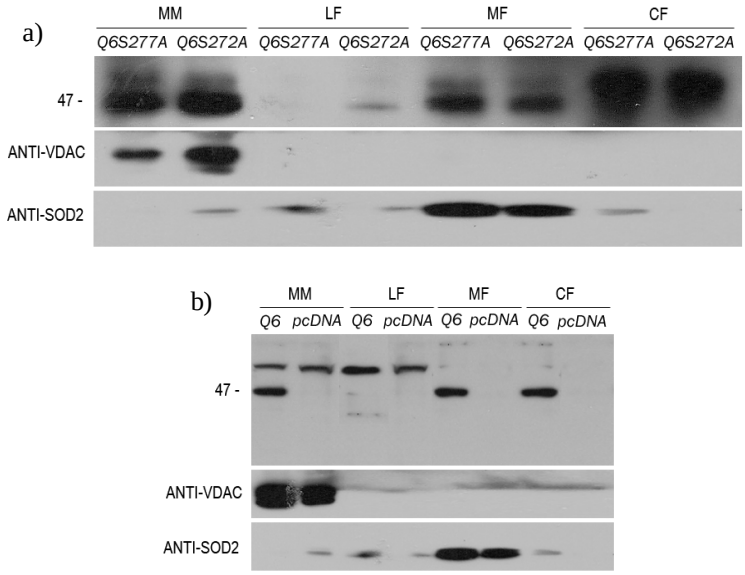

Figure 3.7 Western-blot analysis of AT-3Q6S272A and AT-3Q6S277A mitochondrial localization. *c-myc* tagged AT-3Q6 **(b)** and its mutants AT-3Q6S272A and AT-3Q6S277A **(a)** were expressed in COS-7 cells. Western-blots of mitochondrial membranes and lysosomal, mitochondrial and cytosolic soluble fractions were probed with a polyclonal Z46 antibody. Mitochondrial membranes and mitochondrial soluble fraction controls were performed with anti-VDAC and anti-SOD2 antibodies. **(b)** COS-7 cells were transfected also with empty *pcDNA3.1/myc-His* as a control.

Western-blot analysis of AT-3Q6S272A and AT-3Q6S277A mitochondrial localization (Figure 3.7) shows that they localize in mitochondrial membranes and also in mitochondrial soluble fraction as the wild-type.

3.2.3 AT-3Q6DM AND AT-3Q6TM

3.2.3.1 CONFOCAL MICROSCOPY ANALYSIS

COS-7 cells were plated onto coverslips (2.5×10^4 cells/coverslip) and grown for 24 h before transfection. Cells were transfected overnight with FuGENE6 and AT-3Q6, AT-3Q6DM or AT-3Q6TM. 24 h after transfection cells were doubly stained with anti-*c-myc* mouse monoclonal antibody to visualize C-terminal fragments of AT-3 and anti-HA rabbit polyclonal antibody to visualize N-terminal fragments of AT-3. After extensive washes, cells were incubated with donkey

anti-mouse Cy3 conjugated antibody (red) and donkey anti-rabbit Cy2 conjugated antibody (green).

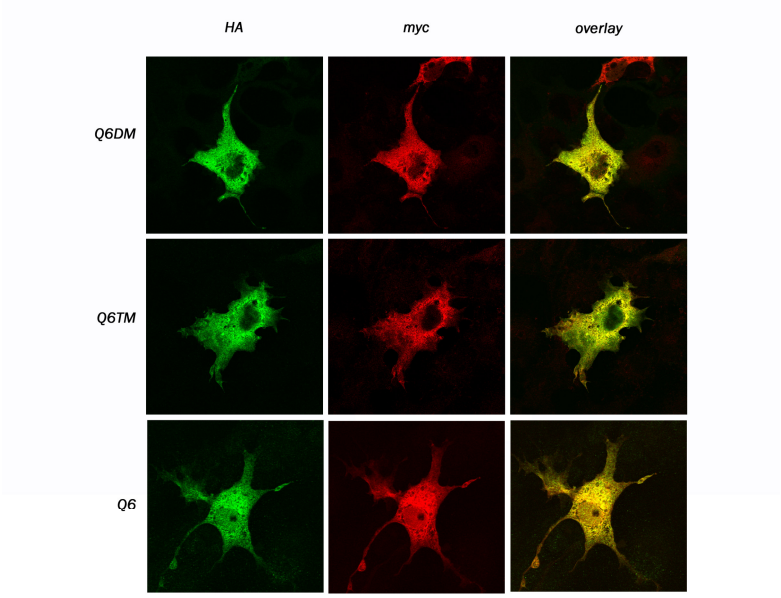

Figure 3.8 Confocal microscopy analysis of AT-3Q6DM and AT-3Q6TM sub-cellular localization. COS-7 cells were transfected with cDNAs coding for AT-3Q6, AT-3Q6DM or AT-3Q6TM mutants. To investigate sub-cellular localization of AT-3, cells were fixed in PFA and probed with mouse monoclonal anti-*c-myc* (red) and rabbit monoclonal anti-HA antibodies (green).

The confocal analysis (Figure 3.8) shows that AT-3Q6DM and AT-3Q6TM localize in the cytoplasm as well as in the nucleus, so they have the same localization of the wild-type. The overlays show that N-terminal and C-terminal fragments co-localize.

Cells were also incubated with anti-*c-myc* rabbit monoclonal antibody to detect AT-3 and mouse anti-*cyt-c* monoclonal antibody for mitochondria visualization. After extensive washes, cells were incubated with donkey anti-rabbit Cy3 (red) and donkey anti-mouse Cy2 (green) antibodies.

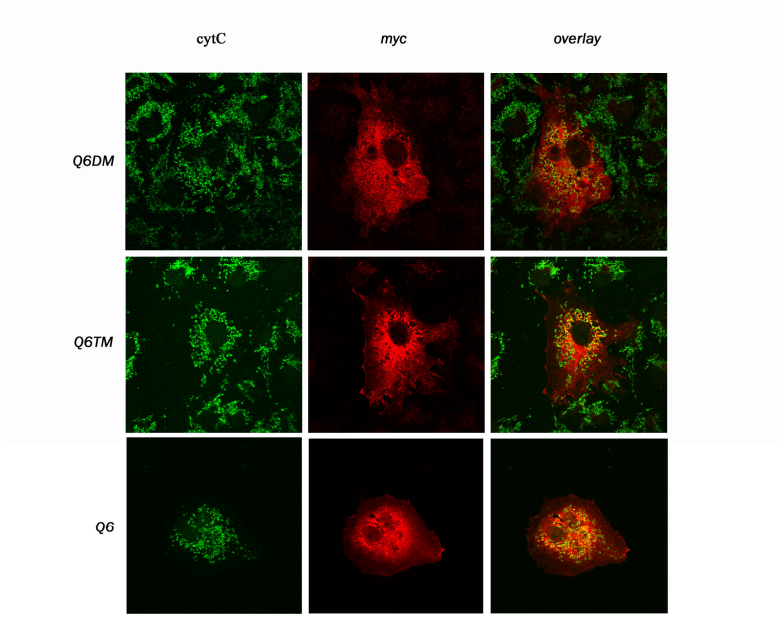

Figure 3.9 Confocal microscopy analysis of AT-3Q6DM and AT-3Q6TM mitochondrial localization. COS-7 cells were transfected with cDNAs coding for AT-3Q6, AT-3Q6DM or AT-3Q6TM mutants. To investigate mitochondrial localization of AT-3, cells were fixed in PFA and probed with rabbit monoclonal anti-*c-myc* (red) and mouse monoclonal anti-*cytocrome-c* antibodies (green).

Confocal microscopy analysis (Figure 3.9) shows that AT-3Q6DM and AT-3Q6TM also localize in mitochondria as the wild-type. The overlays show that AT-3 co-localizes with *cytocrome-c* in mitochondria.

3.2.3.2 CELL FRACTIONATION

COS-7 cells were cultured in 94 mm plates (6×10^5 cells/plate) and grown for 24 h before transfection. Cells were transfected overnight with FuGENE6 and AT-3Q6, AT-3Q6DM or AT-3Q6TM. 24 h after transfection cells were harvested and cytosolic and nuclear fractions were obtained. After SDS-PAGE and Western blot, membranes were incubated with anti-*c-myc* mouse monoclonal antibody to visualize AT-3 and with anti-vinculin, anti-fibrillarin and anti-PGK mouse monoclonal antibodies as fractionation and loading controls.

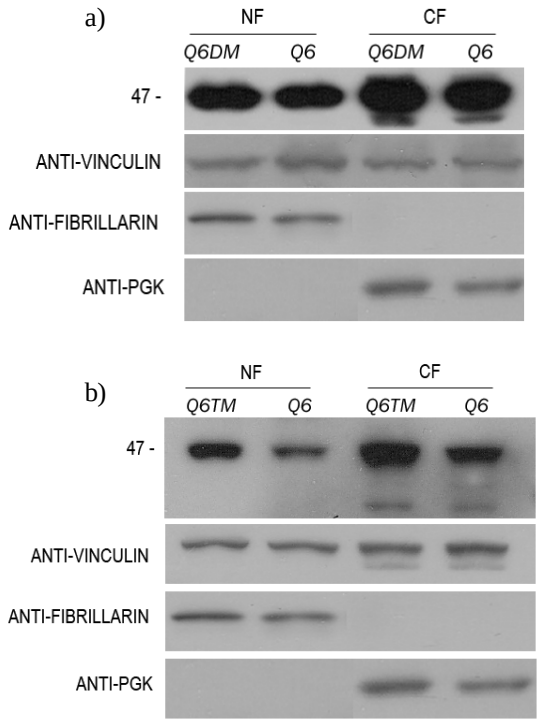

Figure 3.10 Western-blot analysis of AT-3Q6DM and AT-3Q6TM sub-cellular localization. *c-myc* tagged AT-3Q6 and its mutants AT-3Q6DM **(a)** and AT-3Q6TM **(b)** were expressed in COS-7 cells. Western-blots of cytosolic and nuclear fractions were probed with a monoclonal anti-*c-myc* antibody. Cytosolic and nuclear fractions controls were performed with anti-fibrillarin and anti-PGK antibodies, while loading control was performed with anti-vinculin antibody.

Western-blot analysis of AT-3Q6DM and AT-3Q6TM sub-cellular localization (Figure 3.10) shows that they localize in cytosol and also in nucleus as wild-type. Both mutants are subjected to the same proteolytic cleavage as the wild-type.

3.2.3.3 MITOCHONDRIA ISOLATION

COS-7 cells were cultured in 94 mm plates (6×10^5 cells/plate) and grown for 24 h before transfection. Cells were transfected overnight with FuGENE6 and *pcDNA3.1/myc-His*, AT-3Q6, AT-3Q6DM or AT-3Q6TM. 24 h after transfection cells were harvested and mitochondrial membranes, as well as lysosomal, mitochondrial and

cytosolic soluble fractions were obtained. After SDS-PAGE and Western blot, membranes were incubated with Z46 rabbit polyclonal antibody to visualize AT-3 and with anti-VDAC and anti-SOD2 rabbit polyclonal antibodies as mitochondria isolation controls.

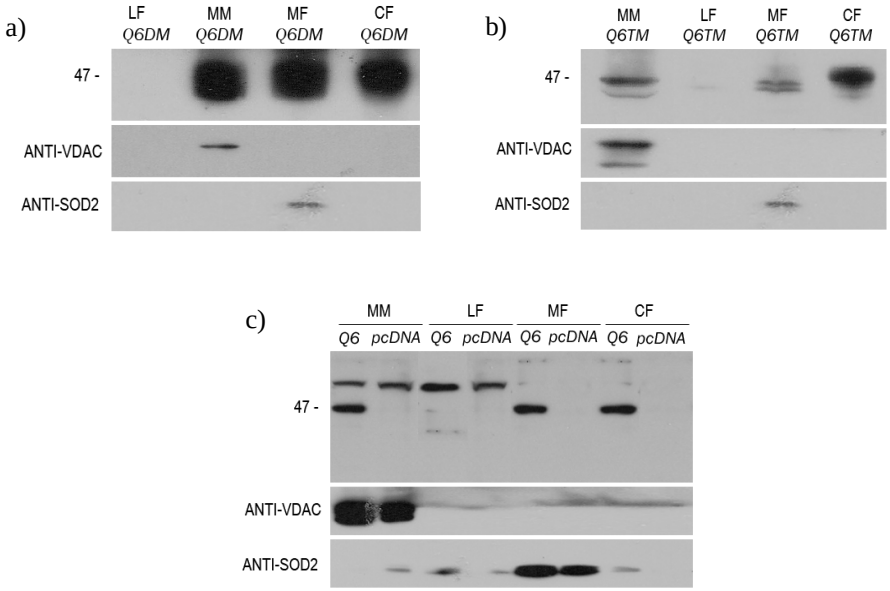

Figure 3.11 Western-blot analysis of AT-3Q6DM and AT-3Q6TM mitochondrial localization. *c-myc* tagged AT-3Q6 **(c)** and its mutants AT-3Q6DM **(a)** and AT-3Q6TM **(b)** were expressed in COS-7 cells. Western-blots of mitochondrial membranes and lysosomal, mitochondrial and cytosolic soluble fractions were probed with a polyclonal Z46 antibody. Mitochondrial membranes and mitochondrial soluble fraction controls were performed with anti-VDAC and anti-SOD2 antibodies. **(c)** COS-7 cells were transfected also with empty *pcDNA3.1/myc-His* as a control.

Western-blot analysis of AT-3Q6DM and AT-3Q6TM mitochondrial localization (Figure 3.11) shows that they localize in mitochondrial membranes and also in mitochondrial soluble fraction as the wild-type.

3.2.4 AT-3Q6QM

3.2.4.1 CELL FRACTIONATION

COS-7 cells were cultured in 94 mm plates (6×10^5 cells/plate) and grown for 24 h before transfection. Cells were transfected overnight with FuGENE6 and AT-3Q6 or AT-3Q6QM. 24 h after transfection cells were harvested and cytosolic and nuclear fractions were obtained. After SDS-PAGE and Western blot, membranes were incubated with anti-*c-myc* mouse monoclonal antibody to visualize AT-3 and with anti-fibrillarin and anti-PGK mouse monoclonal antibodies as fractionation controls.

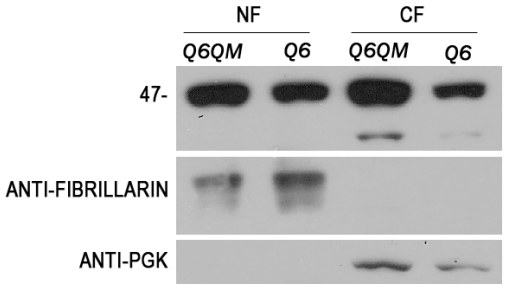

Figure 3.12 Western-blot analysis of AT-3Q6QM sub-cellular localization. *c-myc* tagged AT-3Q6 and its mutant AT-3Q6QM were expressed in COS-7 cells. Western-blots of cytosolic and nuclear fractions were probed with a monoclonal anti-*c-myc* antibody. Cytosolic and nuclear fractions controls were performed with anti-fibrillarin and anti-PGK antibodies.

Western-blot analysis of AT-3Q6QM sub-cellular localization (Figure 3.12) shows that it localizes in cytosol and also in nucleus as wild-type. Moreover, the mutant is subjected to the same proteolytic cleavage as the wild-type.

3.2.4.2 MITOCHONDRIA ISOLATION

COS-7 cells were cultured in 94 mm plates (6×10^5 cells/plate) and grown for 24 h before transfection. Cells were transfected overnight with FuGENE6 and *pcDNA3.1/myc-His*, AT-3Q6 or AT-3Q6QM. 24 h after transfection cells were harvested and mitochondrial membranes, as well as lysosomal, mitochondrial and cytosolic soluble fractions were obtained. After SDS-PAGE and Western blot, membranes were incubated with Z46 rabbit polyclonal antibody to

visualize AT-3 and with anti-VDAC and anti-SOD2 rabbit polyclonal antibodies as mitochondria isolation controls.

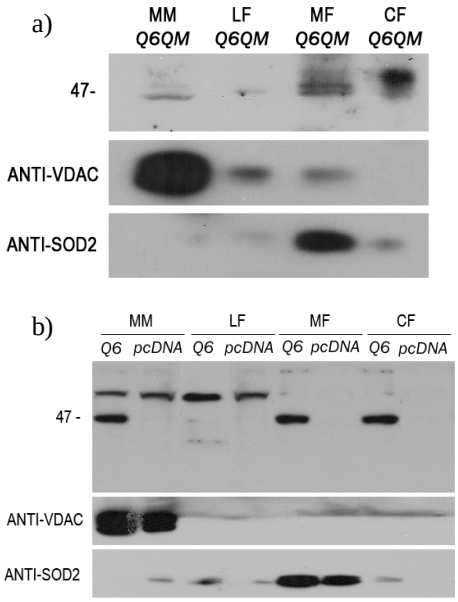

Figure 3.13 Western-blot analysis of AT-3Q6QM mitochondrial localization. *c-myc* tagged AT-3Q6 **(b)** and its mutant AT-3Q6QM **(a)** were expressed in COS-7 cells. Western-blots of mitochondrial membranes and lysosomal, mitochondrial and cytosolic soluble fractions were probed with a polyclonal Z46 antibody. Mitochondrial membranes and mitochondrial soluble fraction controls were performed with anti-VDAC and anti-SOD2 antibodies. **(b)** COS-7 cells were transfected also with empty *pcDNA3.1/myc-His* as a control.

Western-blot analysis of AT-3Q6QM mitochondrial localization (Figure 3.13) shows that it localizes in mitochondrial membranes and also in mitochondrial soluble fraction as the wild-type.

3.2.5 AT-3Q6S29A AND AT-3Q6S29D

3.2.5.1 CONFOCAL MICROSCOPY ANALYSIS

COS-7 cells were plated onto coverslips (2.5×10^4 cells/coverslip) and grown for 24 h before transfection. Cells were transfected overnight with FuGENE6 and AT-3Q6, AT-3Q6S29A or AT-3Q6S29D. 24 h after transfection cells were doubly stained with anti-*c-myc* mouse monoclonal antibody to visualize C-terminal fragments of AT-3 and anti-HA rabbit polyclonal antibody to visualize N-terminal fragments

of AT-3. After extensive washes, cells were incubated with donkey anti-mouse Cy3 conjugated antibody (red) and donkey anti-rabbit Cy2 conjugated antibody (green). At the end cells were incubated with TO-PRO-3 iodide to visualize nuclei.

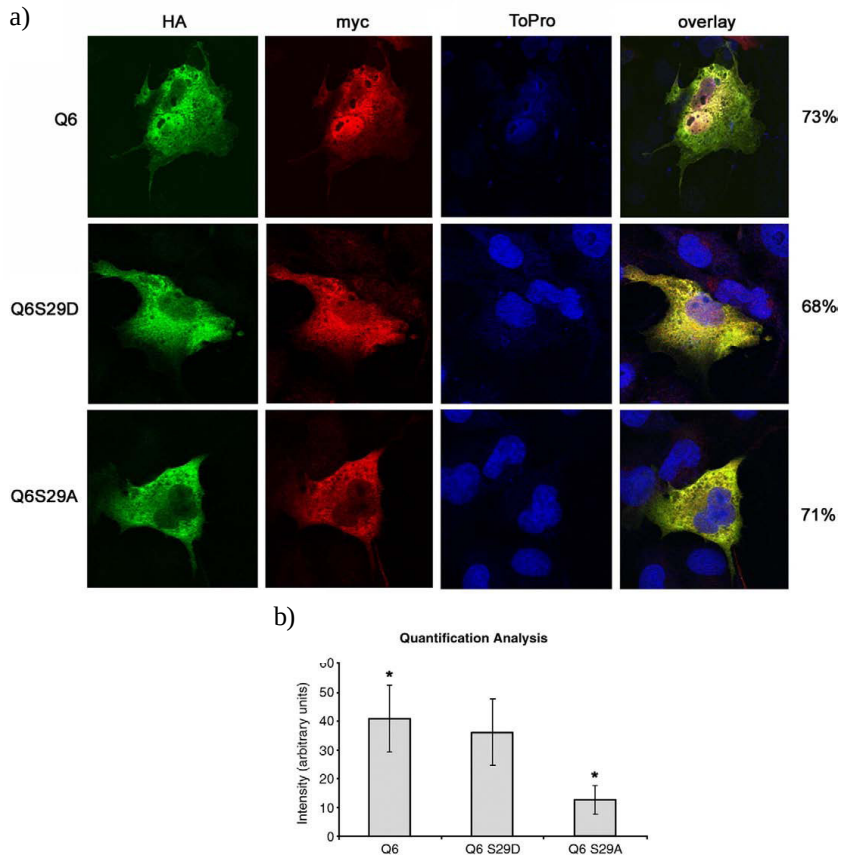

Figure 3.14 Confocal microscopy analysis of AT-3Q6S29A and AT-3Q6S29D sub-cellular localization. (a) COS-7 cells were transfected with cDNAs coding for AT-3Q6, AT-3Q6S29A or AT-3Q6S29D mutants. To investigate sub-cellular localization of AT-3, cells were fixed in PFA and probed with mouse monoclonal anti-*c-myc* (red), rabbit monoclonal anti-HA antibodies (green) and the nuclear marker TO-PRO-3 iodide (blue). **(b)** Quantification analysis of AT-3 nuclear localization. Statistical analysis was performed using t-Student test (*$p<0.05$).

The confocal analysis (Figure 3.14a) shows that AT-3Q6 fluorescence was evenly distributed inside the cells. On the other hand, AT-3Q6S29A mutant fluorescence was found to be much weaker inside the nucleus than in the cytoplasm. The overlay with the blue

fluorescence emission of the nuclear marker confirmed that wild-type AT-3 is found also inside the nucleus, while AT-3Q6S29A mutant is found predominantly in the cytosol. Quantitative analysis of fluorescent emission allowed to assess that AT-3Q6S29A mutant fluorescence in the nuclear region amounted to about 30% of wild-type AT-3 fluorescence in the same area (Figure 3.14b), the significance of this result is demonstrated by a p-value <0.05 of AT-3Q6S29A versus AT-3Q6 nuclear localization.
AT-3Q6S29D shows a uniform fluorescence distribution inside the cells (Figure 3.14a) as the wild-type, the overlay showing colocalization with the nuclear marker. Quantitative fluorescence analysis confirmed that AT-3Q6S29D fluorescence in the nuclear region did not remarkably differ from that of wild-type AT-3Q6 (Figure 3.14b), in fact p-value is >0.05. This result confirms that AT-3Q6S29A phenotype is due to lacking phosphorylation and not to the aminoacidic substitution.
Moreover the same percentage of cells showing the described AT-3 subcellular localization was found in all samples considered, as shown in the last column of Figure 3.14a. Cell viability, assayed through MTT test, showed a 30% reduction for AT-3Q6S29A mutant, when compared to both wild-type protein and AT-3Q6S29D mutant, the significance of this result is demonstrated by a p-value <0.05 of AT-3Q6S29A versus AT-3Q6 cell viability.

Cells transfected with AT-3Q6 and AT-3Q6S29A were also incubated with anti-*c-myc* rabbit monoclonal antibody to visualize AT-3 and mouse anti-*cyt-c* monoclonal antibody for mitochondria visualization. After extensive washes, cells were incubated with donkey anti-rabbit Cy3 (red) and donkey anti-mouse Cy2 (green) antibodies.

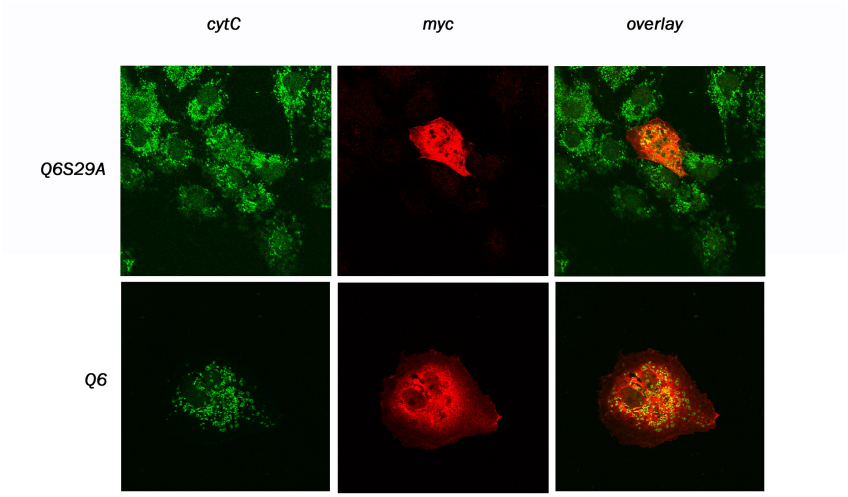

Figure 3.15 Confocal microscopy analysis of AT-3Q6S29A mitochondrial localization. COS-7 cells were transfected with cDNAs coding for AT-3Q6 or AT-3Q6S29A mutant. To investigate mitochondrial localization of AT-3, cells were fixed in PFA and probed with rabbit monoclonal anti-*c-myc* (red) and mouse monoclonal anti-*cytocrome-c* antibodies (green).

Confocal microscopy analysis (Figure 3.15) shows that AT-3Q6S29A localizes also in mitochondria as the wild-type. The overlays show that AT-3 co-localizes with *cytocrome-c* in mitochondria.

3.2.5.2 CELL FRACTIONATION

COS-7 cells (6×10^5 cells/plate) and SHSY-5Y cells (1×10^6 cells/plate) were cultured in 94 mm plates and grown for 24 h before transfection. Cells were transfected overnight with FuGENE6 and AT-3Q6, AT-3Q6S29A or AT-3Q6S29D (COS-7) and with FuGENE6 and AT-3Q6 or AT-3Q6S29A (SHSY-5Y). 24 h after transfection cells were harvested and cytosolic and nuclear fractions were obtained. After SDS-PAGE and Western blot, membranes were incubated with anti-*c-myc* mouse monoclonal antibody to visualize AT-3 and with anti-fibrillarin and anti-PGK mouse monoclonal antibodies as fractionation and loading controls.

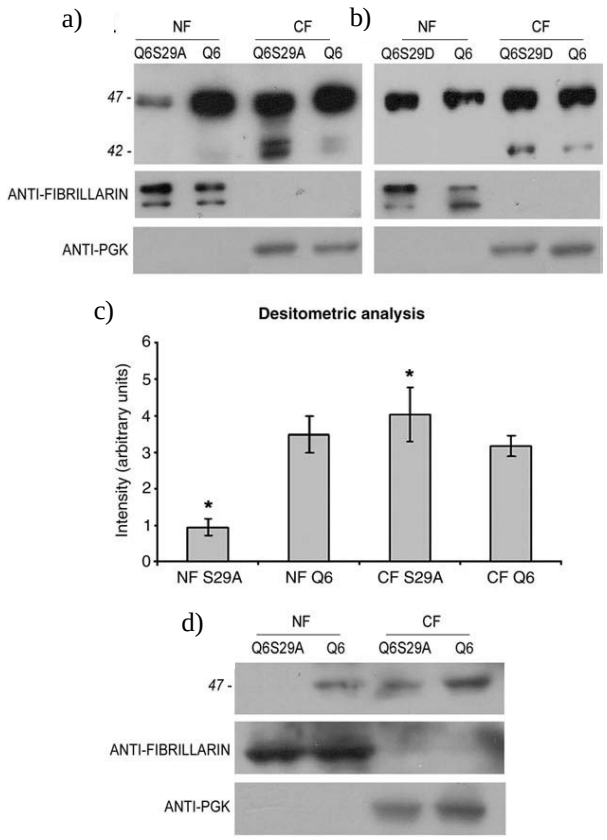

Figure 3.16 Western-blot analysis of AT-3Q6S29A and AT-3Q6S29D sub-cellular localization. *c-myc* tagged AT-3Q6 **(a,b)** and its mutants AT-3Q6S29A **(a)** and AT-3Q6S29D **(b)** were expressed in COS-7 cells. Western-blots of cytosolic and nuclear fractions were probed with a monoclonal anti-*c-myc* antibody. Cytosolic and nuclear fractions controls were performed with anti-fibrillarin and anti-PGK antibodies. **(c)** Densitometric analysis performed with NIH Image-based software Scion Image (Scion Corporation) on blot reported in panel a. Quantification data are a mean of three independent experiments; bands intensities were normalized on fibrillarin and PGK controls. *$p<0.05$ (t-Student test). **(d)** *c-myc* tagged AT-3Q6 and its mutant AT-3Q6S29A were expressed in SHSY-5Y cells. Western-blots of cytosolic and nuclear fractions were probed with a monoclonal anti-*c-myc* antibody. Cytosolic and nuclear fractions controls were performed with anti-fibrillarin and anti-PGK antibodies.

Western blot analysis (Figure 3.16a) shows that the band corresponding to wild-type AT-3Q6 is found equally distributed between the cytoplasm and the nucleus. On the contrary, the band corresponding to AT-3Q6S29A mutant is found much less abundant in the nuclear fraction, being about 25% of the intensity of the

corresponding cytosolic band, as shown by densitometric analysis (Figure 3.16c); this suggests that S29 phosphorylation promotes AT-3 nuclear uptake. The significance of this results is demonstrated by a p-value <0.05 of AT-3Q6S29A nuclear localization versus cytosolic localization.
Results, shown in Figure 3.16b, show that AT-3Q6S29D behaves exactly like the wild-type, being equally distributed in the nucleus and the cytoplasm.
In order to rule out the possibility that the observed phenotype of AT-3Q6S29A mutant might be confined to COS-7 cells, human neuroblastoma SHSY-5Y cells were also transfected with AT-3Q6 or AT-3Q6S29A. Results, reported in Figure 3.16d, show the absence of AT-3Q6S29A in the nuclear fraction, in accordance with what observed in COS-7 cells.

3.2.5.3 MITOCHONDRIA ISOLATION

COS-7 cells were cultured in 94 mm plates (6×10^5 cells/plate) and grown for 24 h before transfection. Cells were transfected overnight with FuGENE6 and *pcDNA3.1/myc-His*, AT-3Q6 or AT-3Q6S29A. 24 h after transfection cells were harvested and mitochondria membranes, lysosomal, mitochondria and cytosolic soluble fractions were obtained. After SDS-PAGE and Western blot, membranes were incubated with Z46 rabbit polyclonal antibody to visualize AT-3 and with anti-VDAC and anti-SOD2 rabbit polyclonal antibodies as mitochondria isolation controls.

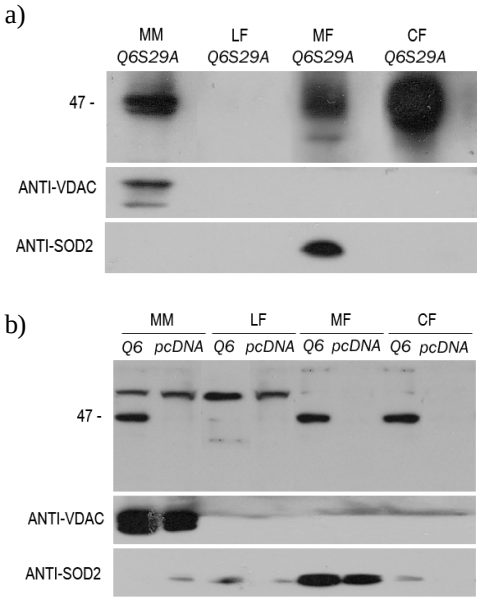

Figure 3.17 Western-blot analysis of AT-3Q6S29A mitochondrial localization. *c-myc* tagged AT-3Q6 **(b)** and its mutant AT-3Q6S29A **(a)** were expressed in COS-7 cells. Western-blots of mitochondrial membranes, as well as lysosomal, mitochondrial and cytosolic soluble fractions were probed with a polyclonal Z46 antibody. Mitochondrial membranes and mitochondrial soluble fraction controls were performed with anti-VDAC and anti-SOD2 antibodies. **(b)** COS-7 cells were transfected also with empty *pcDNA3.1/myc-His* as a control.

Western-blot analysis of AT-3Q6S29A mitochondrial localization (Figure 3.17) shows that it localizes in mitochondrial membranes and also in mitochondrial soluble fraction as the wild-type.

3.2.5.4 INCUBATION WITH CK2 AND GSK3 INHIIBITORS

COS-7 cells were cultured in 94 mm plates (6×10^5 cells/plate) and grown for 24 h before transfection. Cells were transfected overnight with FuGENE6 and AT-3Q6 or AT-3Q6S29D. To inhibit CK2 and GSK3, COS-7 cells were incubated for 24 h with either 5 or 10 μM CK2 inhibitor (TBB) and/or with 10 μM GSK3 inhibitor (SB). 24 h after transfection cells were harvested and cytosolic and nuclear fractions were obtained. After SDS-PAGE and Western blot, membranes were incubated with anti-*c-myc* mouse monoclonal antibody to visualize AT-3 and with anti-fibrillarin and anti-PGK mouse monoclonal antibodies as fractionation and loading controls.

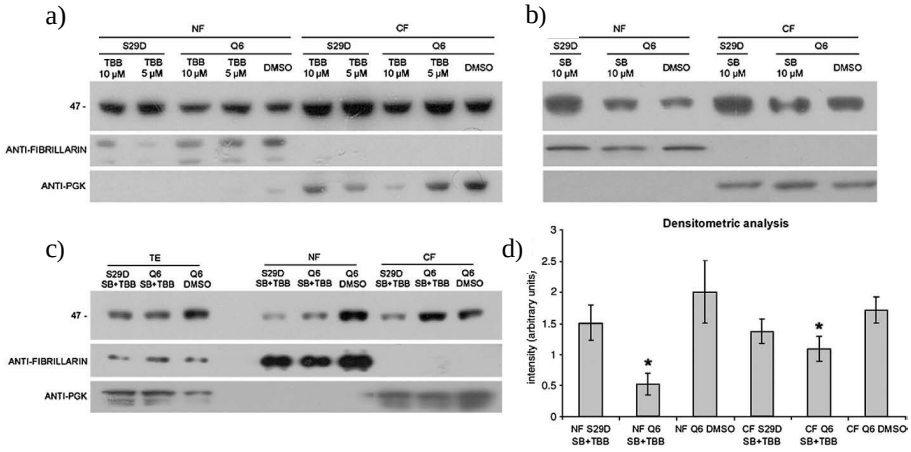

Figure 3.18 Western-blot analysis of COS-7 cells treated with kinase inhibitors. **(a)** *c-myc* tagged full-length AT-3Q6 and its mutant AT-3Q6S29D were expressed in COS-7 cells treated with TBB 5 or 10 μM (CK2 inhibitor) or with DMSO, as a control. **(b)** *c-myc* tagged full-length AT-3Q6 and its mutant AT-3Q6S29D were expressed in COS-7 cells treated with SB 216763 10μM (GSK3 inhibitor) or with DMSO, as a control. **(c)** *c-myc* tagged full-length AT-3Q6 and its mutant AT-3Q6S29D were expressed in COS-7 cells treated with both TBB 10μM (CK2 inhibitor) and SB 216763 10μM (GSK3 inhibitor) or with DMSO, as a control. **(d)** Densitometric analysis performed with NIH Image-based software Scion Image (Scion Corporation) on blot reported in panel c. Quantification data are a mean of three independent experiments; bands intensities were normalized on fibrillarin and PGK controls. *$p<0.05$ (t-Student test). **(a,b,c,)** Western-blots of total extracts, cytosolic fraction and nuclear fraction were probed with a monoclonal anti-*c-myc* antibody. Cytosolic and nuclear fractions controls were performed with anti-fibrillarin and anti-PGK antibodies.

When the culture medium was supplemented with TBB alone, as shown in Figure 3.18a, both wild-type AT-3Q6 and AT-3Q6S29D mutant were found evenly distributed between the cytosol and the nucleus, suggesting that TBB could not prevent S29 phosphorylation even at 10 μM concentration. The same happened when only GSK3 inhibitor SB216763 was administered at 10 μM concentration, as shown in Figure 3.18b.

However, when both inhibitors were added to culture medium, nuclear translocation of wild-type AT-3Q6 appeared to be reduced, a behaviour closely mirroring that of AT-3Q6S29A mutant (Figure 3.18c); on the contrary, AT-3Q6S29D mutant appeared to be uniformly distributed between nucleus and cytosol. Intensities of AT-3 bands in total extracts were found to be similar, showing that the mutation did not affect AT-3 expression levels. These data were

confirmed by densitometric analysis, reported in Figure 3.18d, showing that, when both inhibitors were administered, about 50% of the intensity of the corresponding cytosolic band of wild-type AT-3 was found inside the nucleus, while AT-3Q6S29D mutant was found to be equally distributed between the two cellular compartments. The significance of this results is demonstrated by a p-value <0.05 of AT-3Q6 nuclear localization versus cytosolic localization in the presence of both inhibitors.

3.2.5.5 MASS SPECTROMETRY ANALYSIS

COS-7 cells overexpressing AT-3Q6 were collected 24 h after transfection; the recombinant protein was immunoprecipitated from crude extracts with anti-AT-3Q6 polyclonal Z46 antibody and subsequently loaded onto SDS-PAGE. Bands were detected through acid silver staining and subjected to *in situ* digestion with GluC endoproteinase.

Table 3.5 AT-3 is phosphorylated on Ser29 in transfected cells. Cell homogenate was separated by SDS-PAGE and AT-3Q6 was subjected to reduction, alkylation and *in situ* digestion with GluC endoproteinase (1:10 enzyme/protein, w/w). Upon peptide extraction with 40% CH_3CN in 0.1% TFA, the peptide mixture was analyzed by mass spectrometry.

ATX3	Peptide	Species	Predicted mass	Identified mass
Wild type	^{27}YFSPVE^{32}	P-Ser +80	821.34	821.98
	^{27}YFSPVELSSIAHQLDEEE^{44}	P-Ser +80	2172.97	2173.02

Mass spectrometry analysis of the protein expressed in transfected cells (Table 3.5) unequivocally confirms that AT-3Q6 is phosphorylated at S29, since it is possible to detect phosphopeptides containing S29 upon fingerprint mass analysis (phosphopeptide ^{27}YF**S**PVE^{32}, calculated monoisotopic mass 821.34, experimental mass 821.98, and phosphopeptide ^{27}YF**S**PVELSSIAHQLDEEE^{44}, calculated monoisotopic mass 2172.97, experimental mass 2173.02).
Mass spectrometry analysis, performed on acid silver stained gels after AT-3Q6 immunoprecipitation from COS-7 cells cultured in the presence of both TBB and SB216763, allows to detect only peptides containing unmodified S29 showing that this residue is not phosphorylated when both CK2 and GSK3 inhibitors are present.

3.2.6 AT-3Q6M

3.2.6.1 CELL FRACTIONATION

COS-7 cells were cultured in 94 mm plates (6×10^5 cells/plate) and grown for 24 h before transfection. Cells were transfected overnight with FuGENE6 and AT-3Q6, AT-3Q6S29A or AT-3Q6M. 24 h after transfection cells were harvested and cytosolic and nuclear fractions were obtained. After SDS-PAGE and Western blot, membranes were incubated with anti-*c-myc* mouse monoclonal antibody to visualize AT-3 and with anti-fibrillarin and anti-PGK mouse monoclonal antibodies as fractionation and loading controls.

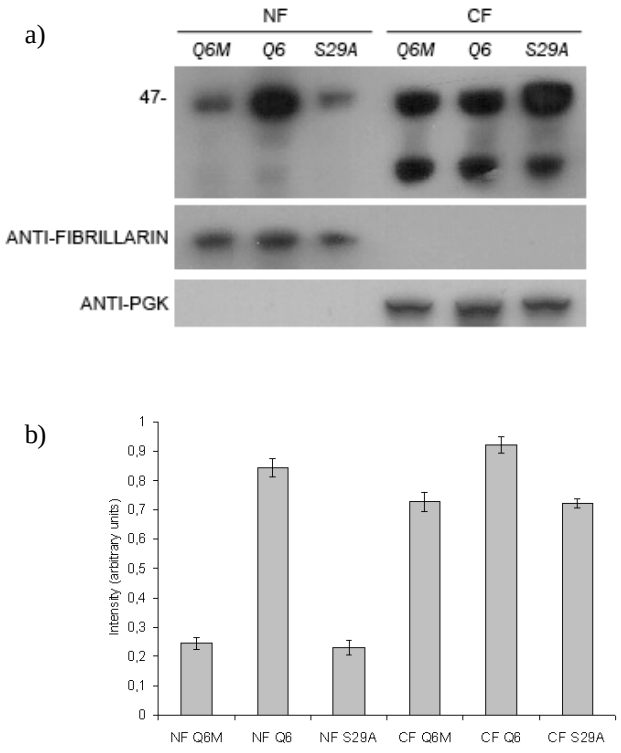

Figure 3.19 Western-blot analysis of AT-3Q6M sub-cellular localization. (a) *c-myc* tagged AT-3Q6 and its mutants AT-3Q6S29A or AT-3Q6M were expressed in COS-7 cells. Western-blots of cytosolic and nuclear fractions were probed with a monoclonal anti-*c-myc* antibody. Cytosolic and nuclear fractions controls were performed with anti-fibrillarin and anti-PGK antibodies. **(b)** Densitometric analysis performed with NIH Image-based software Scion Image (Scion Corporation) on blot reported in panel a. Quantification data are a mean of three independent experiments; bands intensities were normalized on fibrillarin and PGK controls.

Mueller and colleagues (Mueller *et al*., 2009) demonstrated that S329 and S341 control nuclear uptake of AT-3.
Western-blot analysis of AT-3Q6M sub-cellular localization (Figure 3.19a) shows that it has a lower localization in nucleus than wild-type, showing the same localization of AT-3Q6S29A. The lacking of S329 and S341 does not increment S29A phenotype. This result was confirmed by densitometric analysis (Figure 3.19b) that showed for both mutants, AT-3Q6S29A and AT-3Q6M, a band intensity in the nuclear fraction that is 30% of the band intensity in the cytosolic fraction, while AT-3Q6 showed the same band intensity in both fractions.

3.2.7 AT-3Q72S29A

3.2.7.1 CONFOCAL MICROSCOPY ANALYSIS

COS-7 cells were plated onto coverslips (2.5×10^4 cells/coverslip) and grown for 24 h before transfection. Cells were transfected overnight with FuGENE6 and AT-3Q72 or AT-3Q72S29A. 24 h after transfection cells were doubly stained with anti-*c-myc* mouse monoclonal antibody to visualize C-terminal fragments of AT-3 and anti-HA rabbit polyclonal antibody to visualize N-terminal fragments of AT-3. After extensive washes, cells were incubated with donkey anti-mouse Cy3 conjugated antibody (red) and donkey anti-rabbit Cy2 conjugated antibody (green).

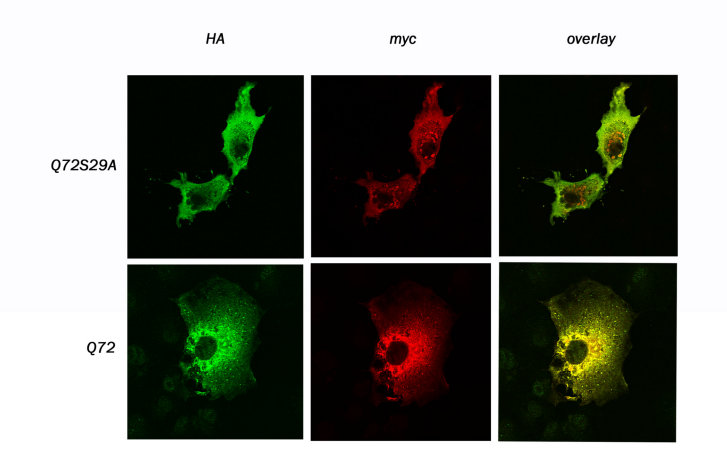

Figure 3.20 Confocal microscopy analysis of AT-3Q72S29A sub-cellular localization. COS-7 cells were transfected with cDNAs coding for AT-3Q72 or AT-3Q72S29A mutant. To investigate sub-cellular localization of AT-3, cells were fixed

in PFA and probed with mouse monoclonal anti-*c-myc* (red) and rabbit monoclonal anti-HA antibodies (green).

The confocal analysis (Figure 3.20) shows that AT-3Q72S29A localizes in the cytoplasm as well as in the nucleus, showing the same localization of AT-3Q72. The overlays show that N-terminal and C-terminal fragments co-localize.

Cells were also incubated with anti-*c-myc* rabbit monoclonal antibody to visualize AT-3 and mouse anti-*cyt-c* monoclonal antibody for mitochondria visualization. After extensive washes, cells were incubated with donkey anti-rabbit Cy3 (red) and donkey anti-mouse Cy2 (green) antibodies.

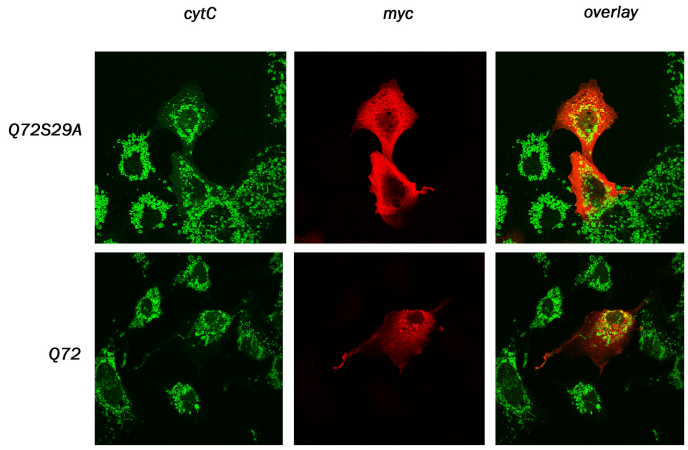

Figure 3.21 Confocal microscopy analysis of AT-3Q72S29A mitochondrial localization. COS-7 cells were transfected with cDNAs coding for AT-3Q72 or AT-3Q72S29A mutant. To investigate mitochondrial localization of AT-3, cells were fixed in PFA and probed with rabbit monoclonal anti-*c-myc* (red) and mouse monoclonal anti-*cytocrome-c* antibodies (green).

Confocal microscopy analysis (Figure 3.21) shows that AT-3Q72S29A localizes also in mitochondria as AT-3Q72. The overlays show that AT-3 co-localizes with *cytocrome-c* in mitochondria.

3.2.7.2 CELL FRACTIONATION

COS-7 cells were cultured in 94 mm plates (6×10^5 cells/plate) and grown for 24 h before transfection. Cells were transfected overnight

with FuGENE6 and *pcDNA3.1/myc-His,* AT-3Q72 or AT-3Q72S29A. 15 h, 24 h or 48 h after transfection cells were harvested and cytosolic and nuclear fractions were obtained. After SDS-PAGE and Western blot, membranes were incubated with anti-*c-myc* mouse monoclonal antibody to visualize AT-3 and with anti-vinculin, anti-fibrillarin and anti-PGK mouse monoclonal antibodies as fractionation and loading controls.

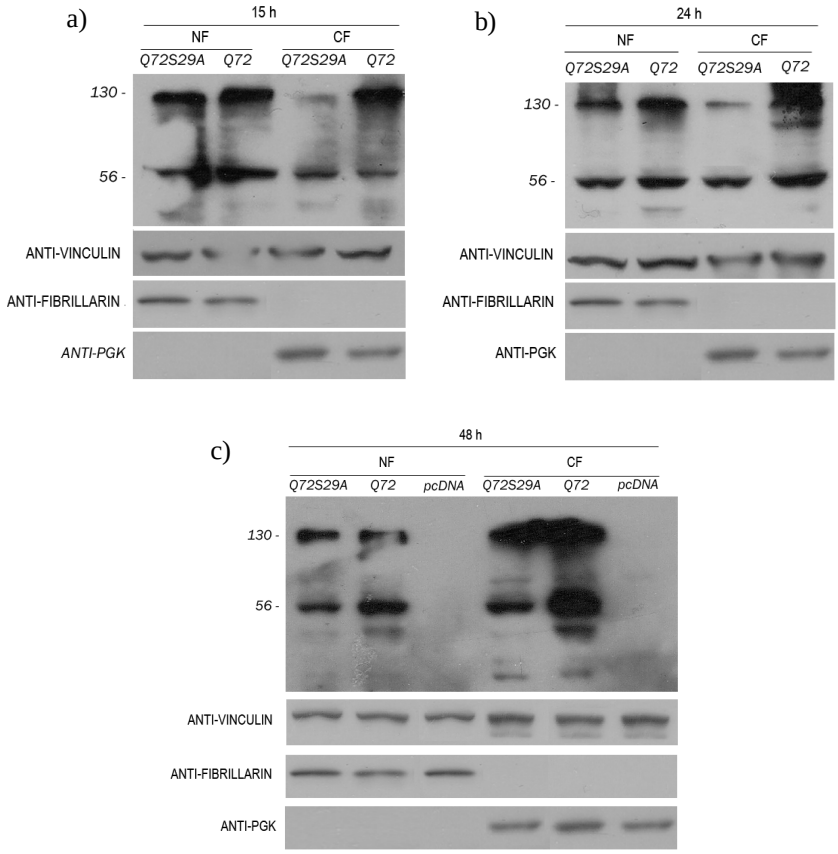

Figure 3.22 Western-blot analysis of AT-3Q72S29A sub-cellular localization. *c-myc* tagged AT-3Q72 and its mutant AT-3Q72S29A were expressed in COS-7 cells. Western-blots of cytosolic and nuclear fractions at 15 **(a)**, 24 **(b)** or 48 h **(c)** post-transfection, were probed with a monoclonal anti-*c-myc* antibody. Cytosolic and nuclear fractions controls were performed with anti-fibrillarin and anti-PGK antibodies, while loading control was performed with anti-vinculin antibody. **(c)** COS-7 cells were transfected also with empty *pcDNA3.1/myc-His* as a control.

Western-blot analysis of AT-3Q72S29A sub-cellular localization (Figure 3.22) shows that it localizes in cytosol and also in nucleus as

AT-3Q72, at all post-transfection times. The mutant is subjected to the same proteolytic cleavage and aggregation of AT-3Q72.

3.2.7.3 MITOCHONDRIA ISOLATION

COS-7 cells were cultured in 94 mm plates (6×10^5 cells/plate) and grown for 24 h before transfection. Cells were transfected overnight with FuGENE6 and AT-3Q72 or AT-3Q72S29A. 24 h after transfection cells were harvested and mitochondrial membranes, as well as lysosomal, mitochondrial and cytosolic soluble fractions were obtained. After SDS-PAGE and Western blot, membranes were incubated with Z46 rabbit polyclonal antibody to visualize AT-3 and with anti-VDAC and anti-SOD2 rabbit polyclonal antibodies as mitochondria isolation controls.

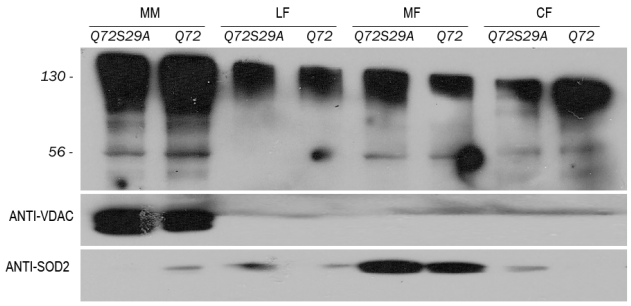

Figure 3.23 Western-blot analysis of AT-3Q72S29A mitochondrial localization. *c-myc* tagged AT-3Q72 and its mutant AT-3Q72S29A were expressed in COS-7 cells. Western-blots of mitochondrial membranes and lysosomal, mitochondrial and cytosolic soluble fractions were probed with a polyclonal Z46 antibody. Mitochondrial membranes and mitochondrial soluble fraction controls were performed with anti-VDAC and anti-SOD2 antibodies.

Western-blot analysis of AT-3Q72S29A mitochondrial localization (Figure 3.23) shows that it localizes in mitochondrial membranes and also in mitochondrial soluble fraction as AT-3Q72.

3.3 INTERACTION BETWEEN AT-3 AND VCP/p97

3.3.1 CONSTRUCTS

cDNA encoding for murine ataxin-3 (AT-3Q6), cloned into plasmid *pcDNA3X(+HA)*, carries only N-terminal HA epitope.
AT-3Q6TM mutant was subcloned from plasmid *pcDNA3.1/myc-His* into plasmid *pcDNA3X(+HA)*, so it carries only N-terminal HA epitope.
AT-3Q6QM (S268A, T271A, S272A, S273A and S277A) was obtained by PCR substituting serines and threonine with alanines.
cDNA encoding for human AT-3Q72, cloned into plasmid *pcDNA3.1/myc-His*, carries N-terminal HA epitope and C-terminal *c-myc* epitope.
cDNA encoding for VCP/p97 was subcloned from plasmid *pCMV-Sport6ccdB* into plasmid *pcDNA3.1/myc-His*, so it carries only C-terminal *c-myc* epitope.

All constructs were hosted and amplified in *E. coli* strain DH5α, while protein expression was achieved after transient co-transfection of COS-7 cells. Cultures were carried out in 94 mm plates in DMEM containing 10% fetal bovine serum (FBS), 100 U/ml penicillin, 100 μg/ml streptomycin and 4 mM glutamine. Cells were subsequently transiently co-transfected with FuGENE6.

3.3.2 IMMUNOPRECIPITATION

COS-7 cells were cultured in 94 mm plates (6×10^5 cells/plate) and grown for 24 h before co-transfection. Cells were co-transfected overnight with FuGENE6 and VCP/p97 and AT-3Q6, AT-3Q6TM, AT-3Q6QM or *pcDNA3X(+HA)*. 24 h after transfection cells were harvested and total extracts were obtained. Then AT-3 was immunoprecipitated with Z46 rabbit polyclonal antibody. After SDS-PAGE and Western blot, membranes were incubated with anti-*c-myc* mouse monoclonal antibody to visualize VCP/p97 and with anti-HA mouse monoclonal antibody to visualize AT-3.

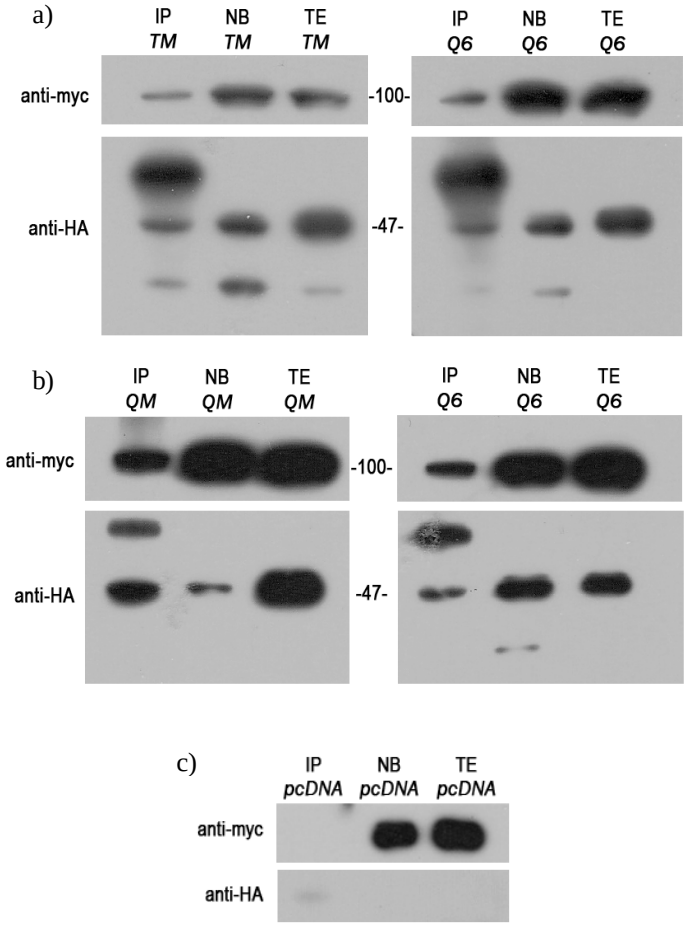

Figure 3.24 Western-blot analysis of AT-3Q6 immunoprecipitation. HA tagged AT-3Q6, its mutants AT-3Q6TM **(a)** or AT-3Q6QM **(b),** or *pcDNA3X(+HA)* **(c)**, and *c-myc* tagged VCP/p97 were expressed in COS-7 cells. Western-blots of immunoprecipitated, not bound and total extract fractions were probed with a monoclonal anti-*c-myc* antibody and a monoclonal anti-HA antibody.

Western blot analysis of AT-3 immunoprecipitation (Figure 3.24) shows that AT-3Q6TM and AT-3Q6QM interact with VCP/p97 as wild-type, suggesting that these phosphorylation sites are not involved in this interaction.

3.3.3 DTT TREATMENT

COS-7 cells were cultured in 94 mm plates (6×10^5 cells/plate) and grown for 24 h before co-transfection. Cells were co-transfected

overnight with FuGENE6 and VCP/p97 and AT-3Q6, AT-3Q6TM or AT-3Q6QM. 24 h after transfection cells were treated with 10 mM DTT for 1 hour to induce an ERAD stress condition, then cells were harvested and total extracts were obtained. Then AT-3 was immunoprecipitated with Z46 rabbit polyclonal antibody. After SDS-PAGE and Western blot, membranes were incubated with anti-*c-myc* mouse monoclonal antibody to visualize VCP/p97 and with anti-HA mouse monoclonal antibody to visualize AT-3.

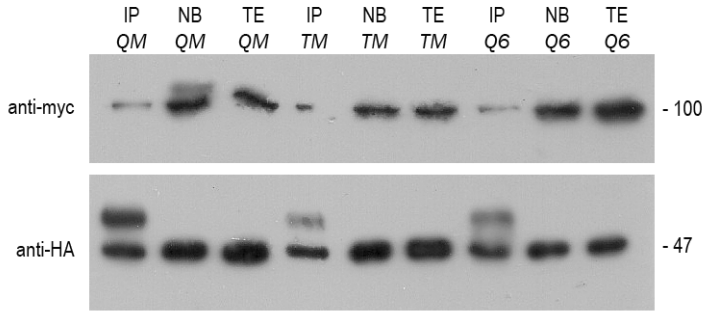

Figure 3.25 Western-blot analysis of AT-3Q6 immunoprecipitation after DTT treatment. HA tagged AT-3Q6 and its mutants AT-3Q6TM or AT-3Q6QM, and *c-myc* tagged VCP/p97 were expressed in COS-7 cells. Western-blots of immunoprecipitated, not bound and total extract fractions were probed with a monoclonal anti-*c-myc* antibody and a monoclonal anti-HA antibody.

Western blot analysis of AT-3 immunoprecipitation after DTT treatment (Figure 3.25) shows that AT-3Q6TM and AT-3Q6QM interact with VCP/p97 as the wild-type, also under stress condition. Nevertheless AT-3, in the presence of ERAD stress, has a lower interaction with VCP than in normal condition. In fact the ratio between the intensity of VCP band and AT-3Q6 band, obtained with NIH Image-based software Scion Image (Scion Corporation), shows a decrease of 50% after DTT treatment (p-value<0.05).

3.3.4 AT-3Q72 AND DTT TREATMENT

COS-7 cells were cultured in 94 mm plates (6×10^5 cells/plate) and grown for 24 h before co-transfection. Cells were co-transfected overnight with FuGENE6 and VCP/p97 and AT-3Q72 or *pcDNA3.1/myc-His*. 24 h after transfection cells were treated or not with 10 mM DTT for 1 hour to induce an ERAD stress condition, then

cells were harvested and total extracts were obtained. AT-3 was subsequently immunoprecipitated with Z46 rabbit polyclonal antibody. After SDS-PAGE and Western blot, membranes were incubated with anti-*c-myc* mouse monoclonal antibody to visualize VCP/p97 and AT-3Q72.

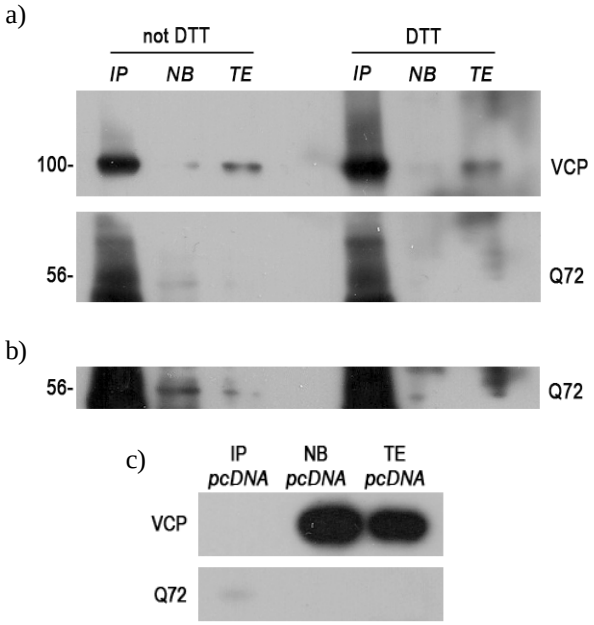

Figure 3.26 Western-blot analysis of AT-3Q72 immunoprecipitation with or without DTT treatment. *c-myc* tagged AT-3Q72 **(a)** or *pcDNA3.1/myc-His* **(c)** and *c-myc* tagged VCP/p97 were expressed in COS-7 cells. Western-blots of immunoprecipitated, not bound and total extract fractions were probed with a monoclonal anti-*c-myc* antibody. **(b)** AT3-Q72 was visualized also with an incremented exposition.

Western blot analysis of AT-3Q72 immunoprecipitation with or without DTT treatment (Figure 3.26) shows that the interaction between AT-3Q72 and VCP/p97 does not change under stress condition. Nevertheless AT-3Q72 has a stronger interaction with VCP than AT-3Q6, as demonstrated by Zhong and coworkers (Zhong X. *et al.*, 2006). In fact the ratio between the intensity of VCP band and AT-3Q72 band, obtained with NIH Image-based software Scion Image (Scion Corporation), is twice as high as the ratio between the intensity of VCP band and AT-3Q6 band (Figure 3.24) (p-value<0.05).

3.4 NITRATION AND AT-3

3.4.1 CONSTRUCTS

cDNAs encoding for murine ataxin-3 (AT-3Q6) and human pathological ataxin-3 (AT-3Q72) were subcloned from plasmid *pcDNA3X(+HA)* into plasmid *pcDNA3.1/myc-His*, they carry N-terminal HA and C-terminal *c-myc* epitopes.
All constructs were hosted and amplified in *E. coli* strain DH5α, while protein expression was achieved after transient transfection of Neuro2a cells. Cultures were carried out in 94 mm plates in DMEM containing 10% fetal bovine serum (FBS), 100 U/ml penicillin, 100 μg/ml streptomycin and 4 mM glutamine. Cells were subsequently transiently transfected with FuGENE6.

3.4.2 NOS EXPRESSION

Neuro2a cells were cultured in 94 mm plates (1×10^6 cells/plate) and grown for 24 h before transfection. Cells were transfected overnight with FuGENE6 and AT-3Q6 or AT-3Q72. 24 h after transfection cells were harvested and total extracts were obtained. After SDS-PAGE and Western blot, membranes were incubated with anti-*c-myc* mouse monoclonal antibody to visualize AT-3, with anti-NOS rabbit polyclonal antibody to visualize NOS and with anti-vinculin mouse monoclonal antibody as loading control.

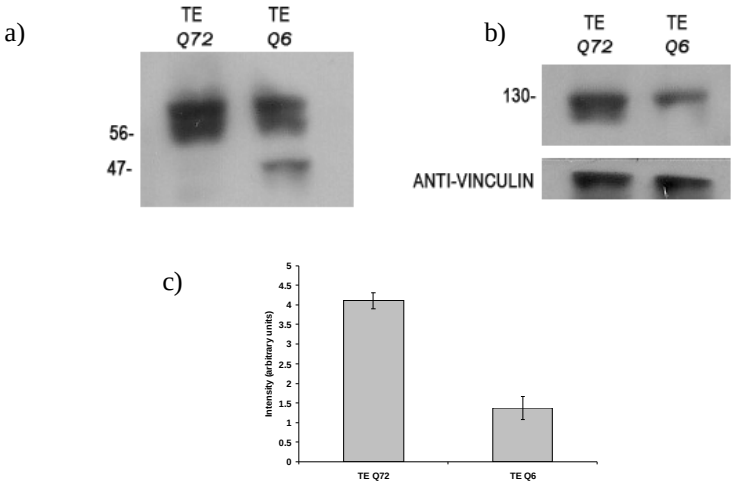

Figure 3.27 Western-blot analysis of NOS expression. *c-myc* tagged AT-3Q6 and AT-3Q72 were expressed in Neuro2a cells. Western-blots of total extracts were

probed with a monoclonal anti-*c-myc* antibody to visualize AT-3 **(a)**, with a polyclonal anti-NOS antibody to visulize NOS and with a monoclonal anti-vinculin antibody as loading control **(b)**. **(c)** Densitometric analysis performed with NIH Image-based software Scion Image (Scion Corporation) on blot reported in panel b. Quantification data are a mean of three independent experiments; bands intensities were normalized on vinculin control.

Western blot analysis of NOS expression in Neuro2a cells transfected with AT-3Q6 or AT-3Q72 (Figure 3.27) shows that in the presence of pathological form of AT-3 there is an increase in NOS expression. This result was confirmed by densitometric analysis (Figure 3.27c) that shows for NOS in presence of AT-3Q72 a band intensity that is four time as high as band intensity of NOS in presence of AT-3Q6 (p-value<0.05).

3.4.3 NITRATION PATTERN

Neuro2a cells were cultured in 94 mm plates (1×10^6 cells/plate) and grown for 24 h before transfection. Cells were transfected overnight with FuGENE6 and AT-3Q6 or AT-3Q72. 24 h after transfection cells were harvested and total extracts were obtained. After 2-D or SDS-PAGE and Western blot, membranes were incubated with anti-nitrotyrosine rabbit polyclonal antibody to visualize nitrated proteins.

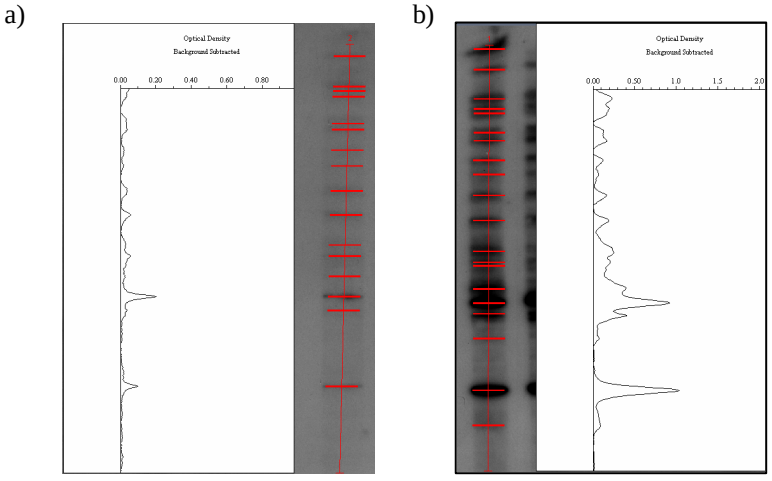

Figure 3.28 Western-blot analysis of nitration pattern. *c-myc* tagged AT-3Q6 **(a)** and AT-3Q72 **(b)** were expressed in Neuro2a cells. Western-blots of total extracts were probed with a polyclonal anti-nitrotyrosine antibody to visualize nitrated proteins. Densitometric analysis was performed with Quantity-one Analysis

software and profiles were obtained through the parameter Trace quantity (the quantity of a band as measured by the area under its intensity profile curve).

Western blot analysis of nitration pattern in Neuro2a cells transfected with AT-3Q6 or AT-3Q72 (Figure 3.28) shows that in the presence of the pathological form of AT-3 there is a remarkable overall increase in protein nitration. This result was confirmed by densitometric analysis performed with Quantity-one Analysis software; in fact nitration profiles obtained show increase in protein nitration.

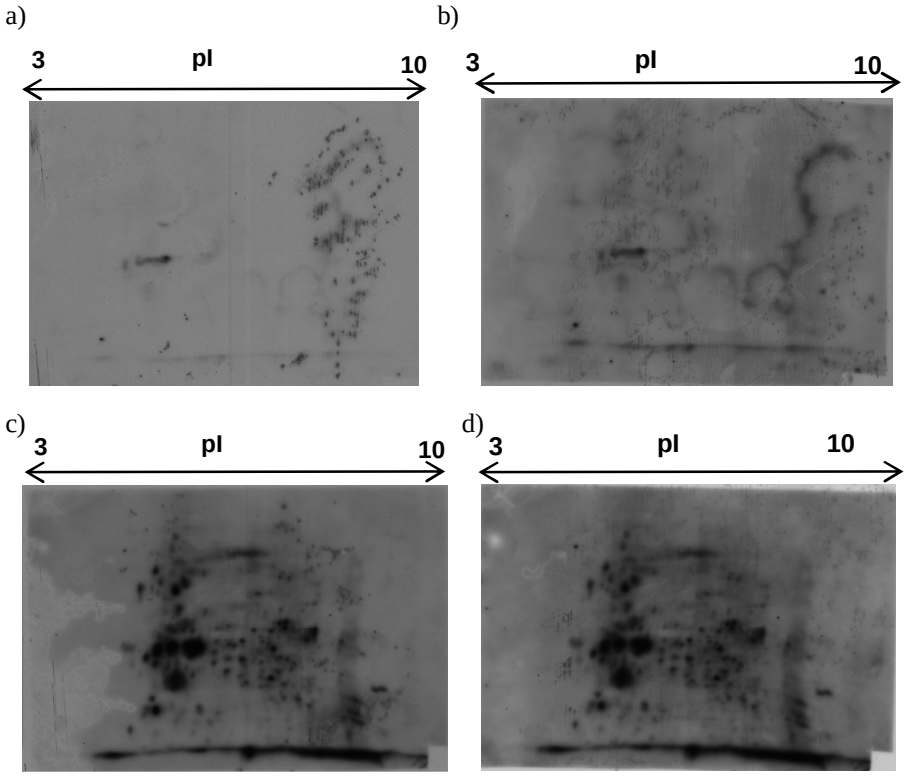

Figure 3.29 2-D analysis of nitration pattern. *c-myc* tagged AT-3Q6 **(a, b)** and AT-3Q72 **(c, d)** were expressed in Neuro2a cells. Western-blots of total extracts subjected to 2-D electrophoresis were probed with a polyclonal anti-nitrotyrosine antibody to visualize nitrated proteins. **(b, d)** Nitrated proteins were visualized also with an incremented exposition.

2-D analysis of nitration pattern in Neuro2a cells transfected with AT-3Q6 or AT-3Q72 (Figure 3.29) shows that in the presence of pathological AT-3 there is a remarkable increase in protein nitration, both as nitration level and as number of nitrated proteins. These data

therefore suggest that pathological AT-3 can induce activation of nitrosative stress.

4. Discussion

DISCUSSION

Phosphorylation is well known to play a role in a number of neurodegenerative diseases, notably in amyloid fibers formation. Nonaka and coworkers (Nonaka T. *et al.*, 2005) have shown that α-synuclein is phosphorylated on Ser 129 and that this is crucial in mediating both protein neurotoxicity and inclusions formation; other authors have shown that hungtintin is phosphorylated by Cdk5 (Luo S. *et al.*, 2005). Phosphorylation has also been reported to protect presenilin-2 from caspase cleavage (Walter J. *et al.*, 1999). Amongst ataxias, SCA14 is caused by mutations on residues which are normally phosphorylated: unphosphorylated proteins do not fold correctly and aggregate (Seki T. *et al.*, 2005); AT-1, the protein responsible for Sca1 has been demonstrated to be phosphorylated by Akt at S776; this phosphorylation creates a binding site for 14-3-3, increasing AT-1 stabilization and accumulation and hence leading to pathogenesis (Chen H. K. *et al.*, 2003; Emamian E. S. *et al.*, 2003).

Amongst the kinases involved in neurodegenerative diseases, CK2 and GSK3 are particularly interesting. In neuronal cells there appears to be a myriad of CK2 substrates that have clear implications in neural development, neuritogenesis, synaptic transmission and plasticity (Chen L. *et al.*, 2005). On the other hand, of the two isoforms of GSK3 which are found in mammals, GSK3β and GSK3α (Woodgett J. R., 1990), GSK3β is particularly abundant in the central nervous system (Kaytor M. D. *et al.*, 2002) and has been found to be involved in Alzheimer disease pathogenesis (Lucas J. J. *et al.*, 2001).

Some authors already addressed the issue of AT-3 phosphorylation (Tait D. *et al.*, 1998; Tao R. S. *et al.*, 2008; Mueller T. *et al.*, 2009; Fei E. *et al.*, 2007), however, their studies were conducted mainly through pull-down assays and co-immunoprecipitations. In this work, we investigated for the first time the role of AT-3 phosphorylation through a proteomic approach.
Amongst the different putative phosphorylation consensus sites which are found along AT-3 sequence, we found that S29, the only phosphorylatable site within the Josephin domain, can be phosphorylated *in vitro* by both CK2 and GSK3. Phosphorylation on S29 was subsequently confirmed in transfected COS-7 cells overexpressing AT-3Q6 and was found to be prevented by the addition of CK2 and GSK3 inhibitors.

Moreover, our data confirmed CK2 phosphorylation at C-terminal sites already described by other authors, such as S329 and S341, corresponding to S340 and S352 respectively in human AT-3 (Mueller T. *et al.*, 2009) and at new C-terminal sites: T271, S272, S277 and S344. Our data also confirmed GSK3 phosphorylation at C-terminal sites already described by Villèn and coworkers, such as S268 and S273 (Villèn J. *et al.*, 2007). It is worth mentioning that Serine29 is recognized, by prediction methods, as part of a consensus sequence for both CK2 and GSK3, although the presence of a proline nearby is known to prevent phosphorylation by CK2 in some instances; experimental data allowed to confirm this prediction.

Our decision to focus, in particular, on S29 phosphorylation is motivated by the fact that this residue is highly conserved in vertebrates; moreover, it is the only putatively phosphorylated site within the Josephin domain and, according to the NMR determined structure (Nicastro G. *et al.*, 2005) is fully exposed to the solvent and presumably easily accessible. On the other hand, we did not focus on all consensus sites located in the C-terminal domain, since they appear to be less conserved and had already been studied by other authors.

In order to assess whether phosphorylation could regulate AT-3 subcellular localization, we substituted S29, S268, T271, S272, S273 and S277 with alanines, through site-directed mutagenesis. Results showed that mutation to alanine does not change mitochondria localization for all mutants, but strongly reduced nuclear uptake only for S29. The fact that, upon substituting S29 with an aspartic acid, the wild-type phenotype is restored shows that the reduction of nuclear uptake is due to the lack of the negative phosphate charge and not to the aminoacid substitution. The site of proteolytic cleavage seems to be unaffected by the lack of phosphorylation; however S29A mutant seems to be cleaved at S29 to a higher extent than both wild-type and S29D mutant, suggesting that phosphorylation at this level might hamper proteolytic cleavage; the double band which is seen in correspondence of S29A 42 kDa fragment is also present in wild-type AT-3 and is probably an artifact. More work will be necessary to elucidate the nature and role of the so far unknown protease involved in the cleavage.

Mass spectrometry analysis also showed beyond any doubt that AT-3 is phosphorylated in transfected cells and this strongly suggests that phosphorylation takes place also *in vivo*. Moreover, the fact that CK2 and GSK3 concur in phosphorylating S29 points to the importance of

AT-3 nuclear translocation. Results obtained with both inhibitors suggest that no other kinases are involved in this process.

All our experiments have been performed on murine AT-3, carrying only six glutamines and sharing a high similarity with normal human AT-3; as stated before (Pozzi C. *et al.*, 2008), the choice of this protein is justified by the effort to avoid aggregate formation, which can be artificially induced by the unnatural raising in concentration which takes place inside transfected cells, since the aggregation process follows a second order kinetic (Shehi E. *et al.*, 2003). The presence of only six glutamines in murine AT-3, makes the event rather unlikely. Moreover we already showed that human AT-3Q26 behaves exactly like murine AT-3Q6 when expressed at low levels in transfected cells, as regards subcellular sorting and proteolytic fragmentation (Pozzi C. *et al.*, 2008).

Our data show a strong reduction in nuclear uptake, which is nevertheless not completely abolished. The possibility that this event is controlled by more than one factor is very likely. In a recent paper, Mueller and coworkers identified CK2 phosphorylation on S340 and S352, two residues which are found downstream of poly-Q, as essential for nuclear translocation (Mueller T. *et al.*, 2009); although, as mentioned above, we did not focus on phosphorylation at these residues, our data are definitely not in contrast with those of Mueller and coworkers. Since S340 and S352 are both found inside UIM3, whose presence in AT-3 structure depends on alternative splicing, phosphorylation at S29 may well be an additional factor promoting nuclear uptake, a process which seems essential for AT-3 function. In addition, AT-3 nuclear uptake does not seem to be completely suppressed in Mueller and coworkers experiments (Mueller T. *et al.*, 2009), neither upon S340/S352 mutagenesis to alanine nor upon addition of CK2 inhibitors. Last but not least, the fact that when S29 is substituted with an alanine, a 30% decrease in cell viability is observed, suggests that nuclear uptake is an important process for AT-3 functionality, possibly in relation to its function as a transcriptional repressor (Li F. *et al.*, 2002; Evert B. O. *et al.*, 2006), and is finely controlled by more than one factor. In contrast to Mueller and coworkers, a recent paper (Reina C. P. *et al.*, 2010) showed that CK2 inhibitors are not effective in preventing AT-3 nuclear localization upon heat-shock; this is well in accordance with our data showing that only simultaneous inhibition of both CK2 and GSK3 can prevent AT-3 nuclear uptake. These authors also showed that S111, which is found inside a Polo-like kinase phosphorylation site, is involved in

AT-3 nuclear uptake following heat-shock; we propose that this residue be involved in nuclear uptake promoted by heat-shock or oxidative stress, while phosphorylation at S29, S340 and S352 could regulate normal AT-3 trafficking between the nucleus and the cytoplasm. This is strongly supported by the fact that, in Reina and coworkers experiments, S111 mutation to alanine decreases AT-3 nuclear localization but does not suppress it.

To assess whether the combination of S29A with Mueller's mutants could suppress AT-3 nuclear uptake, we obtained AT-3Q6M mutant by substituting S29, S329 and S341 with alanines. Our data demonstrated that the removal of phosphorylatable S329 and S341 residues does not increase S29A phenotype, suppressing nuclear localization.

Whether a putative NLS, which is found in AT-3 primary sequence, is essential for AT-3 nuclear translocation is still controversial: in a previous work (Pozzi C. *et al*., 2008) we showed that a truncated mutant lacking this sequence was only slightly less efficiently translocated into the nucleus; Mueller and coworkers, as well as Reina and co-authors, recently confirmed that NLS mutation has no effect on AT-3 subcellular distribution. On the other hand other authors (Macedo-Ribeiro S. *et al*., 2009) showed, through a yeast nuclear import assay, that AT-3 NLS is functional and essential for nuclear uptake.

Nuclear translocation of AT-3 is also of the utmost importance for SCA3 pathogenesis, since amyloid aggregates are found primarily inside the nucleus. Although a growing amount of data suggest that mitochondrial damage is also involved in SCA3 pathogenesis (Tsai H. F. *et al*., 2004; Chou A. H. *et al*., 2006; Yu Y. C. *et al*., 2009), the presence of nuclear aggregates is a hallmark of many neurodegenerative diseases and impairment of nuclear functions is very likely to induce cell death. To assess whether S29 was also involved in nuclear uptake of AT-3 pathological form, we mutated AT-3Q72 S29 to alanine. Our data demonstrate that the mutation does not change AT-3Q72 nuclear localization. The deregulation caused by the expansion of poly-Q probably compensates for the removal of the phosphorylation site; in fact it has been demonstrated that AT-3 associates with the nuclear matrix undergoing a conformational change that causes the poly-Q tract to be exposed (Perez M. K. *et al*., 1999), a modification that could lead to aberrant new interactions both with the nuclear matrix and with other nuclear proteins in the case of an expanded poly-Q.

VCP/p97 is a key protein essential for the extraction of substrates from the endoplasmic reticulum (ER) to the cytosol in ER-associated degradation (ERAD), a quality control system in the secretory pathway responsible for degrading misfolded proteins (Zhong X. *et al.*, 2006). Recent studies revealed that VCP may be involved in the pathogenesis of protein misfolding diseases (Boeddrich A. *et al*, 2006). It colocalizes with abnormal inclusion bodies containing insoluble protein aggregates, which are characteristic features of many neurodegenerative diseases, including Alzheimer's, Parkinson's, and Huntington's disease.

Zhong and coworkers described the interaction between AT-3 and VCP which seems to decrease the binding of the latter with its normal partner Ufd1 and with polyubiquitin chains resulting in a decreased degradation of ERAD substrates. The authors suggest that AT-3 would regulate flow through the ERAD pathway by adjusting the rate of extraction of ERAD substrates and that this regulation is dependent on the poly-Q tract, so that a pathologic AT-3 would aberrantly interact with VCP leading to a deregulation of ERAD. Ataxin-3 interacts with VCP/p97 in a region (aa 257-291) localized between the second ubiquitin interacting motif (UIM) and the poly-Q (Zhong X. *et al.*, 2006).

We identified five phosphorylation sites in this region of interaction between VCP/p97 and AT-3, three for CK2 (T271, S272 and S277) and two for GSK3 (S268 and S273).

To understand if the interaction between ataxin-3 and VCP/p97 is regulated by these phosphorylation sites, we studied the interaction between VCP/p97 and AT-3Q6 or its mutant lacking these phosphorylation sites (AT-3TM and AT-3QM).

We co-transfected VCP/p97 and AT-3 in COS7 cells and subsequently immunoprecipitated AT-3, observing the presence of VCP/p97. We detected no difference in mutants' ability to interact with VCP/p97: they showed the same phenotype as the wild-type.

Then we treated transfected cells with DTT to induce an ER stress in order to study the role of the phosphorylation sites in the interaction between VCP/p97 and its substrates. Also in this condition we detected no difference between AT-3Q6 and its mutants; the interaction between AT-3 and VCP/p97 is probably not so finely regulated through phosphorylation, but it depends by other aminoacids in the involved region.

Nevertheless, in the presence of ERAD stress, AT-3 showed a lower interaction with VCP than in normal conditions. In fact the ratio

between the intensity of VCP band and AT-3Q6 band in immunoprecipitated samples, obtained with NIH Image-based software Scion Image (Scion Corporation), showed a 50% decrease after DTT treatment (p-value<0.05).
Therefore when ER is under stress condition VCP/p97 must increase its interaction with its normal partner Ufd1 and with polyubiquitin chains to degrade ERAD substrates; consequently VCP/p97 must decrease its interaction with AT-3.
We also studied the interaction between VCP/p97 and AT-3Q72 with or without ER stress conditions and we showed that there is no variation in the interaction between AT-3Q72 and VCP/p97 under stress conditions. Nevertheless AT-3Q72 has a stronger interaction with VCP than AT-3Q6, as demonstrated by Zhong and coworkers (Zhong X. *et al.*, 2006). In fact the ratio between the intensity of VCP band and AT-3Q72 band in immunoprecipitated samples, obtained with NIH Image-based software Scion Image (Scion Corporation), is twice as high as the ratio between the intensity of VCP band and AT-3Q6 band (p-value<0.05).
Therefore AT-3 pathological form interacts aberrantly with VCP/p97 also in ER stress conditions, leading to a deregulation of ERAD.
The phosphorylation sites for CK2 and GSK3 at the C-terminal of AT-3, identified in our laboratory, are not involved neither in protein sub-cellular localization nor in the interaction with VCP/p97, their role being still unknown. These sites have not been much conserved during evolution, but they are easily accessible; in fact they are in the unstructured region of AT-3 and they are phosphorylated *in vitro* as dimonstrated by mass spectrometry analysis. Probably these sites are involved in other functions of ataxin-3, such as catalytic activity or interaction with transcription factors CBP and p300, but other studies are necessary to understand the role of these five phosphorylation sites in ataxin-3 physiology.

Overproduction of reactive nitrogen species (RNS) and reactive oxygen species (ROS), which leads to neuronal cell injury and death, is a potential mediator of neurodegenerative disorders including: Parkinson's disease, Alzheimer's disease, amyotrophic lateral sclerosis and polyglutamine diseases such as Huntington's disease (Nakamura T. and Lipton S.A., 2007).
An important feature of most neurodegenerative diseases is the accumulation of misfolded and/or aggregated proteins. These protein aggregates can be cytosolic, nuclear, or extracellular. Importantly,

protein aggregation can result from either a mutation in the disease-related gene encoding the protein, or post-translational changes to the protein engendered by nitrosative/oxidative stress (Nakamura T. and Lipton S.A., 2007).

In particular the role of nitrosative/oxidative stress in Parkinson's disease is well known, in fact nitrosative and oxidative stress are potential causal factors for protein accumulation in the much more common sporadic form of PD. Nitrosative/oxidative stress, commonly found during normal aging, can mimic rare genetic causes of disorders, such as PD, by promoting protein misfolding in the absence of a genetic mutation. For example, S-nitrosylation and further oxidation of parkin or Uch-L1 result in dysfunction of these enzymes and thus of the UPS (ubiquitin-proteasome system).

For Spinocerebellar Ataxia Type 3, Yu and coworkers demonstrated that polyglutamine-expanded ataxin-3 may influence the activity of enzymatic components to remove O_2^- and H_2O_2 efficiently and promote mitochondrial DNA damage or depletion, which leads to dysfunction of mitochondria. In fact they showed that in the presence of the pathological form of ataxin-3 a lower activity of catalase, glutathione reductase, and superoxide dismutase were detected compared to the wild-type. Therefore, they suggest that the cell damage caused by greater oxidative stress in SCA3 mutant cells plays an important role, at least in part, in the disease progression (Yu Y. C. *et al*., 2009)

To understand the role of nitrosative stress in Spinocerebellar Ataxia Type 3 we studied the expression of NO synthase in Neuro2a cells transfected with AT-3Q6 or AT-3Q72. Results demonstrated an increase in NOS expression in the presence of AT-3 pathological form. This result was confirmed by densitometric analysis that showed, when AT-3Q72 was overexpressed, a band intensity for NOS four times higher than the intensity of the NOS band detected in presence of AT-3Q6 (p-value<0.05). Thus we studied nitration pattern through mono and bidimensional analysis and we observed that in the presence of AT-3 pathological form there was a remarkable increase in protein nitration, both as nitration level and as number of nitrated proteins. These data demonstrate that activation of nitrosative stress is induced in the presence of AT-3 pathological form.

Although other studies will be necessary to analyze nitration levels of proteins that interact with ataxin-3, like VCP/p97, CBP or p300; preliminary data suggested that ataxin-3 is also nitrated. The study of wild-type and pathological AT-3 nitration levels could be important to

understand the role of ataxin-3 both in physiological conditions and in the pathogenesis; in fact nitration of tyrosine residues is a relevant posttranslational modification that positively or negatively regulates, signalling pathways, controlling tyrosine phosphorylation, kinases activation and protein-protein interactions (Monteiro H. P. *et al.*, 2008). In AT-3 sequence there are two potentially relevant tyrosine residues: Y27 and Y288. The tyrosine 27 is found close to S29 and to the cleavage site identified as the only one present in every form of ataxin-3 (Pozzi C. *et al.*, 2008); nitration of this residue could prevent S29 phosphorylation by CK2 and GSK3, controlling AT-3 nuclear uptake or possibly the proteolytic cleavage by a putative chimotrypsin-like protease. The tyrosine 288 is located in VCP/p97 binding site, suggesting that nitration of this residue could be regulate the interaction between VCP/p97 and ataxin-3. A detailed study of nitration at both these residues could shed light on AT-3 nuclear aggregate formation and aberrant interaction with VCP/p97 in relation to Sca3 pathogenesis.

REFERENCE LIST

Albrecht M., Hoffmann D., Evert B. O., Schmitt I., Wullner U., and Lengauer T. (**2003**) "Structural modelling of ataxin-3 reveals distant homology to adaptins"; *Proteins* [50] 355-370.

Bates G. P., Mangiarini L., Wanker E. E., and Davies S. W. (**1998**) "Polyglutamine expansion and Huntington's disease"; *Biochem.Soc.Trans.* [26] 471-475.

Berke S. J., Chai Y., Marrs G. L., Wen H., and Paulson H. L. (**2005**) "Defining the role of ubiquitin-interacting motifs in the polyglutamine disease protein, ataxin-3"; *J.Biol.Chem.* [280] 32026-32034.

Berke S. J., Schmied F. A., Brunt E. R., Ellerby L. M., and Paulson H. L. (**2004**) "Caspase-mediated proteolysis of the polyglutamine disease protein ataxin-3"; *J.Neurochem.* [89] 908-918.

Bevivino A. E. and Loll P. J. (**2001**) "An expanded glutamine repeat destabilizes native ataxin-3 structure and mediates formation of parallel beta -fibrils"; *Proc.Natl.Acad.Sci.U.S.A* [98] 11955-11960.

Bienz M., and Clevers H. (**2000**) "Linking colorectal cancer to Wnt signalling"; *Cell* [103] 311–320.

Boeddrich A., Gaumer S., Haacke A., Tzvetkov N., Albercht M., Evert B., Muller E., Lurz R., Breuer P., Schugardt N., Plabmann S., Xu K., Warrik J. M., Suopanki J., Wullner U., Frank R., Hartl U. F., Bonini N. M., and Wanker E.E. (**2006**) "An arginin/lysine-rich motif is crucial for VCP/p97-mediated modulation of ataxin-3 fibrillogenesis"; *The EMBO journal* [25] 1547-1558.

Burnett B., Li F., and Pittman R. N. (**2003**) "The polyglutamine neurodegenerative protein ataxin-3 binds polyubiquitylated proteins and has ubiquitin protease activity"; *Hum.Mol.Genet.* [12] 3195-3205.

Cemal C. K., Carroll C. J., Lawrence L., Lowrie M. B., Ruddle P., Al Mahdawi S., King R. H., Pook M. A., Huxley C., and Chamberlain S. (**2002**) "YAC transgenic mice carrying pathological alleles of the MJD1 locus exhibit a mild and slowly progressive cerebellar deficit"; *Hum.Mol.Genet.* [11] 1075-1094.

Chai Y., Berke S. S., Cohen R. E., and Paulson H. L. (**2004**) "Poly-ubiquitin binding by the polyglutamine disease protein ataxin-3 links its normal function to protein surveillance pathways"; *J.Biol.Chem.* [279] 3605-3611.

Chai Y., Koppenhafer S. L., Shoesmith S. J., Perez M. K., and Paulson H. L. (**1999**) "Evidence for proteasome involvement in polyglutamine disease:

localization to nuclear inclusions in SCA3/MJD and suppression of polyglutamine aggregation *in vitro*"; *Hum.Mol.Genet.* [8] 673-682.

Chai Y., Wu L., Griffin J. D., and Paulson H. L. (**2001**) "The role of protein composition in specifying nuclear inclusion formation in polyglutamine disease"; *J.Biol.Chem.* [276] 44889-44897.

Chen H. K., Fernandez-Funez P., Acevedo S. F., Lam Y. C., Kaytor M. D., Fernandez M. H., Aitken A., Skoulakis E. M., Orr H. T., Botas J., and Zoghbi H. Y. **(2003)** "Interaction of Akt-phosphorylated ataxin-1 with 14-3-3 mediates neurodegeneration in spinocerebellar ataxia type 1"; *Cell* [113] 457–468.

Chen L., and Feany M. B. **(2005)** "Alpha-synuclein phosphorylation controls neurotoxicity and inclusion formation in a Drosophila model of Parkinson disease"; *Nat. Neurosci.* [8] 657–663.

Chiti F., Taddei N., Bucciantini M., White P., Ramponi G., and Dobson C. M. (**2000**) "Mutational analysis of the propensity for amyloid formation by a globular protein"; *EMBO J.* [19] 1441-1449.

Chou A. H., Yeh T. H., Kuo Y. L., Kao Y. C., Jou M. J., Hsu C. Y., Tsai S. R., Kakizuka A., and Wang H. L. (**2006**) "Polyglutamine-expanded ataxin-3 activates mitochondrial apoptotic pathway by upregulating Bax and downregulating Bcl-xL"; *Neurobiol. Dis.* [21] 333-345.

Chou A. H., Yeh T. H., Ouyang P., Chen Y. L., Chen S. Y., and Wang H. L. (**2008**) "Polyglutamine-expanded ataxin-3 causes cerebellar dysfunction of SCA3 transgenic mice by inducing transcriptional dysregulation"; *Neurobiol. Dis.* [31] 89-101.

Chou A. H., Chen S. Y., Yeh T. H., Weng Y. H., and Wang H. L. (**2010**) "HDAC inhibitor sodium butyrate reverses transcriptional downregulation and ameliorates ataxic symptoms in a transgenic mouse model of SCA3"; *Neurobiol. Dis.* [Epub ahead of print]

Chou A. H., Lin A. C., Hong K. J., Hu S. H., Chen Y. L., Chen J. Y., and Wang H. L. **(2010)** "p53 activation mediates polyglutamine-expanded ataxin-3 upregulation of Bax expression in cerebellar and pontine nuclei neurons"; *Neurochem. Int.* [Epub ahead of print]

Chow M. K., Ellisdon A. M., Cabrita L. D., and Bottomley S. P. (**2004**) "Polyglutamine expansion in ataxin-3 does not affect protein stability: implications for misfolding and disease"; *J.Biol.Chem.* [279] 47643-47651.

Cohen E., Bieschke J., Perciavalle R. M., Kelly J. W., and Dillin A. (**2006**) "Opposing activities protect against age-onset proteotoxicity"; *Science* [313] 1604-1610.

Cohen P., and Frame S. (**2001**) "The renaissance of GSK3"; *Mol. Cell. Biol.* [2] 769-776.

DeLaBarre B., and Brunger A. T. (**2003**) "Complete structure of p97/valosincontaining protein reveals communication between nucleotide domains"; *Nat Struct Biol* [10] 856–863.

Emamian E. S., Kaytor M. D., Duvick L. A., Zu T., Tousey S. K., Zoghbi H. Y., Clark H. B., and Orr H. T. **(2003)** "Serine 776 of ataxin-1 is critical for polyglutamine-induced disease in SCA1 transgenic mice"; *Neuron* [38] 375–387.

Evert B. O., Wullner U., and Klockgether T. (**2000**) "Cell death in polyglutamine diseases"; *Cell Tissue Res.* [301] 189-204.

Evert B. O., Araujo J., Vieira-Saecker A. M., de Vos R. A., Harendza S., Klockgether T., and Wullner U. **(2006)** "Ataxin-3 represses transcription via chromatin binding, interaction with histone deacetylase 3, and histone deacetylation"; *J. Neurosci.* [26] 11474–11486.

Fei E., Jia L., Zhang T., Ma X., Wang H., Liu C., Zhang W., Ding L., Nukina N., and Wang G. (**2007**) "Phosphorylation of ataxin-3 by glycogen synthase kinase 3β at serine 256 regulates the aggregation of ataxin-3"; *Biochemical ado Biophysical Resaerch Communications* [357] 487-492.

Fiol C. J., Mahrenholz A. M., Wang Y., Roeske R. W., and Roach P. J. (**1987**) "Formation of protein kinase recognition sites by covalent modification of the substrate. Molecular mechanism for the synergistic action of casein kinase II and glycogen synthase kinase 3"; *J. Biol. Chem.* [262] 14042–14048.

Frame S., Cohen P., and Biondi R. M. (**2001**) "A common phosphate binding site explains the unique substrate specificity of GSK3 and its inactivation by phosphorylation" *Mol. Cell* [7] 1321–1327.

Fujigasaki H., Uchihara T., Takahashi J., Matsushita H., Nakamura A., Koyano S., Iwabuchi K., Hirai S., and Mizusawa H. (**2001**) "Preferential recruitment of ataxin-3 independent of expanded polyglutamine: an immunohistochemical study on Marinesco bodies"; *J.Neurol.Neurosurg.Psychiatry* [71] 518-520.

Goti D., Katzen S. M., Mez J., Kurtis N., Kiluk J., Ben Haiem L., Jenkins N. A., Copeland N. G., Kakizuka A., Sharp A. H., Ross C. A., Mouton P. R., and Colomer V. (**2004**) "A mutant ataxin-3 putative-cleavage fragment in brains of Machado-Joseph disease patients and transgenic mice is cytotoxic above a critical concentration"; *J.Neurosci.* [24] 10266-10279.

Gusella J. F. and MacDonald M. E. (**2000**) "Molecular genetics: unmasking polyglutamine triggers in neurodegenerative disease"; *Nat.Rev.Neurosci.* [1] 109-115.

Hanger D. P., Hughes K., Woodgett J. R., Brion J. P., and Anderton B. H. (**1992**) "Glycogen synthase kinase-3 induces Alzheimer's disease-like phosphorylation of tau: generation of paired helical filament epitopes and neuronal localisation of the kinase"; *Neurosci. Lett.* [147] 58–62.

Hughes K., Nikolakaki E., Plyte S. E., Totty N. F., and Woodgett J. R. (**1993**) "Modulation of the glycogen synthase kinase-3 family by tyrosine phosphorylation"; *EMBO J.* [12] 803–808.

Ikeda H., Yamaguchi M., Sugai S., Aze Y., Narumiya S., and Kakizuka A. (**1996**) "Expanded polyglutamine in the Machado-Joseph disease protein induces cell death *in vitro* and *in vivo*"; *Nat.Genet.* [13] 196-202.

Kaytor M. D., and Orr H. T. **(2002)** "The GSK3 beta signaling cascade and neurodegenerative disease"; *Curr. Opin. Neurobiol.* [12] 275–278.

Kakizuka A. (**1998**) "Protein precipitation: a common etiology in neurodegenerative disorders?"; *Trends Genet.* [14] 396-402.

Kawaguchi Y., Okamoto T., Taniwaki M., Aizawa M., Inoue M., Katayama S., Kawakami H., Nakamura S., Nishimura M., Akiguchi I., and . (**1994**) "CAG expansions in a novel gene for Machado-Joseph disease at chromosome 14q32.1"; *Nat.Genet.* [8] 221-228.

Klement I. A., Skinner P. J., Kaytor M. D., Yi H., Hersch S. M., Clark H. B., Zoghbi H. Y., and Orr H. T. (**1998**) "Ataxin-1 nuclear localization and aggregation: role in polyglutamine-induced disease in SCA1 transgenic mice"; *Cell* [95] 41-53.

Kwong J. Q., Beal M. F., and Manfredi G. (**2006**) "The role of mitochondria in inherited neurodegenerative diseases"; *J.Neurochem* [97] 1659-1675.

Lai C. W., Aronson D. E., and Snapp E. L. (**2010**) "BiP availability distinguishes states of homeostasis and stress in the endoplasmic reticulum of living cells"; *Mol.Biol.of the Cell* [21] 1909-1921.

Li F., Macfarlan T., Pittman R. N., and Chakravarti D. (**2002**) "Ataxin-3 is a histone-binding protein with two independent transcriptional corepressor activities"; *J.Biol.Chem.* [277] 45004-45012.

Lucas J. J., Hernandez F., Gomez-Ramos P., Moran M. A., Hen R., and Avila J. **(2001)** "Decreased nuclear beta-catenin, tau hyperphosphorylation and neurodegeneration in GSK-3beta conditional transgenic mice"; *EMBO J.* [20] 27–39.

Luo S., Vacher C., Davies J. E., and Rubinsztein D. C. **(2005)** "Cdk5 phosphorylation of huntingtin reduces its cleavage by caspases: implications for mutant huntingtin toxicity"; *J.Cell Biol.* [169] 647–656.

Litchfield D. W. (**2003**) "Protein kinase CK2: structure, regulation and role in cellular decisions of life and death"; *Biochem.J.* [369] 1-15.

Macedo-Ribeiro S., Cortes L., Maciel P., and Carvalho A. L. (**2009**) "Nucleocytoplasmic shuttling activity of ataxin-3"; *PloS One* [4] e5834.

Maltecca F., Filla A., Castaldo I., Coppola G., Fragassi N. A., Carella M., Bruni A., Cocozza S., Casari G., Servadio A., and De Michele G. (**2003**) "Intergenerational instability and marked anticipation in SCA-17"; *Neurology* [61] 1441-1443.

Mandel J. L. (**1997**) "Human genetics. Breaking the rule of three"; *Nature* [386] 767-769.

Mao Y., Senic-Matuglia F., Di Fiore P. P., Polo S., Hodsdon M. E., and De Camilli P. (**2005**) "Deubiquitinating function of ataxin-3: insights from the solution structure of the Josephin domain"; *Proc.Natl.Acad.Sci.U.S.A* [102] 12700-12705.

Masino L., Musi V., Menon R. P., Fusi P., Kelly G., Frenkiel T. A., Trottier Y., and Pastore A. (**2003**) "Domain architecture of the polyglutamine protein ataxin-3: a globular domain followed by a flexible tail"; *FEBS Lett.* [549] 21-25.

Mazzucchelli S., De Palma A., Riva M., D'Urzo A., Pozzi C., Pastori V., Comelli F., Fusi P., Vanoni M., Tortora P., Mauri P., and Regonesi M. E. (**2009**) "Proteomic and biochemical analyses unveil tight interaction of ataxin-3 with tubulin"; *Int.J.Biochem.Cell.Biol.* [41] 2485-2492.

Meggio F. and Pinna L. A. (**2003**) "One-thousand-and-one substrates of protein kinase CK2?"; *FASEB J.* [17] 349-368.

Merlino A., Esposito L., and Vitagliano L. (**2006**) "Polyglutamine repeats and beta-helix structure: molecular dynamics study"; *Proteins* [63] 918-927.

Monteiro H. P., Arai R. J., and Travassos L. R. **(2008)** "Protein tyrosine phosphorylation and protein tyrosine nitration in redox signaling"; *Antiox. and.Redox Sign.* [10] 843-889.

Mueller T., Breuer P., Shmitt I., Evert B. O., and Wullner U. (**2009**) "CK2-dependent phosphorylation determines cellular localization and stability of ataxin-3"; *Hum. Mol. Genet.* [17] 3334-3343.

Nakamura T., and Lipton S. A. (**2007**) "Molecular mechanisms of nitrosative stress-mediated protein misfolding in neurodegenerative diseases"; *Cell Mol.Life Sci.* [64] 1609-1620.

Nicastro G., Menon R. P., Masino L., Knowles P. P., McDonald N. Q., and Pastore A. (**2005**) "The solution structure of the Josephin domain of ataxin-3:

structural determinants for molecular recognition"; *Proc.Natl.Acad.Sci.U.S.A* [102] 10493-10498.

Nonaka T., Iwatsubo T., and Hasegawa M. **(2005)** "Ubiquitination of alpha-synuclein"; *Biochemistry* [44] 361–368.

Nucifora F. C., Jr., Ellerby L. M., Wellington C. L., Wood J. D., Herring W. J., Sawa A., Hayden M. R., Dawson V. L., Dawson T. M., and Ross C. A. (**2003**) "Nuclear localization of a non-caspase truncation product of atrophin-1, with an expanded polyglutamine repeat, increases cellular toxicity"; *J.Biol.Chem.* [278] 13047-13055.

Paulson H. L. (**1999**) "Protein fate in neurodegenerative proteinopathies: polyglutamine diseases join the (mis)fold"; *Am.J.Hum.Genet.* [64] 339-345.

Paulson H. L., Das S. S., Crino P. B., Perez M. K., Patel S. C., Gotsdiner D., Fischbeck K. H., and Pittman R. N. (**1997a**) "Machado-Joseph disease gene product is a cytoplasmic protein widely expressed in brain"; *Ann.Neurol.* [41] 453-462.

Paulson H. L., Perez M. K., Trottier Y., Trojanowski J. Q., Subramony S. H., Das S. S., Vig P., Mandel J. L., Fischbeck K. H., and Pittman R. N. (**1997b**) "Intranuclear inclusions of expanded polyglutamine protein in spinocerebellar ataxia type 3"; *Neuron* [19] 333-344.

Perez M. K., Paulson H. L., and Pittman R. N. (**1999**) "Ataxin-3 with an altered conformation that exposes the polyglutamine domain is associated with the nuclear matrix"; *Hum.Mol.Genet.* [8] 2377-2385.

Perutz M. F. (**1996**) "Glutamine repeats and inherited neurodegenerative diseases: molecular aspects"; *Curr.Opin.Struct.Biol.* [6] 848-858.

Perutz M. F., Finch J. T., Berriman J., and Lesk A. (**2002**) "Amyloid fibers are water-filled nanotubes"; *Proc.Natl.Acad.Sci.U.S.A* [99] 5591-5595.

Perutz M. F., Johnson T., Suzuki M., and Finch J. T. (**1994**) "Glutamine repeats as polar zippers: their possible role in inherited neurodegenerative diseases"; *Proc.Natl.Acad.Sci.U.S.A* [91] 5355-5358.

Pozzi C., Valtorta M., Tedeschi G., Galbusera E., Pastori V., Bigi A., Nonnis S., Grassi E., and Fusi P. **(2008)** "Study of subcellular localization and proteolysis of ataxin-3"; *Neurobiol dis* [30] 190-200.

Reina C. P., Zhong X., and Pittman R. N. (**2010**) " Proteotoxic stress increases nuclear localization of ataxin-3"; *Hum.Mol.Genet.* [19] 235-249

Richards R. I. and Sutherland G. R. (**1997**) "Dynamic mutation: possible mechanisms and significance in human disease"; *Trends Biochem.Sci.* [22] 432-436.

Rodrigues A. J., do Carmo Costa M., Silva T. L., Ferreira D., Bajanca F., Logarinho E., and Maciel P. (**2010**) "Absence of ataxin-3 leads to cytoskeletal disorganization and increased cell death"; *Biochim. Biophys. Acta* [1803] 1154-1163.

Ross C. A. (**1995**) "When more is less: pathogenesis of glutamine repeat neurodegenerative diseases"; *Neuron* [15] 493-496.

Sanchez I., Xu C. J., Juo P., Kakizaka A., Blenis J., and Yuan J. (**1999**) "Caspase-8 is required for cell death induced by expanded polyglutamine repeats"; *Neuron* [22] 623-633.

Scheel H., Tomiuk S., and Hofmann K. (**2003**) "Elucidation of ataxin-3 and ataxin-7 function by integrative bioinformatics"; *Hum.Mol.Genet.* [12] 2845-2852.

Scherzinger E., Lurz R., Turmaine M., Mangiarini L., Hollenbach B., Hasenbank R., Bates G. P., Davies S. W., Lehrach H., and Wanker E. E. (**1997**) "Huntingtin-encoded polyglutamine expansions form amyloid-like protein aggregates *in vitro* and *in vivo*"; *Cell* [90] 549-558.

Schmidt T., Landwehrmeyer G. B., Schmitt I., Trottier Y., Auburger G., Laccone F., Klockgether T., Volpel M., Epplen J. T., Schols L., and Riess O. (**1998**) "An isoform of ataxin-3 accumulates in the nucleus of neuronal cells in affected brain regions of SCA3 patients"; *Brain Pathol.* [8] 669-679.

Schmitt I., Brattig T., Gossen M., and Riess O. (**1997**) "Characterization of the rat spinocerebellar ataxia type 3 gene"; *Neurogenetics.* [1] 103-112.

Seki T., Adachi N., Ono Y., Mochizuki H., Hiramoto K., Amano T., Matsubayashi H., Matsumoto M., Kawakami H., Saito N., and Sakai N. **(2005)** "Mutant protein kinase Cgamma found in spinocerebellar ataxia type 14 is susceptible to aggregation and causes cell death"; *J. Biol. Chem.* [280] 29096–29106.

Servadio A., Koshy B., Armstrong D., Antalffy B., Orr H. T., and Zoghbi H. Y. (**1995**) "Expression analysis of the ataxin-1 protein in tissues from normal and spinocerebellar ataxia type 1 individuals"; *Nat.Genet.* [10] 94-98.

Shehi E., Fusi P., Secundo F., Pozzuolo S., Bairati A., and Tortora P. (**2003**) "Temperature-dependent, irreversible formation of amyloid fibrils by a soluble human ataxin-3 carrying a moderately expanded polyglutamine stretch (Q36)"; *Biochemistry* [42] 14626-14632.

Sugiura A., Yonashiro R., Fukuda T., Matsushita N., Nagashima S., Inatome R., and Yanagi S. (**2010**) "A mitochondrial ubiquitin ligase MITOL controls cell toxicity of polyglutamine-expanded protein"; *Mitochondrion* [11] 139-146

Sultana R., Poon H. F., Cai J., Pierce W. M., Merchant M., Klein J. B., Markesbery W. R., and Butterfield D. A. (**2006**) "Identification of nitrated proteins in

Alzheimer's disease brain using a redox proteomics approach"; *Neurobiology of Disease* [22] 76-87.

Tait D., Riccio M., Sittler A., Scherzinger E., Santi S., Ognibene A., Maraldi N. M., Lehrach H., and Wanker E. E. (**1998**) "Ataxin-3 is transported into the nucleus and associates with the nuclear matrix"; *Hum.Mol.Genet.* [7] 991-997.

Takiyama Y., Oyanagi S., Kawashima S., Sakamoto H., Saito K., Yoshida M., Tsuji S., Mizuno Y., and Nishizawa M. (**1994**) "A clinical and pathologic study of a large Japanese family with Machado-Joseph disease tightly linked to the DNA markers on chromosome 14q"; *Neurology* [44] 1302-1308.

Tao R. S., Fei E. K., Ying Z., Wang H. F., and Wang G. H. (**2008**) "Casein kinase 2 interacts with and phosphorylatesataxin-3"; *Neurosci Bull.* [24] 271-277.

Tarlac V. and Storey E. (**2003**) "Role of proteolysis in polyglutamine disorders"; *J.Neurosci.Res.* [74] 406-416.

Trottier Y., Cancel G., An-Gourfinkel I., Lutz Y., Weber C., Brice A., Hirsch E., and Mandel J. L. (**1998**) "Heterogeneous intracellular localization and expression of ataxin-3"; *Neurobiol.Dis.* [5] 335-347.

Trottier Y., Lutz Y., Stevanin G., Imbert G., Devys D., Cancel G., Saudou F., Weber C., David G., Tora L., and . (**1995**) "Polyglutamine expansion as a pathological epitope in Huntington's disease and four dominant cerebellar ataxias"; *Nature* [378] 403-406.

Tsai H. F., Tsai H. J., and Hsieh M. (**2004**) "Full-length expanded ataxin-3 enhances mitochondrial-mediated cell death and decreases Bcl-2 expression in human neuroblastoma cells"; *Biochem.Biophys.Res.Commun.* [324] 1274-1282.

Villén J., Beausoleil S. A., Gerber S. A., and Gygi A. P. (**2007**) "Large-scale phosphorylation analysis of mouse liver"; *PNAS.* [104] 1488-1493.

Walter J., Schindzielorz A., Grunberg J, and Haass C. **(1999)** "Phosphorylation of presenilin-2 regulates its cleavage by caspases and retards progression of apoptosis"; *Proc. Natl. Acad. Sci. U. S. A.* [96] 1391–1396.

Wang G., Sawai N., Kotliarova S., Kanazawa I., and Nukina N. (**2000**) "Ataxin-3, the MJD1 gene product, interacts with the two human homologs of yeast DNA repair protein RAD23, HHR23A and HHR23B"; *Hum.Mol.Genet.* [9] 1795-1803.

Wang Q., Song C., and Li C. (**2003**) "Hexamerization of p97/VCP is promoted by ATP binding to the D1 domain and required for ATPase and biological activities"; *Biochemi Biophys Res Commun* [300] 253-360.

Woodgett J. R. **(1990)** "Molecular cloning and expression of glycogen synthase kinase-3/factor A"; *EMBO J.* [9] 2431–2438.

Wullner U., Seyfried J., Groscurth P., Beinroth S., Winter S., Gleichmann M., Heneka M., Loschmann P., Schulz J. B., Weller M., and Klockgether T. (**1999**) "Glutathione depletion and neuronal cell death: the role of reactive oxygen intermediates and mitochondrial function"; *Brain Res.* [826] 53-62.

Yang W., Tabrizi M., and Yi T. (**2002**) "A bipartite NLS at the SHP-1 C-terminus mediates cytokine-induced SHP-1 nuclear localization in cell growth control"; *Blood Cells Mol.Dis.* [28] 63-74.

Yoshizawa T., Yamagishi Y., Koseki N., Goto J., Yoshida H., Shibasaki F., Shoji S., and Kanazawa I. (**2000**) "Cell cycle arrest enhances the *in vitro* cellular toxicity of the truncated Machado-Joseph disease gene product with an expanded polyglutamine stretch"; *Hum.Mol.Genet.* [9] 69-78.

Yoshizawa T., Yoshida H., and Shoji S. (**2001**) "Differential susceptibility of cultured cell lines to aggregate formation and cell death produced by the truncated Machado-Joseph disease gene product with an expanded polyglutamine stretch"; *Brain Res.Bull.* [56] 349-352.

Yu Y. C., Kuo C. L., Cheng W. L., Liu C. S., and Hsieh M. **(2009)** "Decreased antioxidant enzyme activity and increased mitochondrial DNA damage in cellular models of Machado-Joseph diseas"; *J. Neurosci. Res.* [87] 1884–1891.

Zanuy D., Gunasekaran K., Lesk A. M., and Nussinov R. (**2006**) "Computational study of the fibril organization of polyglutamine repeats reveals a common motif identified in beta-helices"; *J.Mol.Biol.* [358] 330-345.

Zetina C. R. (**2001**) "A conserved helix-unfolding motif in the naturally unfolded proteins"; *Proteins* [44] 479-483.

Zhong X. and Pittman R. N. (**2006**) "Ataxin-3 binds VCP/p97 and regulates retrotranslocation of ERAD substrates"; *Hum.Mol.Genet.* [15] 2409-2420.

Zoghbi H. Y. and Orr H. T. (**2000**) "Glutamine repeats and neurodegeneration"; *Annu.Rev.Neurosci.* [23] 217-247.

Zuccato C., Ciammola A., Rigamonti D., Leavitt B. R., Goffredo D., Conti L., MacDonald M. E., Friedlander R. M., Silani V., Hayden M. R., Timmusk T., Sipione S., and Cattaneo E. (**2001**) "Loss of huntingtin-mediated BDNF gene transcription in Huntington's disease"; *Science* [293] 493-498.

GRAZIE….

- a mamma e papà per aver sempre capito il mio amore per la ricerca universitaria e averlo sempre sostenuto e per essermi sempre stati accanto anche quando non era facile…grazie!!
- ai nonni per essersi sempre interessati al mio lavoro, anche se non è facile capire esattamente cosa faccio e comprendere che, anche se sono ancora in università, non vado più a scuola!!
- a Paola per avermi dato questa opportunità di imparare e crescere tanto e perché comunque vadano le cose so che ha fatto di tutto per darmi la possibilità di restare.
- a Ale, la mia compagna di tanti anni di studio e lavoro, perché le nostre visioni della vita ci hanno sempre reso complementari e so che a lei posso sempre chiedere un consiglio.
- a Elena, la mia Elly, per tante cose…lavorare insieme ha reso unici tanti momenti!
- a Fede, amica e tesista, per i suoi ciaooo che rallegravano la giornata, per il suo sostegno e per la sua tesi…impresa epica!
- a Alessandra, perché è l'anima artistica del laboratorio e perché se non ci fosse bisognerebbe inventarla!
- a Matilde per il suo essere sempre pronta a dire la parola giusta al momento giusto per tirar su il morale.
- a Laura nuova tesista, per le chiacchierate andando a prendere il treno, non preoccuparti per la tua tesi….sarà un successo!
- a Simone per essere diventato subito parte del laboratorio e per tutte le risate.
- a tutte le mie stagiste di questi anni: Roberta, Bianca, Lisa, Daniela, Elena e Rubina, perché da tutte ho imparato qualcosa e perché mi sono laureata di nuovo un po' ogni volta con ognuna di loro.
- a tutti quelli che in questi anni sono stati parte del lab 4010, perché ognuno ha lasciato qualcosa: Marco, Sara, Lavinia Marcella, Vaios, Raffa e soprattutto Alessio, mio primo tesista perché nessuno mi sopportava come lui, e Chiara, mia maestra perché mi ha insegnato tanto e spero che sia soddisfata del risultato.

CK2 and GSK3 phosphorylation on S29 controls wild-type ATXN3 nuclear uptake

V. Pastori [a], E. Sangalli [a], P. Coccetti [a], C. Pozzi [a], S. Nonnis [b], G. Tedeschi [b], P. Fusi [a]

[a] Dipartimento di Biotecnologie e Bioscienze, Università di Milano-Bicocca, P.za della Scienza 2, 20126 Milan, Italy
[b] D.I.P.A.V. (Dipartimento di Patologia Animale, Igiene e Sanità Pubblica Veterinaria), Università degli Studi di Milano, via Celoria 10, 20133, Milan, Italy

a b s t r a c t

In the present work we show that murine ATXN3 (ATXN3Q6) nuclear uptake is promoted by phosphorylation on serine 29, a highly conserved residue inside the Josephin domain. Both casein kinase 2 (CK2) and glycogen synthase kinase 3 (GSK3) are able to carry out phosphorylation on this residue. S29 phosphorylation was initially assessed in vitro on purified ATXN3Q6, and subsequently confirmed in transfected COS-7 cells, by MS analysis. Site-directed mutagenesis of S29 to an alanine was shown to strongly reduce nuclear uptake, in COS-7 transiently transfected cells overexpressing ATXN3Q6, while substitution with phospho-mimic aspartic acid restored the wild-type phenotype. Finally, treatment with CK2 and GSK3 inhibitors prevented S29 phosphorylation and strongly inhibited nuclear uptake, showing that both kinases are involved in ATXN3Q6 subcellular sorting. Although other authors have previously addressed this issue, we show for the first time that ATXN3 is phosphorylated inside the Josephin domain and that S29 phosphorylation is involved in nuclear uptake of ATXN3.

1. Introduction

Ataxin-3 (ATXN3), the protein involved in SCA3 (Spinocerebellar Ataxia type 3), is a ubiquitously expressed protein [1–3], possessing a conserved N-terminal region, the Josephin domain, and a less conserved, unstructured C-terminus containing the poly-Q stretch [4–6]. The structure of the Josephin domain has been determined by NMR [7,8]. Many hypothesis have been formulated as regards ATXN3 function [9–13]. On the whole, recent data suggest a role for ATXN3 in proteasome mediated protein degradation, as a deubiquitinating enzyme which regulates flow through the ERAD (ER Associated Degradation) [7,14]. ATXN3 is mostly cytosolic, although it also localizes in the nucleus [15,16]. Nuclear localization is particularly relevant to SCA3 pathogenesis, in that pathologically expanded ATXN3 gives rise to nuclear aggregates. Different authors [13,17–20] presented evidence suggesting a model of the disease in which the full-length pathological protein is recruited into aggregates by “toxic” poly-Q containing fragments. In our laboratory we observed that purified ATXN3 underwent slow autolytic fragmentation [21] and subsequently showed that pathological ATXN3 was less proteolyzed than its normal counterpart [22]. Besides, some authors showed that ATXN3 is the target of caspase 1 [13], while others demonstrated that ATXN3 is cleaved by calpains [20,23]. The role of phosphorylation in SCA3 pathogenesis has not yet been thoroughly investigated. Tait and coworkers have shown the presence, in ATXN3 primary structure, of two putative casein kinase (CK2) phosphorylation sites [15]. Other authors [24] have shown that ATXN3 interacts with CK2. More recently Mueller and coworkers [25] showed that ATXN3 phosphorylation by CK2 on S340 and S352 promotes ATXN3 nuclear uptake. Protein kinase CK2 is a highly conserved, ubiquitously expressed Ser/Thr kinase, extremely abundant in the brain. This pleiotropic enzyme is involved in the control of various cellular processes [26], amongst which neural development [27]. Moreover, the catalytic α-subunit of CK2 is an inhibitor of the neuronal kinase Cdk5 [28]. Fei and coworkers [29] showed that ATXN3 is also phosphorylated by glycogen synthase kinase 3β (GSK 3β), a Ser/Thr kinase, particularly abundant in the central nervous system [30] that plays a key role in a number of cellular processes [31]. In this work we find that a murine form (ATXN3Q6) [32,33], is phosphorylated by CK2 and GSK3 on serine 29, a highly conserved residue inside the Josephin domain. We also show that phosphorylation at this residue controls nuclear uptake of ATXN3, a key event in SCA3 pathogenesis.

2. Materials and Methods

2.1. Constructs

cDNA coding for murine ATXN3Q6, previously subcloned in our laboratory into plasmid pGEX-6P-1, was cut with BamHI and XhoI restriction enzymes and subcloned into plasmid pcDNA3X(+)HA (Invitrogen UK Ltd. Paisley, England). Subsequently, ATXN3 coding cDNA, tagged with an HA epitope at the N-terminal, was retrieved by PCR from pcDNA3X(+)HA and subcloned into plasmid pcDNA3.1/myc-His, digested with the same enzymes, in frame with a c-myc epitope; the STOP codon was eliminated by site-directed mutagenesis. S29A and S29D mutants were obtained by PCR using Quik-

Change Site directed Mutagenesis Kit (Stratagene La Jolla, CA USA), according to the manifacturer's instructions. The correct insertion of cDNAs in expression vectors and the presence of the mutations were verified by automated sequencing using vector oligonucleotide primers (T7 and BGH). All constructs in pcDNA3.1/myc-His, carrying N-terminal HA and Cterminal c-myc epitopes, were hosted and amplified in E. coli strain DH5α, while protein expression was achieved after transient transfection of COS-7 cells or SHSY-5Y cells. Cultures were carried out in 94 mm plates in DMEM containing 10% fetal bovine serum (FBS), 100 U/ml penicillin, 100 μg/ml streptomycin and 4 mM glutamine (COS-7 cells) or in F12 and DMEM containing 10% fetal bovine serum (FBS), 100 U/ml penicillin, 100 μg/ml streptomycin and 4 mM glutamine (SHSY-5Y cells). Cells were subsequently transiently transfected with FuGENE6 (Roche Diagnostics Mannheim, Germany), according to the manufacturer's instructions. To inhibit CK2 and GSK3, COS-7 cells were incubated for 24 hours at 37 °C with either 5 or 10 μM CK2 inhibitor (TBB, Sigma St. Louis, Mo, USA) and/or with 10 μM GSK3 inhibitor (SB216763, Sigma St. Louis, Mo, USA). 24 h after transfection, cells were harvested and tested for subcellular localization of exogenous ATXN3 by blotting and detection with c-myc antibody. Cell viability was assessed through MTT test (Sigma St. Louis, Mo, USA), performed according to the manufacturer's instructions.

2.2. Cell fractionation

24 h after transfection, COS-7 cells (6×10^5 cells/plate, cultured in 94 mm plates) or SHSY-5Y cells (1×10^6 cells/plate, cultured in 94 mm plates) were harvested and resuspended in 10 mM $(Na)PO_4$, 100 mM NaCl, pH 7.4, 0.5% NP-40, supplemented with protease inhibitors (Roche Diagnostics Mannheim, Germany). After incubating 40 min on ice, nuclei were pelleted by centrifugation at 4000×g for 15 min at 4 °C. The supernatant, was centrifuged at 15,000×g for

30 min at 4 °C, yielding the cytosolic fraction. Nuclei were resuspended in 50 mMHEPES pH 7.9, 0.75 mM $MgCl_2$, 0.5 mM EDTA, 0.5 M NaCl, 12.5% glycerol, 5 mM DTT and protease inhibitors. After incubating 1 h on ice nuclei were centrifuged at 15,000×g for 30 min at 4 °C: the supernatant represented the nuclear fraction.

2.3. Immunoprecipitation

1000 μg total protein extract, obtained from ATXN3Q6 overexpressing COS-7 cells, was incubated overnight at 4 °C with an anti-ATXN-3 polyclonal antibody, (2 μg of Z46 antibody (Primm Cambridge, MA USA). The total extract was subsequently incubated with Protein A-Sepharose ™-CL-4B (Amersham GE Healthcare, Uppsala, Sweden) for 2 h at 4 °C. After incubation the resin was washed 3 times with NP40 buffer (50 mM Tris pH 7.5, 150 mM NaCl, 15 mM$MgCl_2$ and 1% NP40) and ataxin-3 was eluted by boiling in SDS buffer.

2.4. SDS-PAGE and western-blot analysis

SDS-PAGE and Western-blot were carried out by standard procedures. PVDF Immobilon™ P Millipore Billerica, MA USA) membranes were blocked for 1 h in PBS , containing either 5% (w/v) dried milk (for anti-c-myc antibody) or in 5% (w/v) bovine serum albumin (BSA) (Sigma St. Louis, Mo, USA) (for anti-fibrillarin and anti-Phosphoglycerate kinase (PGK) antibodies). Membranes were subsequently probed overnight in PBS 1% dried milk, with anti-c-myc mouse monoclonal antibody (1:1000) (Santa Cruz Biotechnology Inc. Santa Cruz, CA. USA). Control incubations with anti-fibrillarin (1:5000) (Encor Biotechnology Gainesville, FL, USA) and with 22C5 anti-PGK (1:1000) (Molecular Probes, Invitrogen UK Ltd. Paisley, England) mouse monoclonal antibodies were also carried out overnight in PBS, containing 1% (w/v) BSA, 0.1% (v/v) Tween20 and 1% (w/v) BSA respectively. Membranes, probed with mouse antibodies, were incubated for 1 h with an anti-mouse horseradish peroxidase-conjugated IgG (1:3000) (Calbiochem Darmstadt, Germany) in PBS, containing 0.1% (v/v) Tween20 and 1% (w/v) dried milk. Detection of antibody binding was carried out with ECL (Amersham GE Healthcare, Uppsala, Sweden), according to the manufacturer's instructions. Protein levels were quantified by densitometry of scanned not saturated X-ray films using the NIH Image-based software Scion Image (Scion Corporation). Quantification data are a mean of three independent experiments; bands intensities were normalized on fibrillarin and PGK controls. Statistical analysis was performed using t-Student test, results significance was indicated with $p<0.05$.

2.5. Acid silver stain

SDS-PAGE was fixed for 1 h in 40% Ethanol, 10% acid acetic and for 2 days in 5% ethanol, 5% acid acetic; the gel was subsequently washed 3 times for 20 min in 30% ethanol and incubated for 1 min in 0.8 mM sodium tiosulfate. The gel was then incubated in 11.8 mM silver nitrate, 0.02% formaldehyde for 20 min and subsequently washed twice with water for 20 sec and developed with 556 mM sodium carbonate, 0.02% formaldehyde, 0.02 mM sodium tiosulfate. Developing was stopped with 50% ethanol, 12% acid acetic; the gel was washed with water for 10 min and conserved at 4 °C in 1% acid acetic.

2.6. Immunofluorescence and confocal analysis

COS-7 cells were plated onto coverslips (2.5×10^4 cells/coverslip) and grown for 24 h before transfection. Cells were transfected overnight with FuGENE6 (Roche Diagnostics Mannheim, Germany); 24 h after transfection, cells were fixed for 20 min in 3% (w/v) paraformaldehyde in PBS and quenched for 30 min

with 50 mM NH_4Cl in PBS. Permeabilization was carried out by incubating the cells in the presence of 0.3% (w/v) saponin in PBS (7 min for 3 times). Cells were then doubly stained with anti-c-myc mouse monoclonal antibody (Santa Cruz Cruz Biotechnology Inc. Santa Cruz, CA USA) and anti-HA rabbit polyclonal antibody (Sigma St. Louis, Mo USA). After extensive washes, cells were incubated with donkey anti-mouse Cy3 conjugated antibody and donkey anti-rabbit Cy2 conjugated antibody. All antibodies were from Jackson ImmunoResearch Laboratories (West Grove, PA USA). Incubations and washes were carried out at room temperature in PBS, 0.3% (w/v) saponin. Cells were finally incubated for 15 min with the nuclear marker TO-PRO-3 iodide (Molecular Probes, Invitrogen UK Ltd Paisley, England). Confocal microscopy was performed using a Leica Mod. TCS-SP2 (Leica Microsystem). Image processing was performed with Leica Confocal Software (LCS) and Adobe Photoshop Software. Confocal microscopy images were collected under the same conditions in order to compare fluorescence intensities among different images. About 120 cells were examined in each image and 6 images were analyzed for each experiment; the nuclear region was circumscribed and its mean fluorescence intensity was evaluated. Statistical analysis was performed using t-Student test, results significance was indicated with $p<0.05$.

2.7. Purification from E.coli

ATXN3Q6-encoding cDNA, cloned into plasmid pGEX-6P-1, was used to transform E. coli strain BL21 codon plus RIL, to express ATXN3 as a GST-fusion protein. Cells were grown at 37 °C in LB-ampicillin medium and induced at A_{600} 0.8, for 3 h with 50 μM IPTG. In order to obtain crude extracts, cells were resuspended in lysis buffer (10 mM potassium phosphate, pH 7.2, 150 mM NaCl, 1 mM phenylmethanesulfonyl fluoride, 5 mM DTT, 100 mM $MgCl_2$) plus 1 mg/ml lysozyme and incubated for 1 h at 4 °C. Cell suspension was then frozen at -80 °C for 20 min and thawed; DNase I (0.15 mg/g of cells, wet weight) and 1% Triton X-100 were added, and the sample further incubated for 30 min at room temperature. After centrifugation for 30 min at 18,000×g, the supernatant was incubated with Glutathione Sepharose 4B resin (1 ml/g of cells, wet weight) (GE Healthcare, Uppsala, Sweden) for 40 min at 4 °C; the sample was subsequently loaded onto the column. After washing with 10 volumes of PBS (10 mM potassium phosphate, pH 7.2, 150 mM NaCl) and equilibration with 10 volumes of cold Cleavage Buffer (50 mM Tris-HCl, pH 7.0, 150 mM NaCl, 1 mM EDTA, 1 mM DTT), ATXN3 was cleaved from fusion partner by overnight incubation at 4 °C with Prescission Protease (80 U/ml resin) (GE Healthcare, Uppsala, Sweden)). Purified ATXN3 was eluted with 10 ml of Cleavage buffer. Protein concentration was assayed through Coomassie brilliant blue G-250 from Pierce (Pierce Biotechnology, Rockford, IL), using bovine plasma immunoglobulin as a standard protein.

2.8. In vitro phosphorylation by CK2

ATXN3Q6 purified from E. coli was dialyzed for 3 h at 4 °C against 50 mM Tris pH 8, 150 mM NaCl, 10 mM $MgCl_2$, with a 14 kD cut-off membrane. ATXN3Q6 (40 μg) was then incubated for 30 min at 30 °C, under shaking, with 1 μg (200 U) CK2 (BIOMOL international Plymouth Meeting, PA USA) in the presence of 1 mM ATP. The sample was then subjected to MALDI-TOF analysis. If needed, phosphorylation was checked using [γ-^{32}P]ATP, as previously reported [34].

2.9. In vitro phosphorylation by GSK3

ATXN3Q6 purified from E. coli was dialyzed for 3 h at 4 °C in GSK3 buffer (25 mM MOPS pH 7.2, 12.5 mM β-glycerophosphate, 5 mM EGTA, 2 mMEDTA, 25 mM$MgCl_2$, 0.25 mMDTT, 50 ng/ μl BSA) with a 14 kD cut-off membrane. ATXN3Q6 (40 μg) was then incubated with 1 μg (100U) GSK3 (BIOMOL international Plymouth Meeting, PA. USA) and ATP 100 μMat 30 °C for 30 min. The sample was then subjected to analysis.

2.10. Mass spectrometry analysis

ATXN3Q6, phosphorylated in vitro by either CK2 or GSK3 as described above, was subjected to reduction and alkylation in solution by iodoacetamide and incubated with GluC endoproteinases (1:25 enzyme/protein, w/w) overnight at 37 °C. Following acidification, the peptide mixture was loaded onto a MALDI plate using ZipTip C18 (Millipore, Bedfor, MA-USA) with a matrix of α-ciano-4-hydroxycinnamic acid. The same procedure was applied for the analysis of ATXN3Q6 in transfected cells. In the latter case the protein, separated by SDS-PAGE, was subjected to in situ digestion with Glu-C endoproteinase (1:10 enzyme/protein, w/w) and peptide extraction with 40% CH_3CN in 0.1% TFA before loading onto the MALDI plate. Mass spectrometry analysis was carried out on a Bruker Daltonics Reflex IV instrument (Bruker Daltonics, Milano, Italy) equipped with a nitrogen laser, operating in positive and negative linear mode. Each spectrum was accumulated for at least 200 laser shots and Bruker peptide calibration standards were used for calibration. MS/MS analysis was carried out on a MALDI TOF/TOF Autoflex III (Bruker Daltonics, Milano, Italy). Data were acquired and processed using Biotools software (Bruker Daltonics, Milano, Italy).

3. Results

3.1. ATXN3 is phosphorylated in vitro by Casein Kinase II

A bioinformatic analysis, performed through NetPhos 2.0, Net-PhosK 1.0 and ScanProsite servers available at www.expasy.ch, as well as Phosidia server available at Phosidia.com, showed the presence, along ATXN3 aminoacidic sequence, of a series of phosphorylation consensus sites for several kinases. However, within the Josephin domain, the only structured part of the protein, only one residue (S29) was predicted by all four servers to be phosphorylated with a high score. This site appears to be highly conserved in vertebrates, from fish to mammals, as shown in Fig. 1a. According to ScanProsite, NetPhos 2.0 and Phosida servers, S29 is phosphorylated by CK2, despite the presence of a proline at the C-terminal side of the phosphorylated residue; moreover phosphorylation by GSK3 is also predicted at S29 by NetPhosK 1.0 server. As shown in Fig. 1a, another highly conserved consensus site for CK2 is S236, a residue located upstream of the poly-Q stretch, but outside the Josephin domain, which is also predicted to be phosphorylated by CK2 by all servers. S256, another highly conserved phosphorylation site, predicted to be phosphorylated by GSK3 by NetPhos 2.0 and Phosidia servers, was already demonstrated to be phosphorylated by this kinase [29]. Other consensus sites were found in the C-terminal unstructured domain: a cluster of five phosphorylation sites predicted to be phosphorylated either by CK2 or by GSK3 (S268, T271, S272, S273, S277) and the two serines already demonstrated to be phosphorylated by CK2 by Mueller and coworkers (S329 and S341 in murine ATXN3, corresponding to S340 and S352 respectively in human ATXN3) [25]. However, most of these sites (as well as others such as S321 and T344) are not predicted to be phosphorylated by all four servers, nor are they highly conserved, as shown in Fig. 1a. In order to ascertain whether ATXN3 can be phosphorylated by CK2, purified recombinant murine ATXN3Q6, obtained as previously reported [33], was subjected to in vitro phosphorylation by CK2. Autoradiography (Fig. 1b) showed that ATXN3 is actually phosphorylated by this kinase, confirming that sites phosphorylatable by CK2 are present in this protein, as previously reported [25,29]. Lower molecular mass bands are also seen, representing ATXN3 proteolytic fragments, whose characterization was described in a previous work [22]. Since none of the existing studies on ATXN3 phosphorylation had been carried out through mass spectrometry, we decided to investigate ATXN3 phosphorylation through a proteomic approach. The study of the role of CK2 phosphorylation at S29 and S236 appeared of particular interest, since these are the most conserved CK2 phosphorylation sites, the C-terminal domain being more divergent, and because no previous study had investigated phosphorylation of the N-terminus

3.2. ATXN3 is phosphorylated in vitro by CK2 and GSK3 on S29

In order to assess which of the predicted CK2 and/or GSK3 phosphorylatable residues are actually phosphorylated, recombinant ATXN3 was subjected to in vitro phosphorylation by either CK2 or GSK3, digestion with Glu-C and mass spectrometry analysis. Operating in the linear mode, upon incubation of wild-type ATXN3 with either CK2 or GSK3, it was possible to detect peaks corresponding to monophosphorylated peptides containing S29 (Fig. 2). A list of the phosphorylated peptides identified through mass spectrometry is reported in Fig. 2a. The peak at 3002.13 m/z was also analyzed by MS/MS TOF-TOF analysis unequivocally confirming the phosphorylation of ATXN3 on S29 residue (data not shown). Upon phosphatise treatment the corresponding non-phosphorylated peaks were detected (data not shown). Fig. 2b reports three of the spectra relative to the peptides, obtained after phosphorylation with CK2: peak at 2172.32 m/z corresponds to the phosphorylated peptide 27-44 ($_{27}$YFSPVELSSIAHQLDEEE$_{44}$, calculated average mass 2172.97), peak at 3002.13 m/z corresponds to the phosphorylated peptide 8-32 ($_{8}$KQEGSLCAQHCLNNLLQGEYFSPVE$_{32}$, calculated monoisotopic mass 3001.35) and peak at 3516.00 m/z corresponds to the phosphorylated peptide 3-32 ($_{3}$SIFHEKQEGSLCAQHCLNNLLQGEYFSPVE$_{32}$, calculated monoisotopic mass 3516.64). Moreover, mass spectrometric analysis of the protein fingerprint allowed to detect only peptides containing unmodified S236, showing that this residue is not phosphorylated in such conditions. Besides the modification in the Josephin domain, phosphorylation at serine residues in the C-terminal portion of the molecule was also observed: S268, S272, S273, S277, T271, S329 and S341, were all found to be phosphorylated by CK2; S268, S272, S273 and S277 were also found to be phosphorylated by GSK3 (data not shown). These findings are in accordance with previous data reported by Mueller and coworkers [25], who described the phosphorylation of human ATXN3 at S340 and S352, corresponding to murine ATXN3 S329 and S341 respectively. Taken together, our results provide evidence that ATXN3 is phosphorylated in vitro on residue S29 by CK2 and GSK3 and suggest a direct role of these kinases in in vivo phosphorylation of ATXN3 within the Josephin domain.

3.3. ATXN3 is phosphorylated in transfected COS-7 cells

COS-7 cells overexpressing ATXN3Q6 were collected 24 h after transfection; the recombinant protein was immunoprecipitated from crude extracts with anti-ATXN3Q6 polyclonal Z46 antibody and subsequently loaded onto SDS-PAGE. Bands were detected through acid silver staining and subjected to

in situ digestion with Glu-C endoproteinase. Mass spectrometry analysis of the protein expressed in transfected cells unequivocally confirmed that ATXN3Q6 is phosphorylated at S29, since it was possible to detect phosphopeptides containing S29 upon fingerprint mass analysis, as reported in Table 1 (phosphopeptide $_{27}$YFSPVE$_{32}$, calculated monoisotopic mass 821.34, experimental mass 821.98, and phosphopeptide $_{27}$YFSPVELSSIAHQLDEEE $_{44}$, calculated monoisotopic mass 2172.97, experimental mass 2173.02) .

3.4. ATXN3Q6S29A is less efficiently translocated to the nucleus than the wild-type

With the aim of investigating the role of phosphorylation on S29, this residue was substituted with an alanine, through site-directed mutagenesis performed with Quik Change Mutagenesis Kit (Stratagene La Jolla, CA USA). COS-7 cells were transiently transfected with plasmid pcDNA3.1/myc-His, expressing either wild-type ATXN3Q6 or ATXN3Q6S29A carrying an HA epitope at the N-terminus and a c-myc epitope at the C-terminus. Cells were harvested 24 h after transfection and cytosolic and nuclear fractions were analysed by Western blotting, probed with a monoclonal anti-c-myc antibody. Results are shown in Fig. 3a: the band corresponding to wild-type ATXN3Q6 was found equally distributed between the cytoplasm and the nucleus. On the contrary, the band corresponding to S29A mutant was found much less abundant in the nuclear fraction, being about 25% of the intensity of the corresponding cytosolic band, as shown by densitometric analysis (Fig. 3c); statistical analysis confirmed the existence of a significant difference between nuclear and cytosolic S29A mutant ($p<0.05$); no differences were found between nuclear and cytosolic wild-type ATXN3 ($p=0.52$). This suggests that S29 phosphorylation promotes ATXN3 nuclear uptake. Confocal microscopy confirmed these results: as seen in Fig. 4a wild-type ATXN3Q6 fluorescence, both red (due to Cy3 conjugated anti-c-myc antibody) and green (due to Cy2 conjugated anti-HA antibody), was evenly distributed inside the cells. On the other hand, S29A mutant fluorescence was found to be much weaker inside the nucleus than in the cytoplasm. The overlay with the blue fluorescence emission of the nuclear marker confirmed that wild-type ATXN3 is found also inside the nucleus, while S29A mutant is found predominantly in the cytosol. Quantitative analysis of fluorescent emission allowed to assess that S29A mutant fluorescence in the nuclear region amounted to about 30% of wild-type ATXN3 fluorescence in the same area (Fig. 4b); statistically significant differences were found between wild-type ATXN3 and S29A mutant ($p<0.05$). In order to confirm the role of S29 phosphorylation on ATXN3 nuclear uptake, this residue was substituted with an aspartic acid, thus mimicking the presence of the phosphate negative charge. After ATXN3Q6S29D transient expression in COS-7 cells, cytoplasmic and nuclear fractions were analysed by Western blotting. Results, shown in Fig. 3b, showed that S29D behaved exactly like the wild-type, being equally distributed in the nucleus and the cytoplasm. Consistently, a uniform fluorescence distribution inside the cells was detected in confocal microscopy experiments, as shown in Fig. 4a, the overlay showing colocalization with the nuclear marker. Quantitative fluorescence analysis confirmed that S29D fluorescence in the nuclear region did not remarkably differ from that of wild-type ATXN3Q6 (Fig. 4b); statistical analysis yielded a p value 0.53, confirming the absence of any statistically significant differences between wild-type ATXN3 and S29D mutant. Moreover the same percentage of cells showing the described subcellular localization was found in all samples considered, as shown in the last column of Fig. 4a. Cell viability, assayed through MTT test, showed a 30% reduction for S29A mutant, when compared to both wild-type protein and S29D mutant; statistical analysis of three different experiments yielded a p value b0.05 for the comparison between wild-type ATXN3 and S29A mutant, while a p value of 0.21 was found when comparing wild-type ATXN3 with S29D mutant. The previously observed [22] 42 kDa fragment, produced by proteolytic cleavage at S29, was found almost exclusively in the cytosolic fractions and appeared to be more evident in S29A mutant than in the wild-type protein and in S29D mutant. In order to rule out the possibility that the observed phenotype of S29A mutant might be confined to COS-7 cells, human neuroblastoma SHSY-5Y cells were also transfected with plasmid pcDNA3.1/myc-His, expressing either wild-type ATXN3Q6 or ATXN3Q6S29A carrying an HA epitope at the N-terminus and a c-myc epitope at the C-terminus. Cytosolic and nuclear fractions, obtained from harvested cells 24 h after transfection, were analysed by Western blotting, probed with a monoclonal anti-c-myc antibody. Results, reported in Fig. 3d, show the absence of S29A in the nuclear fraction, in accordance with what observed in COS-7 cells.

3.5. CK2 and GSK3 inhibitors demonstrate that both kinases act on S29 in COS-7 transfected cells

COS-7 cells expressing either ATXN3Q6 or ATXN3Q6S29D were grown in the presence of CK2 inhibitor TBB (tetrabromobenzotriazole) and GSK3 inhibitor SB216763. Inhibitors were added to growth media either separately or in combination. Western-blots of nuclear and cytosolic fractions, probed with anti-c-myc antibody, are shown in Fig. 5. When the culture medium was upplemented with TBB alone, as shown in Fig. 5a, both wild-type ATXN3Q6 and S29D mutant were found evenly distributed between the cytosol and the nucleus, suggesting that TBB could not prevent S29 phosphorylation even at 10 μM concentration. The same happened when only GSK3 inhibitor SB216763 was administered at 10 μM concentration, as shown in Fig. 5b. However, when both inhibitors were added to culture medium, nuclear translocation of wild-type ATXN3Q6 appeared to be reduced, a behaviour closely mirroring that

of S29A mutant (see Fig. 5c); on the contrary, S29D mutant appeared to be uniformily distributed between nucleus and cytosol. Intensities of ATXN3 bands in total extracts were found to be similar, showing that the mutation did not affect ATXN3 expression levels. These data were confirmed by densitometric analysis, reported in Fig. 5d, showing that, when both inhibitors were administered, about 50% of the intensity of the corresponding cytosolic band of wild-type ATXN3 was found inside the nucleus, while S29D mutant was equally distributed between the two cellular compartments; the statistically significant difference in nuclear and cytosolic localization of ATXN3 in the presence of the inhibitors was confirmed by a p value <0.05. Mass spectrometry analysis, performed on acid silver stained gels after ATXN3Q6 immunoprecipitation from COS-7 cells cultured in the presence of both TBB and SB216763, allowed to detect a peptide containing unmodified S29, ($_{27}$YFSPVELSSIAHQLDEEE$_{44}$, calculated monoisotopic mass 2092.97, experimental mass 2092.78), showing that this residue is not phosphorylated when both CK2 and GSK3 inhibitors are present. On the whole these data clearly show that CK2 and GSK3 can concur in the phosphorylation of S29, promoting ATXN3 nuclear uptake.

4. Discussion

Phosphorylation is well known to play a role in a number of neurodegenerative diseases, notably in amyloid fibers formation. Nonaka and coworkers [35] have shown that α-synuclein is phosphorylated on Ser 129 and that this is crucial in mediating both protein neurotoxicity and inclusion formation; other authors have shown that hungtintin is phosphorylated by Cdk5 [36]. Phosphorylation has also been reported to protect presenilin-2 from caspase cleavage [37]. Amongst ataxias, SCA14 is caused by mutations on residues which are normally phosphorylated: unphosphorylated proteins do not fold correctly and aggregate [38]; ATXN1, the protein responsible for Sca1 has been demonstrated to be phosphorylated by Akt at S776; this phosphorylation creates a binding site for 14-3-3, increasing ATXN1 stabilization and accumulation and hence leading to pathogenesis [39,40]. Amongst the kinases involved in neurodegenerative diseases, CK2 and GSK3 are particularly interesting. In neuronal cells there appears to be a myriad of CK2 substrates that have clear implications in neural development, neuritogenesis, synaptic transmission and plasticity [27]. On the other hand, of the two isoforms of GSK3 which are found in mammals, GSK3β and GSK3α [41], GSK3β is particularly abundant in the central nervous system [30] and has been found to be involved in Alzheimer disease pathogenesis [42]. Some authors already addressed the issue of ATXN3 phosphorylation [15,24,25,29], however, their studies were conducted mainly through pull-down assays and coimmunoprecipitations. In this work, we investigated for the first time the role of ATXN3 phosphorylation through a proteomic approach. Amongst the different putative phosphorylation consensus sites which are found alongATXN3 sequence, we found that S29, the only phosphorylatable site within the Josephin domain, can be phosphorylated in vitro by both CK2 and GSK3. Phosphorylation on S29 was subsequently confirmed in transfected COS-7 cells overexpressing ATXN3Q6 and was found to be prevented by the addition of CK2 and GSK3 inhibitors. On the contrary, S236, another highly conserved phosphorylation site, was found to be unphosphorylated in mass spectrometry analysis. Moreover, our data confirmed phosphorylation at C-terminal sites already described by other authors, such as S256 [29] and S329 and S341, corresponding to S340 and S352 respectively in human ATXN3 [25]. It is worth mentioning that Serine 29 is recognized, by prediction methods, as part of a consensus sequence for both CK2 and GSK3, although the presence of a proline nearby is known to prevent phosphorylation by CK2 in some instances; experimental data allowed to confirm this prediction. Our decision to focus on S29 phosphorylation is motivated by the fact that this residue is highly conserved in vertebrates; moreover, it is the only putatively phosphorylated site within the Josephin domain and, according to the NMR determined structure [8] is fully exposed to the solvent and presumably easily accessible. On the other hand, we did not focus on consensus sites located in the C-terminal domain, since they appear to be less conserved and had already been studied by other authors. In order to assess whether phosphorylation at S29 could regulate ATXN3 subcellular localization, we substituted S29 with an alanine, through site-directed mutagenesis. Results showed that mutation to alanine strongly reduced nuclear uptake. The fact that, upon substituting S29 with an aspartic acid, the wild-type phenotype is restored, shows that the reduction of nuclear uptake is due to the lack of the negative phosphate charge and not to the aminoacid substitution. The site of proteolytic cleavage seems to be unaffected by the lack of phosphorylation; however S29A mutant seems to be cleaved at S29 to a higher extent than both wild-type and S29D mutant, suggesting that phosphorylation at this level might hamper proteolytic cleavage; the double band which is seen in correspondence of S29A 42 kDa fragment is also present in wild-type ATXN3 and is probably an artifact. More work will be necessary to elucidate the nature and role of the so far unknown protease involved in the cleavage. Mass spectrometry analysis also showed beyond any doubt that ATXN3 is phosphorylated in transfected cells and this strongly suggests that phosphorylation takes place also in vivo. Moreover, the fact that CK2 and GSK3 concur in phosphorylating S29 points to the importance of ATXN3 nuclear translocation. Results obtained with

both inhibitors suggest that no other kinases are involved in this process. All our experiments have been performed on murine ATXN3, carrying only six glutamines and sharing a high similarity with normal human ATXN3; as stated before [22], the choice of this protein is justified by the effort to avoid aggregate formation, which can be artificially induced by the unnatural raising in concentration which takes place inside transfected cells, since the aggregation process follows a second order kinetic [33]. The presence of only six glutamines in murine ATXN3, makes the event rather unlikely. Moreover we already showed that human ATXN3Q26 behaves exactly like murine ATXN3Q6 when expressed at low levels in transfected cells, as regards subcellular sorting and proteolytic fragmentation [22]. Our data show a strong reduction in nuclear uptake, which is nevertheless not completely abolished. The possibility that this event is controlled by more than one factor is very likely. In a recent paper, Mueller at al. identified CK2 phosphorylation on S340 and S352, two residues which are found downstream of poly-Q, as essential for nuclear translocation [25]; although, as mentioned above, we did not focus on phosphorylation at these residues, our data are definitely not in contrast with those of Mueller and coworkers. Since S340 and S352 are both found inside UIM3, whose presence in ATXN3 structure depends on alternative splicing, phosphorylation at S29 may well be an additional factor promoting nuclear uptake, a process which seems essential for ATXN3 function. In addition, ATXN3 nuclear uptake does not seem to be completely suppressed in Mueller and coworkers experiments [25], neither upon S340/S352 mutagenesis to alanine nor upon addition of CK2 inhibitors. Last but not least, the fact that when S29 is substituted with an alanine, a 30% decrease in cell viability is observed, suggests that nuclear uptake is an important process for ATXN3 functionality, possibly in relation to its function as a transcriptional repressor [9,43], and is finely controlled by more than one factor. In contrast to Mueller and coworkers, a recent paper [44] showed that CK2 inhibitors are not effective in preventing ATXN3 nuclear localization upon heat-shock; this is well in accordance with our data showing that only simultaneous inhibition of both CK2 and GSK3 can prevent ATXN3 nuclear uptake. These authors also showed that S111, which is found inside a Polo-like kinase phosphorylation site, is involved in ATXN3 nuclear uptake following heat-shock; we propose that this residue be involved in nuclear uptake promoted by heat-shock or oxidative stress, while phosphorylation at S29, S340 and S352 could regulate normal ATXN3 trafficking between the nucleus and the cytoplasm. This is strongly supported by the fact that, in Reina and coworkers experiments, S111 mutation to alanine decreases ATXN3 nuclear localization but does not suppress it. Whether a putative NLS, which is found in ATXN3 primary sequence, is essential for ATXN3 nuclear translocation is still controversial: in a previous work [22] we showed that a truncated mutant lacking this sequence was only slightly less efficiently translocated into the nucleus; Mueller and coworkers, as well as Reina and coauthors, recently confirmed that NLS mutation has no effect on ATXN3 subcellular distribution. On the other hand other authors [45] showed, through a yeast nuclear import assay, that ATXN3 NLS is functional and essential for nuclear uptake. Nuclear translocation of ATXN3 is also of the utmost importance for SCA3 pathogenesis, since amyloid aggregates are found primarily inside the nucleus. Although a growing amount of data suggest that mitochondrial damage is also involved in SCA3 pathogenesis [46–48], the presence of nuclear aggregates is a hallmark of many neurodegenerative diseases and impairment of nuclear functions is very likely to induce cell death. Our data strongly suggest that inhibiting S29 phosphorylation, strongly reduces ATXN3 nuclear uptake. This in turn leads to the key question of how S29 phosphorylation is involved in SCA3 pathogenesis. In a previous work [22] we suggested that a toxic poly-Q containing fragment is produced from incomplete proteolysis of pathological human ATXN3Q72, which can trigger aggregation of pathological undegraded ATXN3, upon reaching a critical concentration inside mitochondria and the nucleus. Recently, Hubener et al. [49] showed that in transgenic mice nuclear aggregation of pathological ATXN3 occurs even when an expanded ATXN3 carrying a NES is coexpressed and demonstrated that double transgenic mice, expressing both normal and pathological ATXN3 show the same disease progression, as transgenic mice expressing only the pathological proteins; this is consistent with the idea that aggregation is a concentration process and could also be explained by the already
proposed hypothesis of expanded polyQ stretching giving rise to membrane channels. Moreover another recent work [50] showed that the C-terminus of Hsp70-interacting protein (CHIP) suppresses ATXN3Q70 neurotoxicity in transgenic mice, preventing the formation of toxic microaggregates. Ubiquitinylation by either E4B or CHIP is essential to target misfolded ATXN3 to the proteasome [10,24]. Data of different authors [24,25] have shown that pathological ATXN3 is also a substrate of CK2, suggesting that phosphorylation may target pathological ATXN3 to the nucleus, where it will readily form aggregates, escaping ubiquitinylation and targeting to proteasomal degradation. Further work will be undertaken in order to understand the role of CK2 and GSK3 in SCA3 pathogenesis.

Acknowledgements

The authors would like to thank Dr Anna Maria Villa (Dipartimento di Biotecnologie e Bioscienze, Università di Milano-Bicocca, Milan, Italy) for technical support in immunofluorescence experiments.

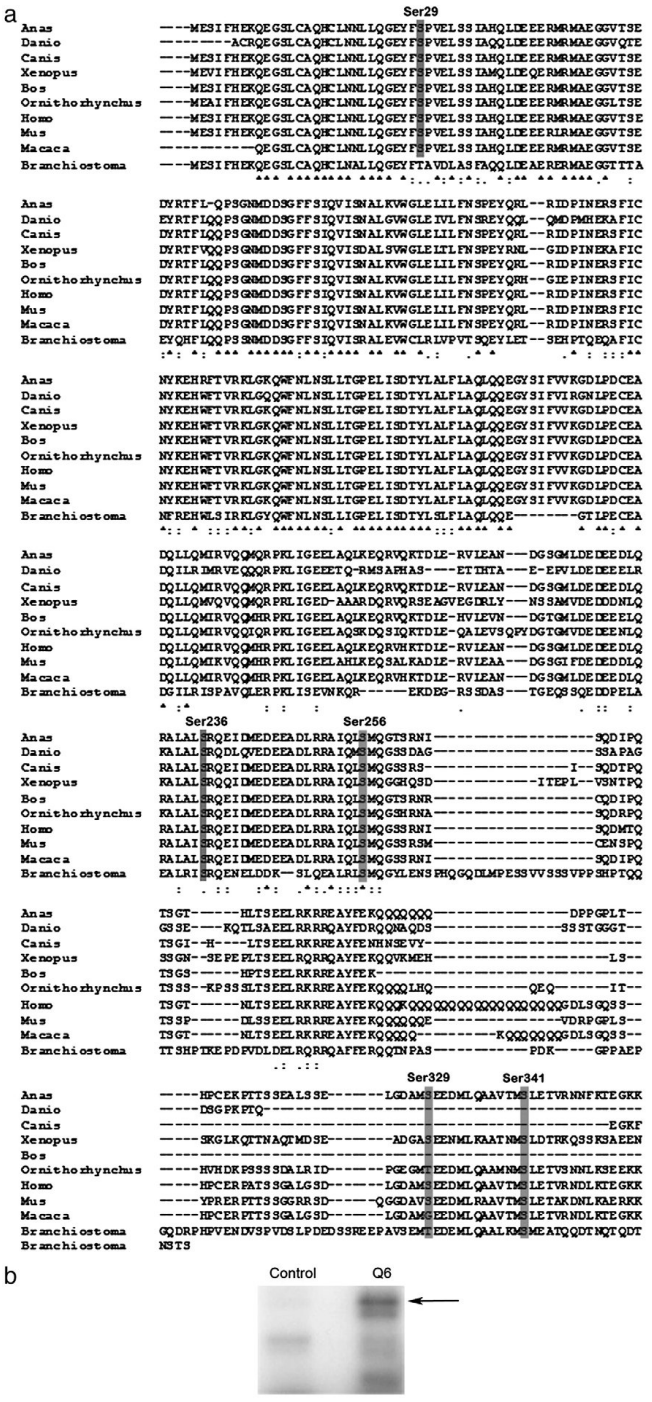

Fig. 1. In vitro CK2 phosphorylation of ATXN3. (a) T-Coffee multiple sequence alignment of ataxins-3: Anas platyrhynchos (duck; ABX10879), Danio rerio (zebrafish; AAY28605), Canis lupus (dog; XP537352), Xenopus laevis (african clawed frog; NP001016389), Bos tauros (domestic cow; AAI46167), Ornithorhynchus anatinus (platypus; XP001507271), Homo sapiens (man; BAI46626), Mus musculus (mouse; NP083981), Macaca rhesus (macaque; XP001116022), Branchiostoma lanceolatum (amphioxus XP002610252); conserved serines are marked. (b) In vitro phosphorylation of purified recombinant murine ATXN3Q6 (arrow); an E. coli crude extract subjected to the same purification procedure (see Materials and Methods) was used as a control.

a

AT-3	Kinase	Peptide	Species	Predicted mass	Identified mass
	CK2				
Wild type		^{27}YF**S**PVE^{32}	P-Ser -18	723.34	723.30
		^{27}YF**S**PVELSSIAHQLDEEE^{44}	P-Ser +80	2172.97	2172.32
		^{8}KQEGSLCAQHCLNNLLQGEYF**S**PVE^{32}	P-Ser +80	3001.35	3002.13
		^{3}SIFHEKQEGSLCAQHCLNNLLQGEYF**S**PVE^{32}	P-Ser -18	3516.64	3516.00
	GSK3				
Wild type		^{27}YF**S**PVE^{32}	P-Ser -18	723.34	723.53
		^{27}YF**S**PVELSSIAHQLDEEE^{44}	P-Ser +80	2172.97	2173.00
		^{8}KQEGSLCAQHCLNNLLQGEYF**S**PVE^{32}	P-Ser +80	3001.35	3001.00

b

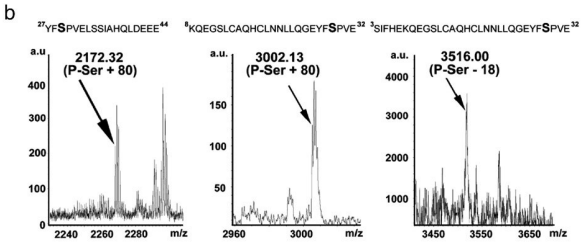

Fig. 2. ATXN3 is phosphorylated on Ser 29 by CK2 and GSK3. (a) 8 μg of ATXN3 was phosphorylated in vitro either by CK2 or GSK3. Samples were denatured in 8 Murea and subjected to reduction and alkylation in solution by iodoacetamide. After dilution and incubation with GluC endoproteinases (1:25 enzyme/protein, w/w) overnight at 37 °C, samples were analysed by Mass analysis (as described in the experimental section). The presence of the phosphate group results in an increase in mass of 80 units or in a decrease of 18 units due to the loss of the phosphate and a water molecule. (b) Peak at 2172.32 m/z corresponds to the CK2 phosphorylated peptide 27-44 ($_{27}$YFSPVELSSIAHQLDEEE$_{44}$, calculated average mass 2172.97), peak at 3002.13 m/z corresponds to the CK2 phosphorylated peptide 8-32 ($_{8}$KQEGSLCAQHCLNNLLQGEYFSPVE$_{32}$, calculated monoisotopic mass3001.35) and peak at 3516.00 m/z corresponds to the CK2 phosphorylated peptide 3-32 ($_{3}$SIFHEKQEGSLCAQHCLNNLLQGEYFSPVE$_{32}$, calculated monoisotopic mass 3516.64) are indicated. Data are representative of one of three experiments

Table 1 ATXN3 is phosphorylated on Ser 29 in transfected cells. Cell homogenate was separated by SDS-PAGE and ATXN3Q6 was subjected to reduction, alkylation and in situ digestion with GluC endoproteinase (1:10 enzyme/protein, w/w). Upon peptide extraction with 40% CH_3CN in 0.1% TFA, the peptide mixture was analyzed by mass spectrometry (as described in Materials and Methods).

ATX3	Peptide	Species	Predicted mass	Identified mass
Wild type	^{27}YFSPVE^{32}	P-Ser + 80	821.34	821.98
	^{27}YFSPVELSSIAHQLDEEE^{44}	P-Ser + 80	2172.97	2173.02

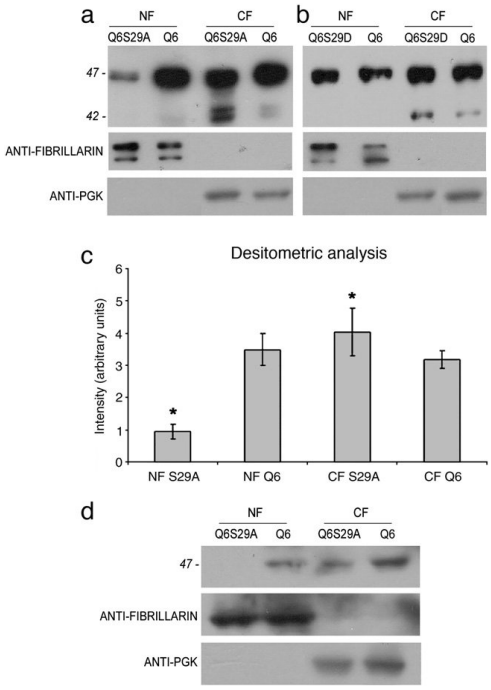

Fig. 3. Western-blot analysis of ataxins-3 in COS-7 and SHSY-5Y cells. c-myc tagged fulllength ATXN3Q6 (a, b) and its mutants ATXN3Q6S29A (a) and ATXN3Q6S29D (b) were expressed in COS-7 cells. Western-blots of cytosolic and nuclear fractions were probed with a monoclonal anti-c-myc antibody. Cytosolic and nuclear fractions controls were performed with anti-fibrillarin and anti-PGK antibodies. (c) Densitometric analysis performed with NIH Image-based software Scion Image (Scion Corporation) on blot reported in panel a. Bands intensities were normalized on fibrillarin and PGK controls.
Data represent mean ± SD of three independent experiments; significant differences were found between nuclear and cytosolic S29A mutant (* $p<0.05$); no differences were found between nuclear and cytosolic wild-type ATXN3 ($p=0.52$) (d) c-myc tagged full-length ATXN3Q6 and its mutant ATXN3Q6S29A were expressed in SHSY-5Y cells. Western-blots of cytosolic and nuclear fractions were probed with a monoclonal anti-c-myc antibody. Cytosolic and nuclear fractions controls were performed with anti-fibrillarin and anti-PGK antibodies.

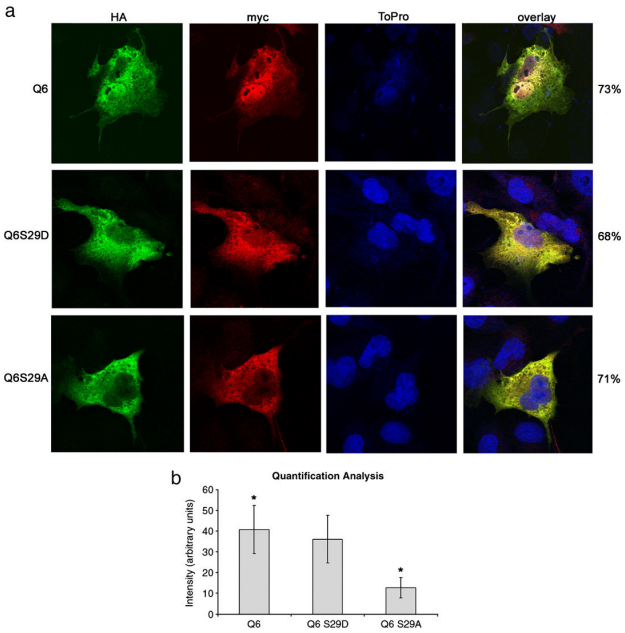

Fig. 4. Confocal microscopy analysis of ATXN3 subcellular localization. (a) COS-7 cells were transfected with cDNAs coding for ATXN3Q6, or ATXN3Q6S29A and ATXN3Q6S29D mutants. To investigate sub-cellular localization of ATXN3, cells were fixed in PFA and probed with mouse monoclonal anti-c-myc (red), rabbit monoclonal anti-HA antibodies (green) and the nuclear marker TO-PRO-3 iodide (blue). Last column reports percentage of observed phenotypes (b) Quantification analysis of fluorescence intensities in the nuclear region of cells overexpressing ATXN3Q6, ATXN3Q6S29A or ATXN3Q6S29D. Data represent mean ± SD of three independent experiments; significant differences were found between wild-type ATXN3 and S29A mutant (* $p<0.05$); no differences were found between wild-type ATXN3 and S29D mutant ($p=0.53$).

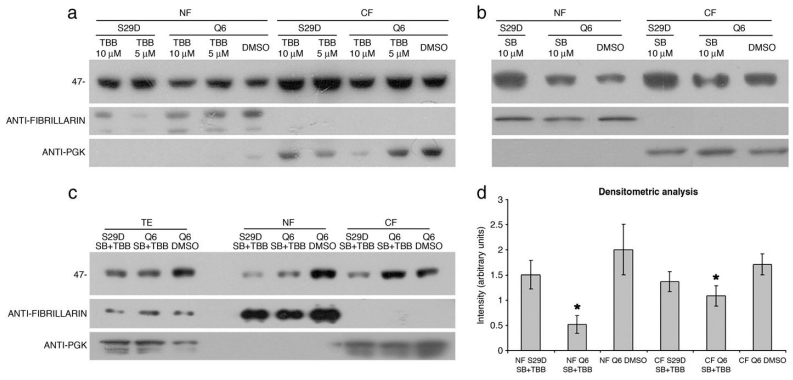

Fig. 5. Western-blot analysis of COS-7 cells treated with kinase inhibitors. (a) c-myc tagged full-length ATXN3Q6 and its mutant ATXN3Q6S29D were expressed in COS-7 cells treated with TBB 5 or 10 μM (CK2 inhibitor) or with DMSO, as a control. (b) c-myc tagged full-length ATXN3Q6 and its mutant ATXN3Q6S29D were expressed in COS-7 cells treated with SB 216763 10 μM(GSK3 inhibitor) or withDMSO, as a control. (c) c-myc tagged full-length ATXN3Q6 and its mutant ATXN3Q6S29D were expressed in COS-7 cells treated with both TBB 10 μM (CK2 inhibitor) and SB 216763 10 μM (GSK3 inhibitor) or with DMSO, as a control. (d) Densitometric analysis performed with NIH Image-based software Scion Image (Scion Corporation) on blot reported in panel c. Bands intensities were normalized on fibrillarin and PGK controls. Data represent mean±SD of three independent experiments; significant differences were found between nuclear and cytosolic wild-type ATXN3 in the presence of CK2 and GSK3 inhibitors (* $p<0.05$); no differences were found between nuclear and cytosolic S29D mutant in the presence of CK2 and GSK3 inhibitors (pN0.5) (a, b, c,) Western-blots of total extracts, cytosolic fraction and nuclear fraction were probed with a monoclonal anti-c-myc antibody. Cytosolic and nuclear fractions controls were performed with anti-fibrillarin and anti-PGK antibodies.

References

[1] H.L. Paulson, S.S. Das, P.B. Crino, M.K. Perez, S.C. Patel, D. Gotsdiner, K.H. Fischbeck, R.N. Pittman, Machado-Joseph disease gene product is a cytoplasmic protein widely expressed in brain, Ann. Neurol. 41 (1997) 453–462.

[2] Y. Trottier, G. Cancel, I. An-Gourfinkel, Y. Lutz, C. Weber, A. Brice, E. Hirsch, J.L. Mandel, Heterogeneous intracellular localization and expression of ataxin-3, Neurobiol. Dis. 5 (1998) 335–347.

[3] A.E. Bevivino, P.J. Loll, An expanded glutamine repeat destabilizes native ataxin-3 structure and mediates formation of parallel beta -fibrils, Proc. Natl. Acad. Sci. U. S. A. 98 (2001) 11955–11960.

[4] M. Albrecht, D. Hoffmann, B.O. Evert, I. Schmitt, U. Wullner, T. Lengauer, Structural modeling of ataxin-3 reveals distant homology to adaptins, Proteins 50 (2003) 355–370.

[5] L. Masino, V. Musi, R.P. Menon, P. Fusi, G. Kelly, T.A. Frenkiel, Y. Trottier, A. Pastore, Domain architecture of the polyglutamine protein ataxin-3: a globular domain followed by a flexible tail, FEBS Lett. 549 (2003) 21–25.

[6] M. Albrecht, M. Golatta, U. Wullner, T. Lengauer, Structural and functional analysis of ataxin-2 and ataxin-3, Eur. J. Biochem. 271 (2004) 3155–3170.

[7] Y. Mao, F. Senic-Matuglia, P.P. Di Fiore, S. Polo, M.E. Hodsdon, P. De Camilli, Deubiquitinating function of ataxin-3: insights from the solution structure of the Josephin domain, Proc. Natl. Acad. Sci. U. S. A. 102 (2005) 12700–12705.

[8] G. Nicastro, R.P. Menon, L. Masino, P.P. Knowles, N.Q. McDonald, A. Pastore, The solution structure of the Josephin domain of ataxin-3: structural determinants for molecular recognition, Proc. Natl. Acad. Sci. U. S. A. 102 (2005) 10493–10498.

[9] F. Li, T. Macfarlan, R.N. Pittman, D. Chakravarti, Ataxin-3 is a histone-binding protein with two independent transcriptional corepressor activities, J. Biol. Chem. 277 (2002) 45004–45012.

[10] M. Matsumoto, M. Yada, S. Hatakeyama, H. Ishimoto, T. Tanimura, S. Tsuji, A. Kakizuka, M. Kitagawa, K.I. Nakayama, Molecular clearance of ataxin-3 is regulated by a mammalian E4, EMBO J. 23 (2004) 659–669.

[11] H. Scheel, S. Tomiuk, K. Hofmann, Elucidation of ataxin-3 and ataxin-7 function by integrative bioinformatics, Hum. Mol. Genet. 12 (2003) 2845–2852.

[12] B. Burnett, F. Li, R.N. Pittman, The polyglutamine neurodegenerative protein ataxin-3 binds polyubiquitylated proteins and has ubiquitin protease activity, Hum. Mol. Genet. 12 (2003) 3195–3205.

[13] S.J. Berke, F.A. Schmied, E.R. Brunt, L.M. Ellerby, H.L. Paulson, Caspase-mediated proteolysis of the polyglutamine disease protein ataxin-3, J. Neurochem. 89 (2004) 908–918.

[14] X. Zhong, R.N. Pittman, Ataxin-3 binds VCP/p97 and regulates retrotranslocation of ERAD substrates, Hum. Mol. Genet. 15 (2006) 2409–2420.

[15] D. Tait, M. Riccio, A. Sittler, E. Scherzinger, S. Santi, A. Ognibene, N.M. Maraldi, H. Lehrach, E.E. Wanker, Ataxin-3 is transported into the nucleus and associates with the nuclear matrix, Hum. Mol. Genet. 7 (1998) 991–997.

[16] M.K. Perez, H.L. Paulson, R.N. Pittman, Ataxin-3 with an altered conformation that exposes the polyglutamine domain is associated with the nuclear matrix, Hum. Mol. Genet. 8 (1999) 2377–2385.

[17] C.L. Wellington, L.M. Ellerby, A.S. Hackam, R.L. Margolis, M.A. Trifiro, R. Singaraja, K. McCutcheon, G.S. Salvesen, S.S. Propp, M. Bromm, K.J. Rowland, T. Zhang, D. Rasper, S. Roy, N. Thornberry, L. Pinsky, A. Kakizuka, C.A. Ross, D.W. Nicholson, D. E. Bredesen, M.R. Hayden, Caspase cleavage of gene products associated with triplet expansion disorders generates truncated fragments containing the polyglutamine tract, J. Biol. Chem. 273 (1998) 9158–9167.

[18] H.L. Paulson, Protein fate in neurodegenerative proteinopathies: polyglutamine diseases join the (mis)fold, Am. J. Hum. Genet. 64 (1999) 339–345.

[19] D. Goti, S.M. Katzen, J. Mez, N. Kurtis, J. Kiluk, L. Ben-Haiem, N.A. Jenkins, N.G. Copeland, A. Kakizuka, A.H. Sharp, C.A. Ross, P.R. Mouton, V. Colomer, A mutant ataxin-3 putative-cleavage fragment in brains of Machado-Joseph disease patients and transgenic mice is cytotoxic above a critical concentration, J. Neurosci. 24 (2004) 10266–10279.

[20] A. Haacke, S.A. Broadley, R. Boteva, N. Tzvetkov, F.U. Hartl, P. Breuer, Proteolytic cleavage of polyglutamine-expanded ataxin-3 is critical for aggregation and sequestration of non-expanded ataxin-3, Hum. Mol. Genet. 15 (2006) 555–568.

[21] P.L.Mauri,M. Riva,D. Ambu, A.De Palma, F. Secundo, L. Benazzi,M. Valtorta, P. Tortora, P. Fusi, Ataxin-3 is subject to autolytic cleavage, FEBS J. 273 (2006) 4277–4286.

[22] C. Pozzi, M. Valtorta, G. Tedeschi, E. Galbusera, V. Pastori, A. Bigi, S. Nonnis, E. Grassi, P. Fusi, Study of subcellular localization and proteolysis of ataxin-3, Neurobiol. Dis. 30 (2008) 190–200.

[23] A. Haacke, F.U. Hartl, P. Breuer, Calpain inhibition is sufficient to suppress aggregation of polyglutamine-expanded ataxin-3, J. Biol. Chem. 282 (2007) 18851–18856.

[24] R.S. Tao, E.K. Fei, Z. Ying, H.F. Wang, G.H. Wang, Casein kinase 2 interacts with and phosphorylates ataxin-3, Neurosci. Bull. 24 (2008) 271–277.

[25] T. Mueller, P. Breuer, I. Schmitt, J. Walter, B.O. Evert, U. Wullner, CK2-dependent phosphorylation determines cellular localization and stability of ataxin-3, Hum. Mol. Genet. 18 (2009) 3334–3343.

[26] H.G. Lee, G. Perry, P.I. Moreira, M.R. Garrett, Q. Liu, X. Zhu, A. Takeda, A. Nunomura, M.A. Smith, Tau phosphorylation in Alzheimer's disease: pathogen or protector? Trends Mol. Med. 11 (2005) 164–169.

[27] L. Chen, M.B. Feany, Alpha-synuclein phosphorylation controls neurotoxicity and inclusion formation in a Drosophila model of Parkinson disease, Nat. Neurosci. 8 (2005) 657–663.

[28] A.C. Lim, Z. Hou, C.P. Goh, R.Z. Qi, Protein kinase CK2 is an inhibitor of the neuronal Cdk5 kinase, J. Biol. Chem. 279 (2004) 46668–46673.

[29] E. Fei, N. Jia, T. Zhang, X. Ma, H. Wang, C. Liu, W. Zhang, L. Ding, N. Nukina, G. Wang, Phosphorylation of ataxin-3 by glycogen synthase kinase 3beta at serine 256 regulates the aggregation of ataxin-3, Biochem. Biophys. Res. Commun. 357 (2007) 487–492.

[30] M.D. Kaytor, H.T. Orr, The GSK3 beta signaling cascade and neurodegenerative disease, Curr. Opin. Neurobiol. 12 (2002) 275–278.

[31] R.S. Jope, G.V. Johnson, The glamour and gloom of glycogen synthase kinase-3, Trends Biochem. Sci. 29 (2004) 95–102.

[32] S. Marchal, E. Shehi, M.C. Harricane, P. Fusi, F. Heitz, P. Tortora, R. Lange, Structural instability and fibrillar aggregation of non-expanded human ataxin-3 revealed under high pressure and temperature, J. Biol. Chem. 278 (2003) 31554–31563.

[33] E. Shehi, P. Fusi, F. Secundo, S. Pozzuolo, A. Bairati, P. Tortora, Temperaturedependent, irreversible formation of amyloid fibrils by a soluble human ataxin-3 carrying a moderately expanded polyglutamine stretch (Q36), Biochemistry 42 (2003) 14626–14632.

[34] P. Coccetti, R.L. Rossi, F. Sternieri, D. Porro, G.L. Russo, A. di Fonzo, F. Magni, M. Vanoni, L. Alberghina, Mutations of the CK2 phosphorylation site of Sic1 affect cell size and S-Cdk kinase activity in Saccharomyces cerevisiae, Mol. Microbiol. 51 (2004) 447–460.

[35] T. Nonaka, T. Iwatsubo, M. Hasegawa, Ubiquitination of alpha-synuclein, Biochemistry 44 (2005) 361–368.

[36] S. Luo, C. Vacher, J.E. Davies, D.C. Rubinsztein, Cdk5 phosphorylation of huntingtin reduces its cleavage by caspases: implications for mutant huntingtin toxicity, J. Cell Biol. 169 (2005) 647–656.
[37] J. Walter, A. Schindzielorz, J. Grunberg, C. Haass, Phosphorylation of presenilin-2 regulates its cleavage by caspases and retards progression of apoptosis, Proc. Natl. Acad. Sci. U. S. A. 96 (1999) 1391–1396.
[38] T. Seki, N. Adachi, Y. Ono, H. Mochizuki, K. Hiramoto, T. Amano, H. Matsubayashi, M. Matsumoto, H. Kawakami, N. Saito, N. Sakai, Mutant protein kinase Cgamma found in spinocerebellar ataxia type 14 is susceptible to aggregation and causes cell death, J. Biol. Chem. 280 (2005) 29096–29106.
[39] H.K. Chen, P. Fernandez-Funez, S.F. Acevedo, Y.C. Lam, M.D. Kaytor, M.H. Fernandez, A. Aitken, E.M. Skoulakis, H.T. Orr, J. Botas, H.Y. Zoghbi, Interaction of Akt-phosphorylated ataxin-1 with 14-3-3 mediates neurodegeneration in spinocerebellar ataxia type 1, Cell 113 (2003) 457–468.
[40] E.S. Emamian, M.D. Kaytor, L.A. Duvick, T. Zu, S.K. Tousey, H.Y. Zoghbi, H.B. Clark, H.T. Orr, Serine 776 of ataxin-1 is critical for polyglutamine-induced disease in SCA1 transgenic mice, Neuron 38 (2003) 375–387.
[41] J.R. Woodgett, Molecular cloning and expression of glycogen synthase kinase-3/factor A, EMBO J. 9 (1990) 2431–2438.
[42] J.J. Lucas, F. Hernandez, P. Gomez-Ramos, M.A. Moran, R. Hen, J. Avila, Decreased nuclear beta-catenin, tau hyperphosphorylation and neurodegeneration in GSK-3beta conditional transgenic mice, EMBO J. 20 (2001) 27–39.
[43] B.O. Evert, J. Araujo, A.M. Vieira-Saecker, R.A. de Vos, S. Harendza, T. Klockgether, U. Wullner, Ataxin-3 represses transcription via chromatin binding, interaction with histone deacetylase 3, and histone deacetylation, J. Neurosci. 26 (2006) 11474–11486.
[44] C.P. Reina, X. Zhong, R.N. Pittman, Proteotoxic stress increases nuclear localization of ataxin-3, Hum. Mol. Genet. 19 (2010) 235-249.
[45] S. Macedo-Ribeiro, L. Cortes, P. Maciel, A.L. Carvalho, Nucleocytoplasmic shuttling activity of ataxin-3, PLoS One 4 (2009) e5834.
[46] H.F. Tsai, H.J. Tsai, M. Hsieh, Full-length expanded ataxin-3 enhances mitochondrial-mediated cell death and decreases Bcl-2 expression in human neuroblastoma cells, Biochem. Biophys. Res. Commun. 324 (2004) 1274–1282.
[47] A.H. Chou, T.H. Yeh, Y.L. Kuo, Y.C. Kao, M.J. Jou, C.Y. Hsu, S.R. Tsai, A. Kakizuka, H.L. Wang, Polyglutamine-expanded ataxin-3 activates mitochondrial apoptotic pathway by upregulating Bax and downregulating Bcl-xL, Neurobiol. Dis. 21 (2006) 333–345.
[48] Y.C. Yu, C.L. Kuo, W.L. Cheng, C.S. Liu, M. Hsieh, Decreased antioxidant enzyme activity and increased mitochondrial DNA damage in cellular models of Machado-Joseph disease, J. Neurosci. Res. 87 (2009) 1884–1891.
[49] J. Hubener, O. Riess, Polyglutamine-induced neurodegeneration in SCA3 is not mitigated by non-expanded ataxin-3: Conclusions from double-transgenic mouse models, Neurobiol. Dis. 38 (1) (2010)116–124.
[50] A.J. Williams, T.M. Knutson, V.F. Colomer Gould, H.L. Paulson, In vivo suppression of polyglutamine neurotoxicity by C-terminus of Hsp70-interacting protein (CHIP) supports an aggregation model of pathogenesis, Neurobiol. Dis. 33 (2009) 342–353.